

NEUTRINO MASS BOUNDS FROM COSMOLOGY

By
SHOUVIK ROY CHOUDHURY
PHYS08201305004

Harish-Chandra Research Institute, Prayagraj

A thesis submitted to the
Board of Studies in Physical Sciences
In partial fulfillment of requirements
for the Degree of
DOCTOR OF PHILOSOPHY
of
HOMI BHABHA NATIONAL INSTITUTE



November, 2019

Homi Bhabha National Institute¹

Recommendations of the Viva Voce Committee

As members of the Viva Voce Committee, we certify that we have read the dissertation prepared by Shouvik Roy Choudhury entitled "Neutrino Mass Bounds from Cosmology" and recommend that it may be accepted as fulfilling the thesis requirement for the award of Degree of Doctor of Philosophy.

Chairman - Prof. Pinaki Majumdar

Pinaki Majumdar

Date:

29/1/20

Guide / Convener - Prof. Sandhya Choubey

for *Sandhya Choubey*

Date:

29/1/2020

Examiner - Prof. Supriya Pan

Supriya Pan

Date: *29/01/2020*

Member 1- Prof. Santosh Kumar Rai

Santosh

Date:

29-01-2020

Member 2- Prof. Anshuman Maharana

A Maharana

Date: *29-01-2020*

Member 3- Prof. Areshkrishna Datta

Areshkrishna Datta

Date:

29/01/2020

Final approval and acceptance of this thesis is contingent upon the candidate's submission of the final copies of the thesis to HBNI.

I/We hereby certify that I/we have read this thesis prepared under my/our direction and recommend that it may be accepted as fulfilling the thesis requirement.

Date: 29.01.2020

Place: Prayagraj

for *Sandhya Choubey*

Prof. Sandhya Choubey
Guide

¹ This page is to be included only for final submission after successful completion of viva voce.

STATEMENT BY AUTHOR

This dissertation has been submitted in partial fulfillment of requirements for an advanced degree at Homi Bhabha National Institute (HBNI) and is deposited in the Library to be made available to borrowers under rules of the HBNI.

Brief quotations from this dissertation are allowable without special permission, provided that accurate acknowledgement of source is made. Requests for permission for extended quotation from or reproduction of this manuscript in whole or in part may be granted by the Competent Authority of HBNI when in his or her judgment the proposed use of the material is in the interests of scholarship. In all other instances, however, permission must be obtained from the author.

Shouvik Roy Choudhury
Shouvik Roy Choudhury

DECLARATION

I, hereby declare that the investigation presented in the thesis has been carried out by me. The work is original and has not been submitted earlier as a whole or in part for a degree / diploma at this or any other Institution / University.

Shouvik Roy Choudhury
Shouvik Roy Choudhury

List of Publications arising from the thesis

Journal

1. “Updated bounds on sum of neutrino masses in various cosmological scenarios”, Shouvik Roy Choudhury and Sandhya Choubey, *JCAP*, **2018**, 1809, 017.
2. “Strong bounds on sum of neutrino masses in a 12 parameter extended scenario with non-phantom dynamical dark energy ($w(z) \geq -1$)”, Shouvik Roy Choudhury and Abhishek Naskar, *Eur. Phys. J.*, **2019**, C79, 262.
3. “Constraining light sterile neutrino mass with the BICEP2/Keck Array 2014 B-mode polarization data”, Shouvik Roy Choudhury and Sandhya Choubey, *Eur. Phys. J.*, **2019**, C79, 557.

Conferences

1. Presented a poster titled “Cosmological Aspect of Light Sterile Neutrinos” at Nu HoRIZons VII, Prayagraj, India, February, 2018.
2. Presented a poster titled “Light sterile neutrinos: Analysis with Planck and Bicep-Keck” at Post Planck Cosmology: Enigma, Challenges and Visions, Pune, India, October, 2017.
3. Presented a poster titled “Light Sterile Neutrinos in Cosmology: Analysis with BK14 data” at Invisibles Workshop 2017, Zurich, Switzerland, June, 2017.
4. Presented a poster titled “Light Sterile Neutrinos in Cosmology: Analysis with BK14 data” at Invisibles School 2017, Murten, Switzerland, June, 2017.

Shouvik Roy Choudhury
Shouvik Roy Choudhury

DEDICATIONS

To my late mother, Mrs. Sikha Roy Choudhury

ACKNOWLEDGEMENTS

I have spent quite some time in HRI and during my stay, I have had opportunity to thank a lot of people. The first of them is my supervisor Prof. Sandhya Choubey. Thank you for all your energy and effort to train me as a physicist, and for the independence you provided me in pursuing my research interests and ideas, and for always pushing me to do my best. I would also like to thank my teachers and thesis committee members, in no particular order, Prof. Jayanta Bhattacharya, Prof. Pinaki Majumdar, Prof. Ashoke Sen, Prof. Dileep Jatkar, Prof. Santosh Rai, Prof. Anshuman Maharana, Prof. Asesh Krishna Datta, Prof. Sumathi Rao, Prof. Anirban Basu, Prof. Rajesh Gopakumar, Prof. S. Naik, Prof. B Mukhopadhyaya, Prof. Ujjwal Sen. I hereby thank my friends at HRI who made HRI an enjoyable experience. Thanks a lot Chiranjib, Gautam, Dhruv, Sarif, Dipyaman, Tanaya, Ratul, Khorshed, Sreetama, Pradeep, Samiran, Atri, Sankha, Soumyananda, Chirag, Samrat, Anoop, Waleed. I also acknowledge the help I received from the administration staff at HRI from time to time. A special thanks to my family members for being there whenever I needed help and support.

Contents

Summary	1
List of Figures	3
List of Tables	11
1 Introduction	15
1.1 Basic Cosmology	15
1.2 Cosmological distances	19
1.3 Neutrino oscillations	21
1.4 The Λ CDM model	24
1.5 Brief thermal history of the universe	26
1.6 Cosmological history of neutrinos	30
1.7 Neutrino mass effects on cosmology	37
1.7.1 Neutrino mass effects on CMB anisotropies	37

1.7.2	Neutrino mass effects on the matter power spectrum	42
1.8	Statistical methods in cosmology	46
2	Results on $\sum m_\nu$ in various cosmological models	51
2.1	Cosmological Models and Analysis Method	54
2.2	Datasets	57
2.3	Results on $\sum m_\nu$	61
2.3.1	Results for the Λ CDM + $\sum m_\nu$ Model	61
2.3.2	Results for the Λ CDM + r + $\sum m_\nu$ Model	77
2.3.3	Results for the w_0w_a CDM + $\sum m_\nu$ Model (DDE)	80
2.3.4	Results for the w_0w_a CDM + $\sum m_\nu$ Model with $w(z) \geq -1$ (NPDDE)	84
2.3.5	Results for the w_0w_a CDM + r + $\sum m_\nu$ Model with $w(z) \geq -1$ (NPDDE+ r)	88
2.4	Discussion and Summary	90
3	Neutrino masses and non-phantom dark energy in a 12 parameter extended scenario	95
3.1	Models	98
3.2	Datasets	101
3.3	Results	101
3.3.1	NPDDE11+ r model	102
3.3.2	NPDDE11 model	109
3.3.3	NPDDE11+ A_{lens} model	114

3.4	τ and A_{lens} : Implications for Planck 2018	117
3.5	Summary	119
4	Constraints on light sterile neutrino mass from cosmology	125
4.1	Cosmological Analysis: Models and Datasets	128
4.2	Results	131
4.2.1	Results for $\Lambda\text{CDM} + r + N_{\text{eff}} + m_s^{\text{eff}}$ model	131
4.2.2	Results for $\Lambda\text{CDM} + r + m_s^{\text{eff}}$ model	141
4.3	Discussion	143
5	Conclusions and future outlook	147
	References	155

List of Figures

- 1.1 Effect of increasing $\sum m_\nu$ on the CMB temperature power spectrum, adjusting h and Ω_Λ to keep Θ_s and z_{eq} fixed. Here $D_l^{TT} \equiv l(l+1)C_l^{TT}/2\pi$ in units of μK^2 . *Upper panel:* the black curve is the power spectrum for the baseline model where $\sum m_\nu = 0.06$ eV, $h = 0.7$, and $\Omega_\Lambda = 0.713$. The red (blue) curve is for $\sum m_\nu = 0.9$ eV ($\sum m_\nu = 1.5$ eV), where the increase in $\sum m_\nu$ is compensated with $h = 0.628$ ($h = 0.586$) and $\Omega_\Lambda = 0.620$ ($\Omega_\Lambda = 0.545$). *Lower panel:* relative change in power compared to the baseline model, with the same color coding as above. 40

LIST OF FIGURES

- 1.2 Impact of increasing $\sum m_\nu$ on the linear matter power spectrum, z_{eq} and Ω_m fixed. *Upper panel:* the black curve is the power spectrum for the baseline model where $\sum m_\nu = 0.06 \text{ eV}$, $h = 0.7$, and $\Omega_m = 0.287$. The red (blue) curves are obtained for $\sum m_\nu = 0.9 \text{ eV}$ ($\sum m_\nu = 1.5 \text{ eV}$), where the increase in $\sum m_\nu$ is compensated for by setting $h = 0.722$ ($h = 0.738$). *Lower panel:* relative change in power with respect to the baseline model, with the same colour coding as above. 44
- 2.1 Comparison of 1-D marginalized posterior distributions for $\sum m_\nu$ for various data combinations in $\Lambda\text{CDM} + \sum m_\nu$, without τ and H_0 priors. The plots are normalized in the sense that area under the curve is same for all curves. 62
- 2.2 Comparison of 1-D marginalized posterior distributions for H_0 for various data combinations in $\Lambda\text{CDM} + \sum m_\nu$, without τ and H_0 priors. 62
- 2.3 1σ and 2σ marginalised contours for τ vs. $\sum m_\nu$ for TT and TT+lowP datasets in the $\Lambda\text{CDM} + \sum m_\nu$ model, showing the reduction in correlation between τ and $\sum m_\nu$ due to addition of lowP data, leading to a stronger bound on $\sum m_\nu$ 65
- 2.4 1σ and 2σ marginalised contours for H_0 vs. $\sum m_\nu$ for TT+lowP, TT+lowP+BAO and TT+lowP+PAN datasets in $\Lambda\text{CDM} + \sum m_\nu$ model, showing the degeneracy breaking effect of BAO and PAN datasets separately. Evidently the BAO data is more effective in breaking the degeneracy between the two parameters. 69

LIST OF FIGURES

2.5 Comparison of 1-D marginalized posterior distributions for $\sum m_\nu$ for various data combinations in $\Lambda\text{CDM} + \sum m_\nu$, with τ and H_0 priors. The plots are normalized in the sense that area under the curve is same for all curves. 70

2.6 Comparison of 1-D marginalized posterior distributions for H_0 for various data combinations in $\Lambda\text{CDM} + \sum m_\nu$, with τ and H_0 priors. . 70

2.7 1σ and 2σ marginalized contours for τ vs. $\sum m_\nu$ for TT+BAO and TT+BAO+ $\tau 0p055$ datasets in $\Lambda\text{CDM} + \sum m_\nu$ model, showing the reduction in correlation between τ and $\sum m_\nu$ due to addition of $\tau 0p055$, leading to a stronger bound on $\sum m_\nu$ 73

2.8 1σ and 2σ marginalized contours for H_0 vs. $\sum m_\nu$ for TT+lowP and TT+lowP+R16 datasets in $\Lambda\text{CDM} + \sum m_\nu$ model, showing the reduction in correlation between H_0 and $\sum m_\nu$ due to addition of the R16 prior, leading to a very strong bound on $\sum m_\nu$ 75

2.9 Comparison of 1-D marginalized posterior distributions for σ_8 for various data combinations in $\Lambda\text{CDM} + \sum m_\nu$ model. Data combinations with FS and SZ prefer a slightly lower value of σ_8 , due to which slightly less stringent upper bounds on $\sum m_\nu$ are obtained. 76

2.10 Comparison of 1-D marginalized posterior distributions for σ_8 for various data combinations in $\Lambda\text{CDM} + r + \sum m_\nu$ model. Addition of BK14 data seems to prefer a higher σ_8 , due to which slightly more stringent upper bounds on $\sum m_\nu$ are obtained. 79

LIST OF FIGURES

2.11 Comparison of 1-D marginalised posterior distributions for $\sum m_\nu$ comparing the Λ CDM + $\sum m_\nu$ and DDE models. The plots are normalized in the sense that area under the curve is same for all curves. 81

2.12 Comparison of 1-D marginalised posterior distributions for H_0 comparing the Λ CDM + $\sum m_\nu$ and DDE models. The DDE model prefers a broader distribution for H_0 and also the mean value of H_0 is higher, thereby reducing the tension between Planck 2015 and R16. Adding the R16 prior in the DDE model leads to even larger H_0 values. . . . 82

2.13 1σ and 2σ marginalised contours in the $\sum m_\nu - H_0$ plane for TT + BAO + PAN + $\tau 0p055$, comparing their correlation in the $w_0 w_a$ CDM + $\sum m_\nu$ (DDE) and Λ CDM + $\sum m_\nu$ models. 82

2.14 1σ and 2σ marginalized contours for w_0 vs. w_a for TT + BAO + PAN + $\tau 0p055$ and TTTEEE + BAO + PAN + R16 + $\tau 0p055$ datasets in the $w_0 w_a$ CDM + $\sum m_\nu$ (DDE) model. The dashed lines are at $w_0 = -1$ and $w_a = 0$ respectively. The two green lines originating from (-1,0) separate the non-phantom region from the rest. The region above the slanted green line and at the right of the vertical green line is the non-phantom region. 83

2.15 Comparison of 1-D marginalized posterior distributions for $\sum m_\nu$ comparing the Λ CDM + $\sum m_\nu$ and NPDDE models. The plots are normalized in the sense that area under the curve is same for all curves. 85

LIST OF FIGURES

2.16 Comparison of 1-D marginalized posterior distributions for H_0 comparing the Λ CDM + $\sum m_\nu$ and NPDDE models. The NPDDE model prefers smaller values for H_0 , thereby increasing the tension between Planck 2015 and R16. Adding the R16 prior in the NPDDE model leads to H_0 values which are somewhat similar to Λ CDM + $\sum m_\nu$ without R16. 85

2.17 Comparison of 1-D marginalized posterior distributions for $\sum m_\nu$ comparing the Λ CDM + $\sum m_\nu$ and NPDDE+r models. The plots are normalized in the sense that area under the curve is same for all curves. 88

2.18 Comparison of 1-D marginalized posterior distributions for H_0 comparing the Λ CDM + $\sum m_\nu$ and NPDDE+r models. 89

2.19 Comparison of 1-D marginalized posterior distributions for σ_8 for NPDDE and NPDDE+r models. Addition of BK14 data seems to prefer a higher σ_8 , due to which slightly more stringent upper bound on $\sum m_\nu$ is obtained. 89

3.1 Comparison of 1-D marginalized posterior distributions for $\sum m_\nu$ (eV) and N_{eff} for various data combinations in NPDDE11+r. 103

3.2 1σ and 2σ marginalized contours for H_0 (km/sec/Mpc) vs. $\sum m_\nu$ (eV) and H_0 (km/sec/Mpc) vs. N_{eff} for Planck+BK14+R16 in the NPDDE11+r model, showing only a small correlation between H_0 and $\sum m_\nu$ whereas a strong positive correlation between H_0 vs. N_{eff} . 104

LIST OF FIGURES

3.3 1σ and 2σ marginalized contours in the $\sigma_8 - \Omega_m$ plane showing that the NPDDE+r model is ineffective in reducing the tension between CFHTLenS and Planck 2015. 104

3.4 Comparison of 1-D marginalized posterior distributions for w_0 and w_a for different data combinations in NPDDE11+r. 105

3.5 Comparison of 1-D marginalized posterior distributions for $\sum m_\nu$ (eV) and N_{eff} for various data combinations in NPDDE11. 110

3.6 1σ and 2σ marginalized contours for H_0 (km/sec/Mpc) vs. $\sum m_\nu$ (eV) and H_0 (km/sec/Mpc) vs. N_{eff} for Planck+R16 in the NPDDE11 model, showing negligible correlation between H_0 and $\sum m_\nu$ whereas a strong positive correlation between H_0 vs. N_{eff} 110

3.7 Comparison of 1-D marginalized posterior distributions for w_0 and w_a for different data combinations in NPDDE11. 111

3.8 Comparison of 1-D marginalized posterior distributions for $\sum m_\nu$ (eV) and N_{eff} for various data combinations in NPDDE11+ A_{lens} 112

3.9 1σ and 2σ marginalized contours in the $\sigma_8 - \Omega_m$ plane showing that the NPDDE11+ A_{lens} model is effective in reducing the tension between CFHTLenS and Planck 2015. 114

3.10 Comparison of 1-D marginalized posterior distributions for w_0 and w_a for different data combinations in NPDDE11+ A_{lens} 117

LIST OF FIGURES

4.1 1σ and 2σ marginalized contours for H_0 [km/sec/Mpc] vs. m_s^{eff} [eV] in the $\Lambda\text{CDM} + r + N_{\text{eff}} + m_s^{\text{eff}}$ model with the following combinations: TT+lowP, TT+lowP+BAO, and TT+lowP+R16. Both BAO and R16 data decrease the correlation between the two parameters significantly. 134

4.2 1-D marginalized posteriors for m_s^{eff} [eV] and r in the $\Lambda\text{CDM} + r + N_{\text{eff}} + m_s^{\text{eff}}$ model with various data combinations. 135

4.3 1σ and 2σ marginalized contours for σ_8 vs. m_s^{eff} [eV] in the $\Lambda\text{CDM} + r + N_{\text{eff}} + m_s^{\text{eff}}$ model with the following combinations: TT+lowP and TT+lowP+BK14. Adding BK14 leads to slightly higher σ_8 ; and due to large anti-correlation present between σ_8 and m_s^{eff} , slightly stronger bound on m_s^{eff} is obtained. 138

4.4 1σ and 2σ marginalized contours for σ_8 vs. Ω_m and σ_8 vs. H_0 in the $\Lambda\text{CDM} + r + N_{\text{eff}} + m_s^{\text{eff}}$ model with the following combinations: TT+lowP and TT+lowP+BK14. We have also presented the contours in the ΛCDM model with Planck 2015 lensing and CFHTLenS data. Adding BK14 leads to slightly higher σ_8 , which worsens the agreement with CFHTLenS and Planck 2015. 139

List of Tables

2.1	Flat priors on cosmological parameters included in this work. For the NPDDE model, hard priors according to Eq. (2.7) are also implemented so as to exclude the parameter space region corresponding to phantom dark energy.	57
2.2	Upper bounds at 95% C.L. on $\sum m_\nu$ (degenerate case), in Λ CDM + $\sum m_\nu$ model for the given datasets. Details about models and datasets are given in Section 2.1 and Section 2.2 respectively.	63
2.3	Upper bounds at 95% C.L. on $\sum m_\nu$ (degenerate case), in Λ CDM + $\sum m_\nu$ model for the given datasets. This is same as Table 2.2 but including the high- l polarization data of Planck 2015. Details about models and datasets are given in Sections 2.1 and 2.2 respectively. . .	63

LIST OF TABLES

2.4	Upper bounds at 95% C.L. on $\sum m_\nu$ (degenerate case), in Λ CDM + $\sum m_\nu$ model for the given datasets. Details about models and datasets are given in Section 2.1 and Section 2.2 respectively.	71
2.5	Upper bounds at 95% C.L. on $\sum m_\nu$ (degenerate case), in Λ CDM + $\sum m_\nu$ model for the given datasets. This is same as Table 2.4 but including the high- l polarization data of Planck 2015. Details about models and datasets are given in Section 2.1 and Section 2.2 respectively.	71
2.6	Upper bounds at 95% C.L. on $\sum m_\nu$ (degenerate case), Λ CDM + $r + \sum m_\nu$ model for the given datasets. Details about models and datasets are given in Section 2.1 and Section 2.2 respectively.	77
2.7	Upper bounds at 95% C.L. on $\sum m_\nu$ (degenerate case), in w_0w_a CDM+ $\sum m_\nu$ model (DDE), for the given datasets. Details about models and datasets are given in Section 2.1 and Section 2.2 respectively.	80
2.8	Upper bounds at 95% C.L. on $\sum m_\nu$ (degenerate), in w_0w_a CDM + $\sum m_\nu$ model with $w(z) \geq -1$ (NPDDE), for the given datasets. Details about models and datasets are given in Section 2.1 and Section 2.2 respectively.	84
2.9	Upper bounds at 95% C.L. on $\sum m_\nu$ (degenerate), in w_0w_a CDM+ $r + \sum m_\nu$ model with $w(z) \geq -1$ (NPDDE with tensors), for the given datasets. Details about models and datasets are given in Section 2.1 and Section 2.2 respectively.	88

LIST OF TABLES

3.1	Flat priors on the main cosmological parameters constrained in this chapter.	100
3.2	Bounds on cosmological parameters in the NPDDE11+r model. Marginalized limits are given at 68% C.L. whereas upper limits are given at 95% C.L. Note that H_0 and σ_8 are derived parameters.	102
3.3	Bounds on cosmological parameters in the Λ CDM model. Marginalized limits are given at 68% C.L. whereas upper limits are given at 95% C.L. Note that H_0 and σ_8 are derived parameters.	103
3.4	Bounds on cosmological parameters in the NPDDE11 model. Marginalized limits are given at 68% C.L. whereas upper limits are given at 95% C.L.. Note that H_0 and σ_8 are derived parameters.	109
3.5	Bounds on cosmological parameters in the NPDDE11+ A_{lens} model. Marginalized limits are given at 68% C.L. whereas upper limits are given at 95% C.L. Note that H_0 and σ_8 are derived parameters. . . .	113
4.1	Flat priors on cosmological parameters included in this work.	131
4.2	Bounds on cosmological parameters in the Λ CDM + r + N_{eff} + m_s^{eff} model without BK14 data. Marginalized limits are given at 68% C.L. whereas upper limits are given at 95% C.L. Note that H_0 and σ_8 are derived parameters.	132

LIST OF TABLES

4.3	Bounds on cosmological parameters in the Λ CDM + r + N_{eff} + m_s^{eff} model with BK14 data. Marginalized limits are given at 68% C.L. whereas upper limits are given at 95% C.L.. Note that H_0 and σ_8 are derived parameters.	132
4.4	Bounds on a cosmological parameters in the Λ CDM + r + m_s^{eff} model with $N_{\text{eff}} = 4.046$, assuming complete thermalization of sterile neutrinos. Marginalized limits are given at 68% C.L. whereas upper limits are given at 95% C.L. Note that H_0 and σ_8 are derived parameters.	141
4.5	Bounds on a cosmological parameters in the Λ CDM + r + m_s^{eff} model with $N_{\text{eff}} = 3.5$, assuming partial thermalization of sterile neutrinos. Marginalized limits are given at 68% C.L. whereas upper limits are given at 95% C.L. Note that H_0 and σ_8 are derived parameters.	141

Summary

This thesis is a thorough study on the constraints on neutrino masses coming from recent cosmological data, in various cosmological models. While the first two parts of the thesis deals with the sum of active neutrino masses $\sum m_\nu$, the last part incorporates a 3+1 scenario incorporating a light eV scale sterile neutrino. In the first part, we deal with base $\Lambda\text{CDM} + \sum m_\nu$ model and some of its simple extensions with tensor perturbations and dynamical dark energy. Neutrino mass bounds are dependent on the model and dataset combination being used, and we currently have only upper bounds instead of a detection. In the base $\Lambda\text{CDM} + \sum m_\nu$ model, the 95% bound is very close to the minimum mass required by inverted hierarchy of neutrino masses. However, current experiments do not have the sensitivity to determine the mass hierarchy of neutrinos. On the other hand, in extended models, the bounds on $\sum m_\nu$ can relax by a factor of two or more. However, that is not the case for an extended model with non-phantom dynamical dark energy, where the bound on $\sum m_\nu$ is actually stronger than $\Lambda\text{CDM} + \sum m_\nu$. Noticing this, we study 12

parameter extended cosmology with massive neutrinos and non-phantom dynamical dark energy and see that the bounds are stronger than $\Lambda\text{CDM} + \sum m_\nu$ even in such an extended scenario. However, introducing a parameter like A_{lens} which is strongly correlated with $\sum m_\nu$ relaxes the bound greatly. In the final part, we study light sterile neutrinos. We study the improvement of the bounds on a sterile neutrino effective mass due to CMB B-mode data from BICEP2/Keck collaboration (BK14). Fully thermalized sterile neutrinos with 1 eV mass (as predicted by short baseline experiments) are disfavoured by cosmology. These become slightly more disfavoured with BK14 data, due to tighter bounds on the mass, the effect likely coming from the lensing information encoded in the BK14 data.

Cosmological observations are a powerful probe of neutrino properties, namely energy density and mass. In this chapter, we mainly discuss the role of neutrinos in shaping the cosmological evolution. Later chapters of this thesis are devoted to constraints on the neutrino mass from cosmological observables.

1.1 Basic Cosmology

Einstein's field equations of classical General Relativity state that [1]:

$$G_{\mu\nu} = 8\pi GT_{\mu\nu}. \quad (1.1)$$

In Eq. (1.1), the Einstein tensor $G_{\mu\nu}$ corresponds to the geometry of the spacetime, whereas the energy-momentum tensor $T_{\mu\nu}$ is determined by the matter and energy content of the spacetime. The universe is homogeneous and isotropic on large scales, a notion that is known as the cosmological principle. The general form of

a metric which preserves this notion is the Friedmann-Lemaître-Robertson-Walker (FLRW) metric, given by the following line element [2–4]:

$$ds^2 = dt^2 - a^2(t) \left[\frac{dr^2}{1 - Kr^2} + r^2(d\theta^2 + \sin^2\theta d\phi^2) \right], \quad (1.2)$$

where t is time, r , θ , and ϕ are the spherical comoving coordinates, and K is the curvature parameter. The function $a(t)$ is the scale factor. We choose to define $a(t)$ such that at present time $t = t_0$, $a(t_0) = 1$.

Assuming that $T_{\mu\nu} = \text{diag}(\rho, P, P, P)$ (corresponding to a perfect fluid with energy density ρ and pressure P) one can arrive at the following Friedmann equations [1]:

$$H(a)^2 = \frac{8\pi G}{3}\rho(a) - \frac{K}{a^2} \quad (1.3)$$

$$\frac{\ddot{a}}{a} = -\frac{4\pi G}{3}(\rho + 3P), \quad (1.4)$$

with the dot denoting a time derivative.

Here, $H(a) \equiv \dot{a}/a$ is usually known as the Hubble parameter, and provides a measure of the expansion rate of the universe. The value of the Hubble parameter at present time, $H_0 = H(t_0)$, is called the Hubble constant. The reduced Hubble constant h is given by: $h \equiv H_0/(100 \text{ km s}^{-1} \text{ Mpc}^{-1})$.

The contribution to the energy density $\rho(a)$ comes from various sources: photons (γ), massive neutrinos (ν), baryons(b), dark matter (c), dark energy (DE).

Introducing the redshift as $z = 1/a - 1$, we can write,

$$\rho(z) = \rho_\gamma(z) + \rho_c(z) + \rho_b(z) + \rho_{\text{DE}}(z) + \rho_\nu(z). \quad (1.5)$$

If $K = 0$, i.e. the universe is flat, then from Eq. (1.3), evaluated today, i.e. $a = 1$, gives the total density (i.e. critical density required at present day for a flat spatial geometry),

$$\rho_{\text{cr},0} = \frac{3H_0^2}{8\pi G}. \quad (1.6)$$

In general, we use the subscript 0 to denote quantities evaluated at the present time. We redefine the densities of the constituents of the universe in the following way,

$$\Omega_i = \frac{\rho_{i,0}}{\rho_{\text{cr},0}}, \quad (1.7)$$

for $i \equiv \gamma, \nu, b, c, \text{DE}$. We also define $\Omega_k = -K/H_0^2$, as the curvature density.

From the first Friedmann equation (1.3), evaluated at present time, we can write,

$$\sum_i \Omega_i = 1, \quad (1.8)$$

where i now sums over curvature also, along with all the other components. In this thesis, we also use another notation for the densities, defined as $\omega_i \equiv \Omega_i h^2$. Thus, $\sum_i \omega_i = h^2$.

The Equation of State (EoS) w_i of a particular component of the universe (except curvature) is defined as $P_i = w_i \rho_i$. Here we introduce another useful equation, which

is not independent from Eqs. (1.3) and (1.4), often known as the continuity equation,

$$\dot{\rho} + 3H(\rho + P) = 0. \quad (1.9)$$

Solving this continuity equation by incorporating the EoS, one can show that,

$$\rho_i(z) \propto (1 + z)^{3(1+w_i)}. \quad (1.10)$$

Since photons always behave as radiation, $w_\gamma = 1/3$, whereas for CDM and baryons behave as matter for most of the evolution of the universe and thus one can take $w_c = w_b = 0$. For DE, we for now allow for an arbitrary but constant EoS, i.e. $w_{DE} = w$. If dark energy is described by a cosmological constant, Λ , then $w = -1$, and in that case we shall denote Ω_{DE} as Ω_Λ . We can now recast Eq. (1.3) as,

$$H(z)^2 = H_0^2 \left[\Omega_\gamma (1 + z)^4 + (\Omega_c + \Omega_b) (1 + z)^3 + \Omega_{DE} (1 + z)^{3(1+w)} + \Omega_k (1 + z)^2 + \frac{\rho_\nu(z)}{\rho_{cr,0}} \right]. \quad (1.11)$$

Here we have not explicitly mentioned the redshift dependence of neutrino energy density, since neutrinos behave as radiation in the early universe but can turn non-relativistic and behave as matter at late times, with the redshift of non-relativistic transition depending on their mass. An important quantity to note here is Ω_m , which includes the present day matter density from all matter, i.e. CDM, baryons, and

neutrinos whose masses are large enough so that they are non-relativistic currently.

1.2 Cosmological distances

In this section we introduce some distance scales frequently used in cosmology. The comoving causal horizon r_h at time t is the comoving distance covered by a photon from $t = 0$ until time t , i.e.,

$$r_h(t) = \int_0^t \frac{dt'}{a(t')} = \int_{z(t)}^{\infty} \frac{dz'}{H(z')}. \quad (1.12)$$

This is same as conformal time, which is usually denoted by $\eta(t)$ (as long as $\eta(0)$ is taken to be zero). If two particles are separated by a comoving distance larger than r_h today, they were not in causal contact since $t = 0$. Another important length scale is the Hubble length or time or radius $t_H(t) \equiv H(t)^{-1}$. In an ever accelerating universe, two particles presently separated by more than the present Hubble radius cannot communicate between each other from now on, though they might have communicated in the past.

An analogous quantity to r_h is the comoving sound horizon $r_s(t)$, i.e., the distance covered by an acoustic wave in the baryon-photon plasma in time t since $t = 0$. It is given by,

$$r_s(t) = \int_0^t \frac{c_s(t')}{a(t')} dt' = \int_{z(t)}^{\infty} \frac{c_s(z')}{H(z')} dz', \quad (1.13)$$

where c_s is the speed of the sound in the plasma, and it is given by $c_s = 1/\sqrt{3(1+R)}$, with $R = (P_b + \rho_b)/(P_\gamma + \rho_\gamma)$.

The comoving distance χ between us and a particle at a redshift z is

$$\chi(z) = \int_0^z \frac{dz'}{H(z')}, \quad (1.14)$$

and as can be seen from Eq. (1.12), this is equal to $\eta_0 - \eta(z)$, where η_0 is the present value of the comoving causal horizon. On the other hand, the comoving angular diameter distance $D_A(z)$ is defined as,

$$D_A(z) \equiv \frac{\sin(\sqrt{K}\chi)}{\sqrt{K}}. \quad (1.15)$$

Hence, if we are in a flat universe, i.e., $\Omega_k = 0$,

$$D_A(z) = \chi(z) = \int_0^z \frac{dz'}{H(z')}. \quad (1.16)$$

The angular size θ (that is observed by us) of an object is related to its comoving linear size l through $\theta = l/D_A(z)$. Thus if we know the linear size of an object, we can use it as a “standard ruler” to measure its angular diameter distance.

Another distance measure is given by the luminosity distance $d_L(z)$, that relates the observed flux F to the intrinsic luminosity L of an object at redshift z :

$$d_L(z) \equiv \sqrt{\frac{L}{4\pi F}} = (1+z)\chi(z) = (1+z)D_A(z). \quad (1.17)$$

Similar to the standard ruler case, here we can have “standard candles” which are objects of known intrinsic luminosity, and they can be used to measure their lumi-

nosity distance via the measurement of their flux. In both cases, such measurements can be used to make inferences about the cosmological parameters which participate in the integral in Eq. (1.14).

Since in this thesis, we are interested in neutrinos, in the next section we move away from cosmology and briefly describe the phenomenon of neutrino oscillations, which is an important step in understanding the neutrino mass parameter, $\sum m_\nu$ used in cosmology.

1.3 Neutrino oscillations

Standard model of particle physics was constructed with 3 massless neutrinos. However, neutrino oscillation experiments [5–9] have confirmed that neutrinos have distinct but small masses, with the lightest one having the option of having a zero mass. Neutrinos are produced in a particular flavor eigenstate $|\nu_\alpha\rangle$ ($\alpha = e, \mu, \tau$) via charged-current weak interactions. The flavor of the neutrino is determined by the charged lepton involved in the interaction, namely electron, muon, or tau. A flavor eigenstate is a quantum superposition of the three mass eigenstates $|\nu_i\rangle$ ($i = 1, 2, 3$) with individual masses m_i ,

$$|\nu_\alpha\rangle = \sum_i U_{\alpha i}^* |\nu_i\rangle. \quad (1.18)$$

Here U is the Pontecorvo Maki Nakagawa Sasaka (PMNS) matrix [10, 11]. Neutrinos are produced at the source as a particular flavor eigenstate, and while they travel, the three mass eigenstates can each obtain different phases due to having different phase

velocities. Thus, when the neutrinos reach their destination and are detected, there is a non-vanishing probability that the flavor of the detected neutrino is different from the original one, i.e. the neutrino oscillates among the flavors. The probability that a particular neutrino with flavor α transforms into a neutrino with flavor β is given by [12],

$$P(\nu_\alpha \rightarrow \nu_\beta) \simeq \sum_{i,j} U_{\alpha i}^* U_{\beta i} U_{\alpha j} U_{\beta j}^* e^{-i \frac{\Delta m_{ij}^2 L}{2E}}, \quad (1.19)$$

where L is the distance travelled, $\Delta m_{ij}^2 \equiv m_i^2 - m_j^2$ is the squared mass splitting, and E is the energy of the neutrino. In Eq. (1.19), the neutrinos are taken to be ultra-relativistic. Things are easier to understand if we assume only two family mixing, where the mixing matrix takes the simple form,

$$U = \begin{pmatrix} \cos \theta & \sin \theta \\ -\sin \theta & \cos \theta \end{pmatrix}. \quad (1.20)$$

For such a scenario the probability in Eq. (1.19) is simply written as:

$$P(\nu_\alpha \rightarrow \nu_\beta) \simeq \sin^2(2\theta) \sin^2 \left[1.27 \frac{\Delta m^2 [\text{eV}^2] L [\text{km}]}{E [\text{GeV}]} \right] \quad (\alpha \neq \beta). \quad (1.21)$$

where we have chosen some convenient units. Here Δm^2 is the squared mass splitting. Thus, for neutrino oscillation to happen, the mass-squared differences cannot be zero, i.e., at least two of the three active neutrinos must be massive, which we know from the data from the neutrino oscillations experiments.

While neutrino oscillation experiments are able to determine the squared mass splittings Δm_{21}^2 (+ve) and $|\Delta m_{31}^2|$ with reasonable accuracy (with $|\Delta m_{31}^2| \gg \Delta m_{21}^2$), the sign of Δm_{31}^2 is not known. This gives rise to two possible hierarchies of neutrino masses: normal ($m_1 < m_2 \ll m_3$) and inverted ($m_3 \ll m_1 < m_2$), based on whether the sign of Δm_{31}^2 is +ve or -ve, respectively. From now on, we denote the normal hierarchy as NH, and inverted hierarchy as IH. A recent global analysis of data from neutrino oscillation experiments [13] puts the following bounds on the squared mass splittings (in units of eV^2 , limits are given at 1σ):

$$\begin{aligned}\Delta m_{21}^2 &= 7.39_{-0.20}^{+0.21} \times 10^{-5}, \\ \Delta m_{31}^2 &= 2.525_{-0.032}^{+0.033} \times 10^{-3} \quad (\text{NH}), \\ \Delta m_{32}^2 &= -2.512_{-0.032}^{+0.034} \times 10^{-3} \quad (\text{IH}).\end{aligned}\tag{1.22}$$

Let us denote the mass of the lightest neutrino with m_0 . In case of normal hierarchy, $m_0 = m_1$, whereas for the inverted case, $m_0 = m_3$. Then, the sum of neutrino masses, $\sum m_\nu = m_1 + m_2 + m_3$ in a particular hierarchy will be given by,

$$\sum m_\nu = m_0 + \sqrt{m_0^2 + \Delta m_{21}^2} + \sqrt{m_0^2 + \Delta m_{31}^2} \quad (\text{NH}),\tag{1.23}$$

and

$$\sum m_\nu = m_0 + \sqrt{m_0^2 - \Delta m_{32}^2} + \sqrt{m_0^2 - \Delta m_{32}^2 - \Delta m_{21}^2} \quad (\text{IH}),\tag{1.24}$$

We can determine the minimum mass sum, $\sum m_\nu^{\min}$, required by a particular hierarchy by putting $m_0 = 0$. This leads to $\sum m_\nu^{\min} = 0.05885_{-0.00044}^{0.00045}$ eV (1σ) for NH, and $\sum m_\nu^{\min} = 0.09950_{-0.00067}^{0.00070}$ eV (1σ) for IH. For convenience, we approximate these values to $\sum m_{\nu,\text{NH}}^{\min} = 0.06$ eV and $\sum m_{\nu,\text{IH}}^{\min} = 0.1$ eV from now on. Note that, the neutrino oscillation experiments are not sensitive to the lightest neutrino mass m_0 or $\sum m_\nu$, and thus cannot put an upper bound on $\sum m_\nu$. This is where cosmological data becomes important, which is sensitive to the $\sum m_\nu$. Strongest upper bounds on $\sum m_\nu$ come from cosmological data.

1.4 The Λ CDM model

One of the most successful theories in cosmology is the Λ CDM model the main constituents of the universe are cold dark matter, and a cosmological constant Λ describing dark energy (i.e. $w = -1$), with other constituents of the universe like radiation and ordinary matter are given by the standard model of particle physics (except massive neutrinos), with adiabatic, nearly scale-invariant initial conditions for scalar perturbations to explain the inhomogeneity and anisotropy observed in the universe. Here cold dark matter describes a pressure-less, stable form of matter which interacts with other constituents of the universe only through gravity. In Λ CDM model, the universe is spatially flat, i.e. $\Omega_k = 0$. In this model, it is presently usual to take one massive and two massless neutrinos, with $\sum m_\nu$ fixed to 0.06 eV (the minimum mass required by normal hierarchy).

The Λ CDM model has six free parameters: the physical baryon and CDM den-

sities $\omega_b \equiv \Omega_b h^2$ and $\omega_c \equiv \Omega_c h^2$, The amplitude of the primordial power spectrum of scalar fluctuations, A_s , the tilt of the primordial power spectrum n_s ($n_s = 1$ for complete scale invariance), the angular size of the sound horizon at the time of photon decoupling $\Theta_s = r_s(z_{\text{dec}})/\chi(z_{\text{dec}})$ (with z_{dec} the redshift of decoupling and $\chi(z_{\text{dec}})$ the comoving distance to the CMB last scattering surface), and the optical depth to reionization τ . Looking at Eq (1.11), one can see that only three free parameters control the background evolution: h , ω_b , and ω_c , given the flatness assumption, the neutrino density being fixed, and the background photon energy density is precisely measured from the CMB blackbody temperature. However, since CMB observations directly measure the angle subtended by the sound horizon at decoupling, instead of h , Θ_s is used. On the other hand, A_s and n_s are related to perturbations, as they parametrize the power spectrum of initial scalar fluctuations. Instead of A_s , we usually vary $\ln(10^{10} A_s)$, since A_s takes values of order $\approx 10^{-9}$. Finally, the parameter τ takes care of the ionization history in the late universe, which we shall come back to later.

In this thesis, we are interested inferring neutrino masses from cosmology. Thus we shall consider the sum of neutrino masses $\sum m_\nu$ as a free parameter in Chapters 2 & 3, whereas the effective mass of a sterile neutrino m_s^{eff} will be treated as a free parameter in Chapter 4. Along with that, we shall not restrict ourselves to a Λ CDM cosmology only. We shall consider various extensions to the Λ CDM model, details of which will be provided in the following chapters as and when required.

1.5 Brief thermal history of the universe

At the very early times, all the standard model particles were in thermal equilibrium with each other at a common temperature T , through frequent interactions with each other. Due to universal expansion, however, the universe cooled down. If a particle maintains its equilibrium with the plasma with some particular interaction, and its rate Γ falls below the expansion rate H at that particular time ($\Gamma \ll H$), then the particle can be considered effectively decoupled from the plasma. Also, as long as $T_i \gg m_i$, where m_i is the mass and T_i is the temperature of some particle species, that particular species can be considered relativistic, i.e. its energy density contributes to radiation. Also, at early times (large z), the universe is radiation dominated, since from Eq. (1.11) we can see that the contribution from radiation scales as $(1+z)^4$, whereas the matter contribution scales as $(1+z)^3$, i.e. the contribution from radiation is much larger than matter. To understand how neutrinos affect the cosmological evolution, it would be beneficial to understand the main events in the history of the universe first. Thus, below we describe those main events briefly:

- **Baryogenesis, Electroweak phase transition, QCD phase transition.**

Baryogenesis is a physical process that generated the baryon asymmetry in the universe (i.e. more matter than anti-matter). There are several models of baryogenesis [14–16], but they have not been experimentally verified. Assuming that baryogenesis actually took place, it likely happened before the electroweak phase transition, which occurred at around $T \gtrsim 125 \text{ GeV}$ ($z \approx 10^{15}$,

$t \approx 10^{-11}$ s) when the Higgs field acquired a non-zero vacuum expectation value and broke the electro-weak symmetry [17–23]. Next big event is the QCD phase transition ($T \approx 100$ MeV, $z \approx 10^{12}$, $t \approx 10^{-5}$ s) [24] when quarks confine to form hadrons and mesons.

- **Neutrino decoupling.** At $T \approx 1$ MeV ($z \approx 5 \times 10^9$, $t \approx 1$ s) the rate of weak interactions falls below the Hubble expansion rate at that time [25–28]. Neutrinos decouple from the primordial plasma and start free-streaming.
- **Electron-positron annihilation.** As the temperature of the universe plummets below the electron mass, $T \approx 0.5$ MeV ($z \approx 3 \times 10^9$, $t \approx 6$ s) the annihilation/pair-production process $e^+ + e^- \rightarrow \gamma\gamma$ becomes unfavourable in the reverse direction.
- **Big Bang Nucleosynthesis (BBN).** At a temperature of $T \approx 100$ keV ($z \approx 4 \times 10^8$, $t \approx 3$ min), the synthesis of light elements (mostly ^4He , some ^2H and ^7Li and traces of some other elements) begins [29–32] as nuclear reactions bind nucleons into light nuclei.
- **Matter-radiation equality.** Matter-radiation equality happens at the time when the energy density of matter and radiation become equal. i.e. $\rho_m(z_{\text{eq}}) = \rho_r(z_{\text{eq}})$, where $z_{\text{eq}} = \Omega_m/\Omega_r - 1$ is the redshift of matter-radiation equality. Given the current estimates, $z_{\text{eq}} \approx 3400$ ($T \approx 0.75$ eV, $t \approx 60000$ yrs) [33].
- **Recombination and Photon decoupling.** As the temperature drops further the reaction $e^- + p^+ \rightarrow H + \gamma$ (where H is neutral Hydrogen) becomes

energetically disfavoured in the reverse direction, leading to free electrons getting captured in neutral Hydrogen and Helium atoms. This process is known as “recombination.” Photon decoupling is a separate event but happens nearly at the same time of recombination, because of recombination. Drop in the free electron density due to recombination leads to a drop in the rate of Thomson scattering $e^- + \gamma \rightarrow e^- + \gamma$. Hence the photons start to free-stream, and are usually referred as the Cosmic Microwave Background. These events take place at around $T \approx 0.26$ eV ($z \approx 1090$, $t \approx 380000$ yrs.) [33].

- **Drag epoch.** The very small baryon-to-photon-ratio $\eta_b \sim 10^{-9}$ leads to the baryons being dragged along with photons for some time after photon decoupling. This drag epoch ends when baryons stop feeling the photon drag and are released from the photons. This occurs at a redshift $z_{\text{drag}} \approx 1060$ [33].
- **Reionization.** From the drag epoch until the first stars form, the universe is transparent to the CMB photons. This period is called the “dark ages” [34–36], because there were no sources of photons in the visible frequency range. When the first stars form, the UV radiation emitted by them reionizes neutral Hydrogen present in the universe. As a result the universe again becomes (partially) opaque to radiation since CMB photons get scattered again by free electrons. Given current estimates, the mid-point of reionization redshift is $z_{\text{re}} \approx 7.5$ [33].
- **Matter-dark energy equality.** If we assume dark energy is described by a cosmological constant, matter-dark energy equality happens at a redshift

$z_\Lambda = (\Omega_\Lambda/\Omega_m)^{1/3} - 1 \approx 0.3$ [33]. After this, the universe becomes cosmological constant dominated.

- **Today.** Today, the average temperature of the universe is $T \approx 0.24$ meV, redshift is $z = 0$ by definition. The current energy content as per the Λ CDM model: 68.5% dark energy, for about 26.5% dark matter, around 4.9% by baryons and rest by photons and neutrinos [33].

We would like to mention here that for a particular interaction, equilibrium holds as long as the rate of a given interaction, Γ , is greater than the Hubble rate, H . When the interaction rate falls with universal expansion and $\Gamma \sim H$, the reaction is said to freeze-out. When all the interactions that are keeping a given particle species in thermal equilibrium freeze-out, the particle decouples from the primordial plasma. The evolution of the phase space distribution f of a particle species (baryons, dark matter, dark energy, photons, neutrinos) throughout the expansion history of the Universe is governed by the Boltzmann equation:

$$\mathcal{L}[f] = \mathcal{C}[f], \tag{1.25}$$

where the Liouville operator \mathcal{L} is a total derivative with respect to time and \mathcal{C} is the collision operator. For each particle species the Boltzmann equations result in a set of coupled differential equations for the evolution of perturbations. See [37–41] for details regarding Boltzmann equations and cosmological perturbation theory. Solving the Boltzmann equations is done through numerical codes known as Boltzmann solvers. Two popular Boltzmann solvers are **CAMB** [42] and **CLASS** [43].

1.6 Cosmological history of neutrinos

In the very early universe (with neutrino temperature $T_\nu \gg 1$ MeV), neutrinos were in thermal equilibrium with the primeval plasma, through standard weak interactions with an interaction rate, $\Gamma \sim G_F^2 T_\nu^5$, which was more than the Hubble expansion rate, i.e. $\Gamma \gg H$. Here G_F is the Fermi coupling constant. The frequent weak interactions ensure that the neutrino temperature is same as that of photons (T_γ), i.e. $T_\nu = T_\gamma$. In thermal equilibrium, the background neutrino distribution is given by the Fermi-Dirac distribution function,

$$f_\nu(p, z) = \frac{1}{e^{\frac{p}{T_\nu(z)}} + 1} \quad (1.26)$$

for a particular momentum p , and redshift $z = 1/a - 1$, where a is the scale factor of the universe. And in the very early universe, considering that the temperature of the neutrinos is far greater than their mass, i.e. $T_\nu \gg m_\nu$, we have made the approximation in Eq. (1.24) that the energy of the neutrinos, $E_\nu \simeq p$. Due to the assumption of homogeneity and isotropy of the background universe (i.e. without perturbations), the background distribution doesn't depend on the spatial coordinates or direction of the momentum.

The expansion of the universe leads to a decrease in temperature, and this causes the weak interaction rate to fall. At around $T_{\nu,dec} \sim 1$ MeV, the interaction rate falls below the expansion rate (i.e. $\Gamma < H$), and the neutrinos decouple from the primeval plasma. After decoupling, neutrinos can affect the other components of the universe only through gravitational effects, as far as only the known physics is considered.

Since neutrinos are decoupling when they are relativistic, they keep the shape of their distribution with an effective temperature $T_\nu(a) \propto a^{-1}$ (i.e. $T_\nu(z) \propto (1+z)$). Note that after decoupling neutrinos are no longer in equilibrium, and thus their “temperature” is ill-defined. However, we can still assign an effective “temperature” to neutrinos since lack of any interaction preserves the shape of their Fermi-Dirac distribution.

If we assume instantaneous decoupling of neutrinos at $T_\gamma \sim 1$ MeV, then neutrinos don’t get exposed to the entropy released to the photons during the electron-positron annihilation which takes place shortly after the neutrinos decouple, at around $T_\gamma \sim 0.5$ MeV. The photon temperature, thus decreases at a rate slower than $T_\gamma \propto (1+z)$, whereas T_ν continues to decrease at the rate of $(1+z)$. Using conservation of entropy of the universe, one can show that the electron-positron annihilation leads to a higher photon temperature compared to neutrinos, with the ratio $T_\nu/T_\gamma = (4/11)^{1/3} \simeq 0.714$. Considering the current photon temperature, measured very precisely from the CMB blackbody spectrum, is $T_{\gamma,0} \simeq 2.725$ K, the temperature of the Cosmic Neutrino Background (CνB) should be around the value of $T_{\nu,0} \simeq 1.95$ K. While neutrinos remain relativistic in the early universe, the temperature ratio is useful in determining the neutrino energy density with respect to the photon energy density, $\rho_\gamma(T_\gamma) = (\pi^2/15)T_\gamma^4$. The background energy density of any particle species can be calculated from the following equation,

$$\rho(T) = g \int \frac{d^3p}{(2\pi)^3} f(p, T) E(p), \quad (1.27)$$

where g is the degeneracy, p is the momentum, T is the temperature, E is the energy of a particle with momentum p , and $f(p, T)$ is the distribution function. For photons and each species of neutrinos, $g = 2$. For photons, this is to account for the two spin states whereas for neutrinos, this is to take care of a neutrino and anti-neutrino. For photons, $E(p) = p$, whereas for neutrinos $E(p) \approx p$ when relativistic.

The neutrino energy density is usually parametrized by N_{eff} , which is the effective number of neutrino species, so that the total neutrino energy density is given by, $\rho_\nu(T_\nu) = (7/8)(\pi^2/15)N_{\text{eff}}T_\nu^4$. The $(7/8)$ factor comes because neutrinos are fermions and follow Fermi-Dirac statistics, while photons are bosons and follow Bose-Einstein statistics. It is important to remember that broadly, N_{eff} pertains to any relativistic species which are not photons. Thus, the total radiation density in the early universe is given by,

$$\rho_r = \left[1 + \frac{7}{8} \left(\frac{4}{11} \right)^{4/3} N_{\text{eff}} \right] \rho_\gamma. \quad (1.28)$$

With the assumption of instantaneous decoupling of neutrinos, if we consider neutrinos and photons to be the only relativistic species remaining in the early universe after electron-positron annihilation, then we simply have $N_{\text{eff}} = 3$.

In reality, neither neutrino decoupling, nor electron-positron annihilation are instantaneous processes. Consequently, some neutrinos continue to remain in equilibrium even during the electron-positron annihilation process at around $T \sim 0.5$ MeV, and receive a part of the entropy released. This, and some other known effects like finite temperature QED radiative corrections and flavor oscillations, can be accommodated with a slight increase of the energy density of neutrinos, giving

$N_{\text{eff}} = 3.046$ [26] (or $N_{\text{eff}} = 3.045$ by a newer analysis [27]) instead of a simple $N_{\text{eff}} = 3$. A departure of N_{eff} from this theoretical prediction would be due to non-standard effects or to the contribution of other relativistic species like a sterile neutrino or dark radiation [44].

As the universe expands and cools down further, neutrinos turn non-relativistic roughly when their average momentum becomes similar to their mass, $\langle p \rangle = m_\nu$. The average momentum of a neutrino depends on its temperature [45],

$$\langle p \rangle(z) \approx 3.15 T_\nu(z) = 3.15 \left(\frac{4}{11} \right)^{(1/3)} (1+z) T_{\gamma,0}. \quad (1.29)$$

The redshift for this non-relativistic transition z_{nr} is given by [45]:

$$1 + z_{\text{nr}} \approx 1900 \left(\frac{m_\nu}{\text{eV}} \right). \quad (1.30)$$

The matter radiation equality happens at a redshift of $z_{\text{eq}} \simeq 3400$. Thus, from Eq. (1.30) we can see that neutrinos with masses $m_\nu \lesssim 1.8$ eV become non-relativistic after matter-radiation equality. Recombination happens at a temperature of $T_\gamma \approx 0.3$ eV, which roughly corresponds to the redshift $z_{\text{rec}} \approx 1090$. Consequently, neutrinos with mass $m_\nu \simeq 0.6$ eV or less become non-relativistic after recombination. On the other hand, $z_{\text{nr}} = 0$ (note: $z = 0$ at present, by definition) implies that $m_\nu \approx 1/1900$ eV = 5.3×10^{-4} eV. Any m_ν less than this value corresponds to a neutrino which is relativistic currently. Given the values of the squared mass splittings in Eq. (1.22), at least two of the three active neutrinos are non-relativistic today. The lightest mass eigenstate, however, can be massless

and hence might be relativistic at present. After neutrinos become non-relativistic, their energy density adds to the matter energy density, along with cold dark matter (CDM) and baryons. Due to their small masses, neutrinos are the only known particle species which behave as radiation deep into the matter dominated era, and then turn non-relativistic to behave as matter.

The average number density of a particle species at a temperature T is given by,

$$n(T) = g \int \frac{d^3p}{(2\pi)^3} f(p, T). \quad (1.31)$$

Number density of a neutrinos species, using Eq. (1.31), can be calculated to be,

$$n_\nu(T_\nu) = \frac{6\zeta(3)}{4\pi^2} T_\nu^3. \quad (1.32)$$

Considering all the three species, the number density of cosmic neutrinos comes out to be around $336/\text{cm}^3$. As in case of energy density, it is possible to get a simple ratio of the number densities of photons and one species of neutrinos at the same redshift z (simply from Eq. (1.31)), which is given by,

$$\frac{n_\nu(T_\nu)}{n_\gamma(T_\gamma)} = \frac{3}{4} \left(\frac{T_\nu}{T_\gamma} \right)^3 = \frac{3}{11}, \quad (1.33)$$

which sets the present number density of CMB photons to be $411/\text{cm}^3$.

The energy density of neutrinos, when they turn relativistic, is different from the relativistic case, since it is no longer possible to approximate $E(p) \approx p$ in Eq. (1.27) when neutrinos are non-relativistic. Now we must write $E(p) = \sqrt{p^2 + m_\nu^2}$ and

then evaluate the integral. In the limiting case $m_\nu \gg p$, and we can approximate the energy as $E \approx m_\nu$. As a function of the effective neutrino temperature T_ν the neutrino energy density ρ_ν (for a single species) is given by:

$$\rho_\nu(T_\nu) = \begin{cases} \frac{7\pi^2}{120} T_\nu^4 & (T_\nu \gg m_\nu), \\ m_\nu n_\nu & (T_\nu \ll m_\nu). \end{cases}, \quad (1.34)$$

Since $T_\nu(z) \propto (1+z)$, we have $\rho_\nu(z) \propto (1+z)^4$ in the early universe and $\rho_\nu(z) \propto (1+z)^3$ in the late universe.

After neutrinos decouple from the primeval plasma at $T_{\nu,\text{dec}} \sim 1$ MeV, neutrinos travel at an average speed which is close to the speed of light, i.e. neutrinos free-stream. Later, when they turn non-relativistic, they can still have high thermal velocities (when compared to CDM, baryons). This has a very important impact on cosmological structure formation. Since neutrinos can free-stream out of gravitational potential wells in over-dense regions of the universe due to high thermal velocities, neutrinos hamper structure formation below a length scale, called the neutrino *free-streaming scale*, denoted with λ_{fs} . Let $c_\nu(z)$ denote neutrino speed at a particular redshift z . Then λ_{fs} is roughly the distance travelled by a neutrino over a Hubble time, $t_{\text{H}} \equiv 1/H$.

It is defined as follows [40]:

$$\lambda_{\text{fs}}(z) \equiv (1+z)^{-1} \frac{2\pi}{k_{\text{fs}}(z)} \equiv 2\pi \sqrt{\frac{2}{3}} \frac{c_\nu(z)}{H(z)}. \quad (1.35)$$

Here k_{fs} is the free-streaming wavenumber.

As long as neutrinos are relativistic, $c_\nu(z) \approx 1$, and $\lambda_{\text{fs}}(z) = 2\pi\sqrt{\frac{2}{3}}t_{\text{H}}$. Thus,

$$k_{\text{fs}}(z) = (1+z)^{-1}\sqrt{\frac{3}{2}}H(z) = \sqrt{\frac{3}{2}}aH(z) \quad (1.36)$$

On the other hand, after the non-relativistic transition $c_\nu(z)$ can be written as [40] :

$$c_\nu(z) = \frac{\langle p \rangle(z)}{m_\nu} \approx 3.15 \frac{T_\nu(z)}{m_\nu} \approx 158(1+z) \left(\frac{1 \text{ eV}}{m_\nu} \right) \frac{\text{km}}{\text{s}}. \quad (1.37)$$

Here we have used Eq. (1.29). We can see that $c_\nu(z)$ decreases with $T_\nu(z)$ as $(1+z)$. Using Eq. (1.37) in Eq. (1.35) we can get [40]:

$$\begin{aligned} \lambda_{\text{fs}} &\approx 8.1(1+z) \frac{H_0}{H(z)} \left(\frac{m_\nu}{1 \text{ eV}} \right) \quad h^{-1}\text{Mpc}, \\ k_{\text{fs}} &\approx 0.776(1+z)^{-2} \frac{H(z)}{H_0} \left(\frac{m_\nu}{1 \text{ eV}} \right) \quad h\text{Mpc}^{-1}. \end{aligned} \quad (1.38)$$

To understand the variation of k_{fs} with redshift, we note that during matter domination, $H(z) \approx H_0\sqrt{\Omega_m}(1+z)^{3/2}$. Before the non-relativistic transition but within the matter domination era, $k_{\text{fs}}(z)$ decreases as $(1+z)^{1/2}$, as we can see from Eq. (1.36). After the non-relativistic transition $k_{\text{fs}}(z)$ begins increasing with time as $(1+z)^{-1/2}$. Hence it can be inferred that during the non-relativistic transition, k_{fs} goes through a minimum value, which corresponds to a maximum neutrino free-streaming scale. This minimum is denoted with k_{nr} . It is the wavenumber above which free-streaming effects of neutrinos should be incorporated. We denote the corresponding free-streaming length scale by λ_{nr} , the scale below which neutrino free-

streaming effects are not negligible, and on these scales neutrino density fluctuations are damped leading to suppressed structure formation. k_{nr} is obtained by evaluating k_{fs} [from Eq. (1.38)] at z_{nr} [from Eq. (1.30)]:

$$k_{\text{nr}} \approx 0.0178 \sqrt{\Omega_m} \left(\frac{m_\nu}{1 \text{ eV}} \right)^{\frac{1}{2}} h \text{Mpc}^{-1}. \quad (1.39)$$

Modes with $k < k_{\text{nr}}$ are, on the other hand, not affected by free-streaming. Thus on scales larger than λ_{nr} , neutrinos behave as cold dark matter.

1.7 Neutrino mass effects on cosmology

In the literature there are a lot of excellent articles describing the effects of neutrinos on cosmological observations [44, 46–59]. Below we briefly describe the effects neutrinos impart on the CMB and LSS probes.

1.7.1 Neutrino mass effects on CMB anisotropies

The information in the CMB anisotropies is the power spectrum coefficients C_ℓ^{TT} . These are the coefficients of the expansion in Legendre polynomials (P_ℓ) of the two-point correlation function. In the case of the angular fluctuations in the temperature in direction \hat{n} , $\Delta T(\hat{n})/T$ [45]:

$$\left\langle \frac{\Delta T(\hat{n})}{T} \frac{\Delta T(\hat{n}')}{T} \right\rangle = \sum_{\ell=0}^{\infty} \frac{2\ell+1}{4\pi} C_\ell^{TT} P_\ell(\hat{n} \cdot \hat{n}'). \quad (1.40)$$

Where T is the average temperature. A similar expression holds for the E mode polarization field (sourced by scalar perturbations) and for its cross-correlation with temperature, and also for B mode polarization (which are not produced by scalar fluctuations). Primordial B modes can only be sourced in the presence of tensor modes, i.e., gravitational waves, whereas some E-mode polarization are also converted to B mode through gravitational lensing.

As a consequence of the opposite action of gravity and radiation pressure in the photon-baryon fluid in the early Universe acoustic waves are generated which get “frozen” in the CMB spectrum once photons decouple [60], and thus we see a series of peaks and troughs in the temperature power spectrum. The scale of the oscillations is given by the sound horizon at decoupling $r_s(z_{\text{dec}})$.

After decoupling photon perturbations are affected by time variations in the gravitational potentials. This effect is known as integrated Sachs-Wolfe (ISW) effect. The gravitational potentials don’t change in the completely matter-dominated era. So the ISW effect has two contributions: the early ISW contribution right after recombination, when the radiation component is not negligible, and a late ISW contribution, when the dark energy density begins to dominate [45].

One can classify effect of neutrino masses on the CMB anisotropies in two categories: background effects and perturbation effects. Background effects are related to changes to the background evolution of $H(z)$. CMB anisotropy spectra are sensitive to the following characteristic scales: z_{eq} , $r_s(z_{\text{dec}})$, and $\chi(z_{\text{dec}})$. In fact, the angular position of the first peak is given by $\Theta_s = r_s(z_{\text{dec}})/\chi(z_{\text{dec}})$, and the height of the first peak is very sensitive to the redshift of matter-radiation equality, z_{eq} .

As far as the latest CMB data is concerned, z_{eq} and Θ_s are well constrained, and thus to understand the impact of $\sum m_\nu$ or N_{eff} on the CMB anisotropies, it makes sense to vary other parameters also, so that these characteristic scales remain fixed. This is the approach advocated in [40]. The perturbation effects are related to the impact of neutrinos on metric fluctuations (gravitational potentials). Since current cosmological bounds on neutrino masses from different probes are $m_\nu \ll 1$ eV, we consider neutrinos to be radiation at matter-radiation equality. Thus

$$z_{\text{eq}} = \frac{\omega_b + \omega_c}{\omega_\gamma \left[1 + \frac{7}{8} \left(\frac{4}{11} \right)^{\frac{4}{3}} N_{\text{eff}} \right]} \equiv \frac{\omega_b + \omega_c}{\alpha \omega_\gamma}, \quad (1.41)$$

where $\alpha \equiv [1 + 7/8(4/11)^{4/3} N_{\text{eff}}] \approx (1 + 0.2271 N_{\text{eff}})$. In this section we consider $\Omega_k = 0$, and $\Omega_{\text{DE}} = \Omega_\Lambda$. Then we can rewrite the sum rule in Eq. (1.8) as,

$$\omega_\gamma + \omega_b + \omega_c + \omega_\Lambda + \omega_\nu = h^2. \quad (1.42)$$

Also the background evolution of $H(z)$ in Eq. (1.11) can be rewritten as,

$$H(z) = H_0 \sqrt{(\Omega_b + \Omega_c)(1+z)^3 + \Omega_\gamma(1+z)^4 + \Omega_\Lambda + \frac{\rho_\nu(z)}{\rho_{\text{crit}}}}. \quad (1.43)$$

The effect of increasing $\sum m_\nu$ on the CMB temperature power spectrum while keeping Θ_s and z_{eq} fixed is shown in Fig. 1.1.

Neutrinos with mass $m_\nu \ll 0.6$ eV become non-relativistic long after photon decoupling. If we increase the neutrino mass while keeping ω_b and ω_c fixed, the

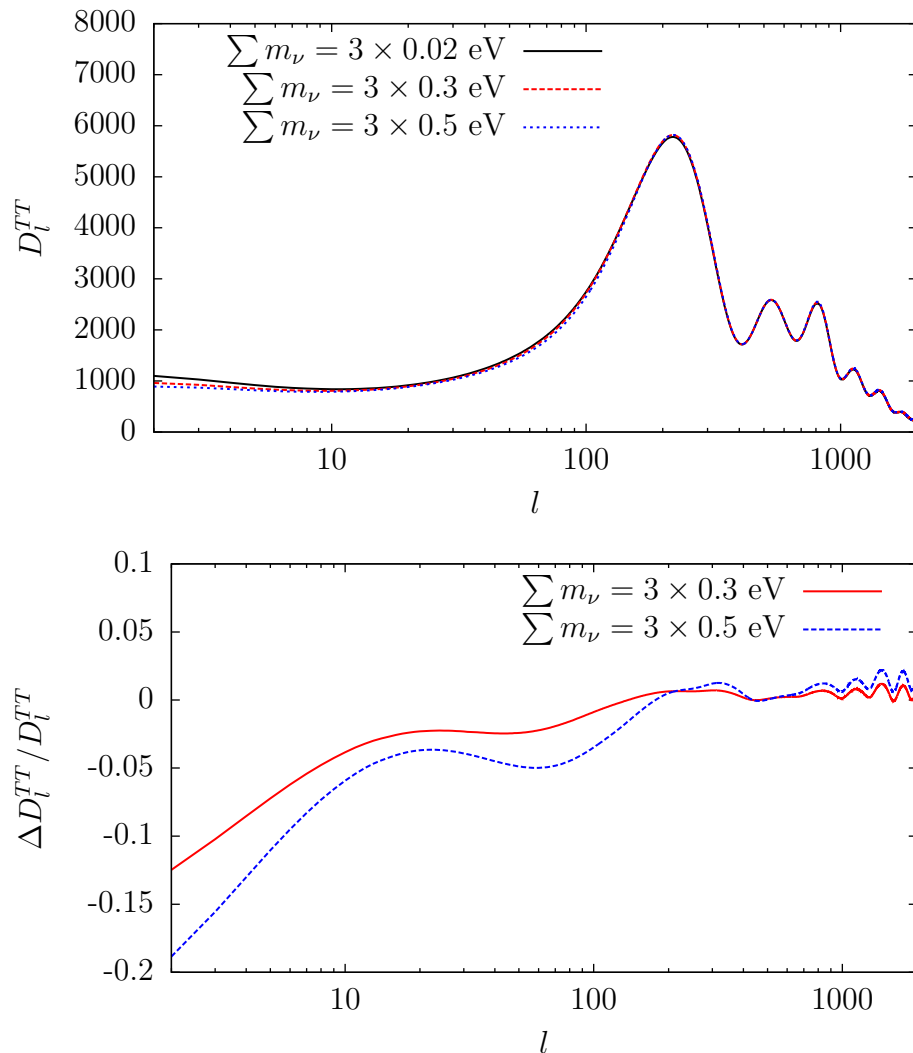


Figure 1.1: Effect of increasing $\sum m_\nu$ on the CMB temperature power spectrum, adjusting h and Ω_Λ to keep Θ_s and z_{eq} fixed. Here $D_l^{TT} \equiv l(l+1)C_l^{TT}/2\pi$ in units of μK^2 . *Upper panel*: the black curve is the power spectrum for the baseline model where $\sum m_\nu = 0.06$ eV, $h = 0.7$, and $\Omega_\Lambda = 0.713$. The red (blue) curve is for $\sum m_\nu = 0.9$ eV ($\sum m_\nu = 1.5$ eV), where the increase in $\sum m_\nu$ is compensated with $h = 0.628$ ($h = 0.586$) and $\Omega_\Lambda = 0.620$ ($\Omega_\Lambda = 0.545$). *Lower panel*: relative change in power compared to the baseline model, with the same color coding as above.

early time evolution remains unchanged (z_{eq} and $r_s(z_{\text{dec}})$ also) and independent of the neutrino mass up to the time of the non-relativistic transition. Moreover presence of baryons introduce an asymmetry between even and odd peaks, and thus varying ω_b can be problematic. Thus neutrino masses $m_\nu \ll 0.6$ eV have small effect on the CMB, but we can still discern some of the effects.

First, the neutrino density increases the total non-relativistic density at late times, $\omega_m = \omega_b + \omega_c + \omega_\nu$, with $\omega_\nu \propto \sum m_\nu$. The late background evolution affects the CMB anisotropy spectrum via changes in the $\chi(z_{\text{dec}})$ which depends on $H(z)$ via Eq. (1.14), and on the redshift of matter-to- Λ equality through late ISW effect. Increasing $\sum m_\nu$ modifies these two quantities. By tuning h and Ω_Λ , it is possible to keep one of them fixed, but not both at the same time. Since the CMB temperature anisotropy spectrum measures Θ_s with great precision, and is only slightly sensitive to the late ISW effect due to cosmic variance, with increase in $\sum m_\nu$ we choose in Fig. 1.1 to decrease the Hubble parameter to maintain a fixed scale $\chi(z_{\text{rec}})$. With such a choice, an increase in neutrino mass comes together with a decrease in ω_Λ , and hence a decrease in the late ISW effect explaining the reduction of the CMB spectrum for $l \leq 20$ in Fig. 1.1. In practice however, this change is difficult to measure due to cosmic variance and CMB anisotropy data alone cannot provide useful information on sub-eV neutrino masses [44]. Since both $\sum m_\nu$ and h enter the expression of $H(z)$ and hence $\chi(z_{\text{rec}})$ means that $\sum m_\nu$ will be strongly correlated with h in CMB data in the $\Lambda\text{CDM} + \sum m_\nu$ model. This is an issue we shall get back to in later chapters. Second, the non-relativistic transition of neutrinos changes the total pressure-to-density ratio of the universe, and leads to a small change in the metric fluctuations.

If this transition happens not long after photon decoupling (i.e. the neutrinos are massive enough), this variation can be seen via the early ISW effect [40, 44, 61]. It is responsible for the dip seen in Fig. 1.1 for $20 \leq l \leq 200$ which is of the order of $\Delta C_l/C_l \sim -(\sum m_\nu/10 \text{ eV})$ in the temperature spectrum. Third, when the neutrino mass is higher, due to a decrease in the matter power spectrum due to neutrino free streaming effects, the CMB photons are exposed to less lensing. Lensing causes smearing in the high- l peaks in the CMB spectra. This reduced lensing effect is the reason of most of the the oscillations visible in Fig. 1.1 for $l \geq 200$. Fourth, the neutrinos having the smallest momenta begin to become non-relativistic before the neutrinos with average momenta. The photon perturbations are affected by this via gravitational coupling with neutrinos. This leads to a small enhancement of C_l^{TT} for $l \geq 500$, not properly visible on Fig. 1.1 because of the lensing effect. Seeing the overall effect of neutrino masses on CMB anisotropies, we see that CMB anisotropy alone cannot be a very powerful probe of sub eV neutrino masses.

1.7.2 Neutrino mass effects on the matter power spectrum

The clustering of matter at large scales is another useful probe of neutrino masses. It can be described by the following two-point correlation function :

$$\langle \delta_m(\vec{k}, z) \delta_m(\vec{k}', z) \rangle = P_m(k, z) \delta^{(3)}(\vec{k} - \vec{k}') , \quad (1.44)$$

where $\delta_m(\vec{k}, z)$ is the Fourier transform of the matter energy density perturbation, and $P_m(k, z)$ is called the power spectrum of matter energy density fluctuations, at

the redshift z .

For matter power spectrum, z_{eq} is an important quantity, as it is the redshift at which $P_m(k)$ turns around, because different growth is experienced by modes which enter the horizon before to matter radiation equality vs after matter-radiation equality. During radiation dominated era, the radiation pressure hampers the growth of matter overdensities, and matter perturbations can only grow logarithmically with the scale factor: $\delta_m \propto \ln a$, whereas, during the matter dominated era, matter perturbations can grow faster: $\delta_m \propto a$ [37–40]. The turn-around happens at a wavenumber $k_{\text{eq}} = \sqrt{2\Omega_m(1+z_{\text{eq}})}$ which corresponds to a mode entering the horizon at z_{eq} [40]. Also, the overall amplitude of $P_m(k)$ depends strongly on Ω_m (we are considering a spatially flat Λ CDM scenario), whereas ω_b and ω_b/ω_c govern the high- k (small scale) part of the spectrum [40]. Increasing ω_b/ω_c causes a suppression in the small scale power spectrum CDM perturbations have a slower growth rate in presence of baryons. Again, the acoustic oscillations in the photon-baryon fluid during recombination gets “frozen” in the baryons also, when baryons are decoupled from photons after the drag epoch, with $r_s(z_{\text{drag}})$ setting the characteristic scale. Imprint of this Baryon Acoustic Oscillations (BAO) are seen on the matter power spectrum in the form of wiggles, whose amplitude and phase depends on ω_b [40]. Measurement of the BAO signal from matter power spectrum is useful for constraining neutrino masses, since the BAO data is helpful in breaking the degeneracy between h and $\sum m_\nu$ present in the CMB data.

Thus any useful comparison of the matter power spectra for different values of $\sum m_\nu$ should be done keeping z_{eq} , Ω_m , ω_b , and ω_b/ω_c fixed. Since z_{eq} is given by

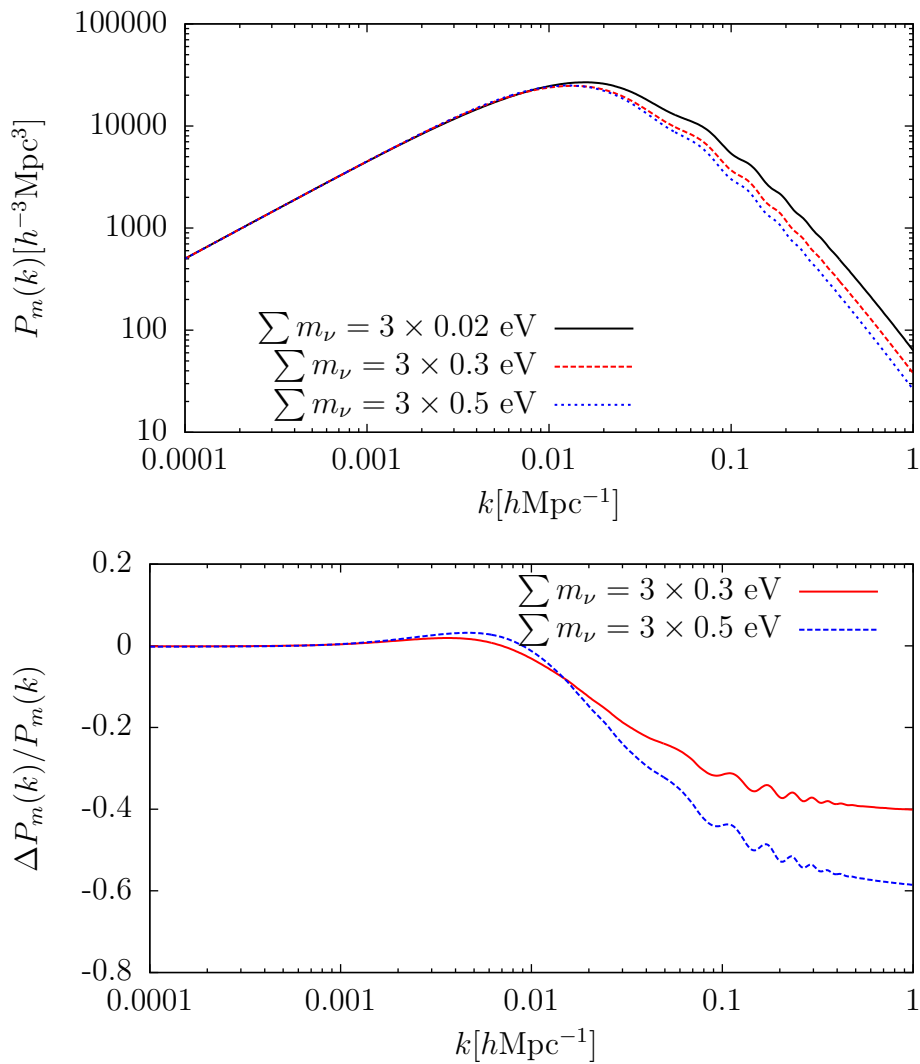


Figure 1.2: Impact of increasing $\sum m_\nu$ on the linear matter power spectrum, z_{eq} and Ω_m fixed. *Upper panel*: the black curve is the power spectrum for the baseline model where $\sum m_\nu = 0.06 \text{ eV}$, $h = 0.7$, and $\Omega_m = 0.287$. The red (blue) curves are obtained for $\sum m_\nu = 0.9 \text{ eV}$ ($\sum m_\nu = 1.5 \text{ eV}$), where the increase in $\sum m_\nu$ is compensated for by setting $h = 0.722$ ($h = 0.738$). *Lower panel*: relative change in power with respect to the baseline model, with the same colour coding as above.

Eq. (1.41), if we keep ω_b and ω_c fixed, both z_{eq} and ω_b/ω_c remain unchanged. Things are slightly complicated for Ω_m , which, at late times, is given by $\Omega_m = \Omega_c + \Omega_b + \Omega_\nu = (\omega_c + \omega_b + \omega_\nu)/h^2$, considering neutrinos have become non-relativistic. Since ω_c and ω_b are already fixed, the only way to keep Ω_m fixed is to increase h as we increase $\sum m_\nu$.

In Fig. 1.2, we show the effect of increasing $\sum m_\nu$ on the matter power spectrum with Ω_m and z_{eq} fixed. The signature of neutrino masses seen as a step-like suppression in $P(k)$ on small scales (large k) due to a combination of two main effects. Firstly, due to their high thermal velocities, below their free-streaming scale neutrinos do not cluster, therefore don't contribute to the matter fluctuations δ_m . Secondly, CDM and baryon perturbations grow slower in the presence of massive neutrinos, since massive neutrinos behave as radiation below their free-streaming scale and thus increase the radiation-to-matter fraction. Above the neutrino free-streaming scale matter perturbation δ_m grows as in a purely matter dominated universe, i.e. $\delta_m \propto a$ (for $k \ll k_{\text{nr}}$). However, below the neutrino free-streaming scale, numerical calculations find that $\delta_m \propto a^{1-3f_\nu/5}$ (for $k \gg k_{\text{nr}}$), where $f_\nu \equiv \Omega_\nu/\Omega_m$ [40]. These two effects together result in a suppression of $\Delta P_m(k)/P_m(k) \approx -8f_\nu$ as long as we can consider the matter perturbations to be linear [40, 62]. Furthermore, numerical simulations incorporating non-linear effects have found the suppression to be around $\Delta P_m(k)/P_m(k) \approx -10f_\nu$ [63–66].

Since neutrinos with different masses become non-relativistic at different times, it is expected that the suppression of matter power spectrum happens in three steps (or two if the lightest eigenstate is massless) as per the k_{nr} of each eigenstate. However,

the imprint of individual masses is found to be too small to be probed by current or near-future surveys [67–69]. Thus in this thesis, we use the $\sum m_\nu$ parameter, since cosmological data is currently found to be sensitive only to the total mass.

1.8 Statistical methods in cosmology

Before we move to analysis of cosmological data and present results on neutrino masses, in this section we provide a brief description of the statistical methods (which are relevant to this thesis) used in cosmological studies to estimate model parameters from the vast amount of cosmological data currently available. See [70–74] for an in-depth overview of application of Bayesian statistics and data analysis in cosmology.

Let A and B be two events which can be assigned probabilities, $p(A)$ and $p(B)$ respectively. Let $p(A|B)$ denote the probability of A being true on the condition that B is true. Let $p(A, B)$ denote the joint probability of A and B .

Then *Bayes' theorem* [75] states that,

$$p(B|A) = \frac{p(A|B)p(B)}{p(A)} \quad (1.45)$$

While A and B correspond to discrete events, we now switch to continuous random variables, with ps now describing probability distribution functions rather than probabilities. In cosmology, we usually have some data from observations \mathbf{d} and a cosmological model \mathcal{M} described by some parameters $\boldsymbol{\theta}$. Then, we can rewrite

Eq. (1.45) for the model \mathcal{M} as,

$$p(\boldsymbol{\theta}|\mathbf{d}) = \frac{p(\mathbf{d}|\boldsymbol{\theta})p(\boldsymbol{\theta})}{p(\mathbf{d})}. \quad (1.46)$$

In the field of cosmological parameter estimation, the quantity on the left hand side, $p(\boldsymbol{\theta}|\mathbf{d})$ in a particular model \mathcal{M} is what we want to calculate, i.e. the probability distribution of the model parameters given the data, often called the *posterior distribution*. On the right hand side of Eq. 1.46 lie three quantities. $p(\mathbf{d}|\boldsymbol{\theta})$ is often called the *likelihood function* which gives the probability distribution function of the observed outcome of an experiment, \mathbf{d} given a particular parameter set $\boldsymbol{\theta}$ of the model \mathcal{M} . $p(\boldsymbol{\theta})$ is known as the *prior distribution* of model parameters which depends on our initial belief about the model parameters (irrespective of the data). The quantity in the denominator is $p(\mathbf{d})$, which is usually known as *evidence*.

Since $p(\boldsymbol{\theta}|\mathbf{d})$ is a probability distribution, we must have

$$\int d\boldsymbol{\theta} p(\boldsymbol{\theta}|\mathbf{d}) = \frac{1}{p(\mathbf{d})} \int d\boldsymbol{\theta} p(\mathbf{d}|\boldsymbol{\theta})p(\boldsymbol{\theta}) = 1 \quad (1.47)$$

which immediately gives us an expression for the *evidence*,

$$p(\mathbf{d}) = \int d\boldsymbol{\theta} p(\mathbf{d}|\boldsymbol{\theta})p(\boldsymbol{\theta}). \quad (1.48)$$

Evidence $p(\mathbf{d})$ doesn't depend on model parameters and is thus useful in comparison between various models for some particular data \mathbf{d} . In this thesis we have not used any *evidence* based model comparison and thus we do not discuss it fur-

ther. However if someone is only interested in parameter inference instead of model comparison, that person will only care about the ratio of the values of the posterior distribution at different values of the model parameters. The overall normalization, *evidence*, is irrelevant in such a scenario. We can then use a simpler form of Bayes' theorem,

$$p(\boldsymbol{\theta}|\mathbf{d}) \propto p(\mathbf{d}|\boldsymbol{\theta})p(\boldsymbol{\theta}). \quad (1.49)$$

It is evident that the posterior distribution depends both on the likelihood and the prior. Here comes one important point. If the data is informative, then the posterior should mostly depend on the likelihood instead of the prior. On the other hand, if the data is not informative, or only weakly informative, then the posterior will largely depend on the prior [71]. This is particularly important in the case of neutrino masses. It is usual to take a $\sum m_\nu \geq 0$ prior since a mass is a positive quantity (to leave out the un-physical negative masses from the analysis). Over and above this prior, it is possible to add other priors on $\sum m_\nu \geq 0$ based on what one believes to be the correct mass model for neutrinos. Currently, cosmological data is not informative enough to detect the neutrino mass sum, and we only get various upper bounds for various dataset and model combinations. For a particular dataset, this upper bound can vary greatly depending on the choice of the prior on $\sum m_\nu$. This issue has gained a lot of attention in recent literature: [76–81].

In a Bayesian analysis, the joint posterior distribution $p(\boldsymbol{\theta}|\mathbf{d})$ of all varying parameters in the model is computed. Let us consider that there are n free parameters

in the model: $(\theta_1, \theta_2, \dots, \theta_n)$. We can then compute the 1D posterior distribution $p(\theta_1|\mathbf{d})$ for a single parameter θ_1 by integrating out other parameters:

$$p(\theta_1|\mathbf{d}) = \int d\theta_2 \dots d\theta_n p(\boldsymbol{\theta}|\mathbf{d}). \quad (1.50)$$

This method of integrating out other parameters is known as *marginalization*. Similarly for the 2D posterior distribution $p(\theta_1, \theta_2|\mathbf{d})$ we integrate out all other parameters except θ_1 and θ_2 , i.e. a straightforward generalization of Eq. 1.50.

We now move to the discussion of credible regions or confidence levels (C.L.). A $f\%$ credible region, denoted by \mathcal{R} encloses a fraction $f/100$ of the posterior probability, considering a normalized posterior distribution (such that $\int d\boldsymbol{\theta} p(\boldsymbol{\theta}|\mathbf{d}) = 1$).

$$\int_{\mathcal{R}} d\boldsymbol{\theta} p(\boldsymbol{\theta}|\mathbf{d}) = f/100. \quad (1.51)$$

Usually credible regions are typically used for $f \approx 68.3$, $f \approx 95.4$, and $f \approx 99.7$, and these are referred to as 1σ , 2σ , and 3σ confidence levels. In the case of a single parameter, confidence regions known as confidence intervals. Another important thing is, the region \mathcal{R} is not unique, and several such regions which are different from each other, can be constructed. One way to chose a credible region is to use the highest posterior density regions, \mathcal{R}^* , such that $p(\boldsymbol{\theta}|\mathbf{d}) \geq p$ for all points in parameter space belonging to \mathcal{R}^* , with $p(\boldsymbol{\theta}|\mathbf{d}) = p$ being the boundary of \mathcal{R}^* .

Now we want to apply Bayesian statistics in cosmology is to perform parameter

estimation. Given some data \mathbf{d} and a model \mathcal{M} with a given parametrization θ with a prior distribution $p(\theta)$, we want to determine the posterior distributions of the parameters. In cosmological analyses, each evaluation of the likelihood involves a call to one Boltzmann solver (e.g. `CAMB` [42] or `CLASS` [82]). Evaluation of the posterior distribution in cosmological studies is usually not very easy, considering it usually involves dealing with $\mathcal{O}(10)$ parameters. For instance the minimal Λ CDM model alone has 6 parameters, and cosmological datasets usually have a number of nuisance parameters to account for calibration, systematics, etc. One needs an efficient way of sampling the posterior distribution and nowadays the predominantly used method is Markov Chain Monte Carlo (MCMC) method [83]. In this thesis, we have exclusively used the popular MCMC sampler `CosmoMC` [84] interfaced with the Boltzmann solver `CAMB` [42] which takes care of the background and perturbation evolution equations.

Results on $\sum m_\nu$ in various cosmological models

This chapter is based on my paper: “Updated Bounds on Sum of Neutrino Masses in Various Cosmological Scenarios” (arXiv: 1806.10832)[85]. In this thesis, we are interested in neutrino mass bounds from cosmology. In this work we start with Λ CDM model and some of its simple extensions with tensor perturbations and dynamical dark energy. Our main goal in the above paper was to understand how strong the upper bound on $\sum m_\nu$ can be with the latest cosmological datasets available at that time, in various cosmologies. We provide bounds on $\sum m_\nu$ in the background of five different cosmological models: (1) Λ CDM + $\sum m_\nu$ (2) Λ CDM + r + $\sum m_\nu$, where r is the tensor to scalar ratio, (3) $w_0 w_a$ CDM + $\sum m_\nu$, where we assume Chevallier-Polarski-Linder (CPL) parametrization for dynamical dark energy instead of a simple cosmological constant, (4) $w_0 w_a$ CDM + $\sum m_\nu$ with $w(z) \geq -1$, i.e., we restrict the $w_0 - w_a$ parameter space to exclude phantom dark energy, and (5) $w_0 w_a$ CDM + r + $\sum m_\nu$ with $w(z) \geq -1$, a model extended with both tensors

and non-phantom dynamic dark energy.

We use combinations of the following datasets: (1) Cosmic Microwave Background (CMB) temperature, polarization and their cross-correlation data from Planck 2015; (2) BAO signal from SDSS-III BOSS DR12, MGS and 6dFGS; (3) the Type Ia supernovae (SNe Ia) luminosity distance measurements from Pantheon Sample; (4) the data released from the BICEP2/Keck Collaboration for the BB mode of the CMB spectrum up to and including 2014; (5) and also local measurements of the Hubble parameter (H_0) from the Hubble Space Telescope; (6) the 2016 measurement of the optical depth to reionization (τ) obtained from the analysis of the data from High Frequency Instrument of the Planck satellite; and (7) the galaxy cluster data from the observation of the Sunyaev-Zel'dovich (SZ) signature from the 2500 square degree South Pole Telescope Sunyaev Zel'dovich (SPT-SZ) survey.

The two low redshift priors (on τ and H_0) are particularly important in constraining $\sum m_\nu$ because of presence of significant degeneracy of these two parameters with $\sum m_\nu$ [86] in the CMB data. We emphasize here that at the time of completion of this work, apart from Planck 2015 and the two redshift priors, the other datasets had not been studied widely in literature for obtaining bounds on $\sum m_\nu$ and we are the first to use combinations of these above mentioned datasets and priors to obtain the very strong bounds presented in this paper, in the above mentioned cosmological models.

As noted in previous chapter, current cosmological measurements are primarily sensitive to the sum of the three masses, $\sum m_\nu$. Same total mass, but different mass splittings should result in slightly different signatures in the cosmological ob-

servables. However current experiments do not have the sensitivity to distinguish these differences with reasonable significance [76]. For this reason, in this work, we present results which are obtained with the approximation of 3 degenerate neutrino masses (from now on DEG), i.e.,

$$m_1 = m_2 = m_3 = \frac{\sum m_\nu}{3} \quad (\text{DEG}). \quad (2.1)$$

This approximation is predominant in literature in analyses where $\sum m_\nu$ is varied. Planck 2015 data combined with others led to a bound of $\sum m_\nu < 0.23$ eV at 95% C.L. (Planck 2015 TT + lowP + lensing + BAO + JLA + H₀) [87]. Depending on the used data and variations in the analysis, different analyses [33, 78, 86, 88–94] obtain 95% C.L. upper bounds from current data approaching the value of 0.1 eV, minimum mass required for IH. These results suggest IH is under pressure from cosmology. However, getting a 95% limit of $\sum m_\nu$ less than the minimum required mass for IH does not rule out IH. Recent papers [76, 78] have suggested a rigorous but simple statistical method of computing the confidence level at which the hypothesis of IH can be rejected against NH using results from both cosmological and oscillations data. These recent analyses indicate that cosmology does slightly prefer NH compared to IH, but no statistically significant conclusion can be reached yet. In this work, we, however, do not perform this statistical analysis and concentrate only on obtaining bounds on $\sum m_\nu$.

This chapter is structured as follows: in Section 2.1 we describe our analysis method, the varying parameters of various cosmological models analyzed in this

paper and the priors on the said parameters. We also briefly describe the Chevallier-Polarski-Linder (CPL) parametrization for dynamical dark energy. In Section 2.2, we briefly describe the various datasets we have used in this work. In Section 2.3 we provide the results of the analyses. We summarize Section 2.4.

2.1 Cosmological Models and Analysis Method

As mentioned in the previous section, in this work we have considered 5 different models of cosmology to obtain bounds on the sum of three active neutrino masses. Below we list the vector of parameters to vary in each of these cosmological models.

- For Λ CDM + $\sum m_\nu$ model:

$$\theta \equiv \left[\omega_c, \omega_b, \Theta_s, \tau, n_s, \ln[10^{10} A_s], \sum m_\nu \right]. \quad (2.2)$$

- For Λ CDM + r + $\sum m_\nu$ model:

$$\theta \equiv \left[\omega_c, \omega_b, \Theta_s, \tau, n_s, \ln[10^{10} A_s], \sum m_\nu, r \right]. \quad (2.3)$$

- For both the $w_0 w_a$ CDM + $\sum m_\nu$ models (with or without phantom dark energy) :

$$\theta \equiv \left[\omega_c, \omega_b, \Theta_s, \tau, n_s, \ln[10^{10} A_s], \sum m_\nu, w_0, w_a \right]. \quad (2.4)$$

- For the $w_0 w_a$ CDM + r + $\sum m_\nu$ model (non-phantom dark energy with tensors)

:

$$\theta \equiv \left[\omega_c, \omega_b, \Theta_s, \tau, n_s, \ln[10^{10} A_s], \sum m_\nu, w_0, w_a, r \right]. \quad (2.5)$$

We fix N_{eff} to the theoretical value of 3.046 in all our analyses in this chapter. In $\Lambda\text{CDM} + r + \sum m_\nu$, along with scalar perturbations we also include tensor perturbations and let another parameter r to vary, which is the tensor-to-scalar ratio at the pivot scale of $k_* = 0.05 h Mpc^{-1}$. The choice to study this model is motivated by the results from the publicly available dataset from the measurement of the BB mode spectrum of the CMB from BICEP2/Keck collaboration, namely BK14, which provides an upper bound to $r < 0.07$ at 95% C.L, when combined with Planck 2015 and other datasets [95]; while the bound without BK14 data is much more relaxed at $r < 0.12$ [87]. We expect this data to modify the constraints on the neutrino related parameters.

The motivation to study the dynamical dark energy models stems from the fact that from the quantum field theoretic point of view, a cosmological constant has been a very difficult thing to explain [96]. For the two dynamical dark energy models, we again only concentrate on scalar perturbations, but the background ΛCDM cosmology with the dark energy equation of state (EoS) $w = -1$ is replaced by a varying equation of state with the following parametrization in terms of the redshift z :

$$w(z) = w_0 + w_a \frac{z}{1+z}. \quad (2.6)$$

This parametrization is famously known as the Chevallier-Polarski-Linder (CPL) parametrization [97, 98]. This parametrization uses Taylor expansion of $w(a)$ (only

the first two terms). This parametrization is suitable for describing the past expansion history of the universe, especially at high redshifts [98], but other parametrizations might be needed to describe future evolution [99] since as $z \rightarrow -1$, $w(z)$ diverges.

Notice that $w(z = 0) = w_0$ corresponds to the dark energy EoS today, whereas $w(z \rightarrow \infty) = w_0 + w_a$ refers to the dark energy EoS in the very far past. Between these two times, it is easy to see that $w(z)$ is a monotonic function. Therefore, to explore only the non-phantom dark energy region of the parameter space, i.e., $w(z) \geq -1$, it is sufficient to apply the following hard priors [100]:

$$w_0 \geq -1; \quad w_0 + w_a \geq -1. \quad (2.7)$$

We abbreviate the model, $w_0 w_a \text{CDM} + \sum m_\nu$ ($w(z) \geq -1$) as the NPDDE model, whereas this same model without any such prior on the EoS will be simply called the DDE model. A Universe with a phantom dark energy component ($w(z) \leq -1$) would lead to a Big Rip in most cosmological models, where dark energy density becomes infinite in a finite time, resulting in dissociation of any bound state, i.e., the ‘‘Big Rip’’ [101]. Such a universe is unphysical in a sense and hence we study the NPDDE model separately.

In our work, we conduct a Bayesian analysis to derive constraints on $\sum m_\nu$. For all the parameters listed in Eq. (2.2-2.5), we impose flat priors in our analysis. The prior ranges are listed on the Table 2.1. We obtain the posteriors using the Markov Chain Monte Carlo (MCMC) sampler CosmoMC [84] which uses CAMB

Parameter	Prior
ω_c	[0.001,0.99]
ω_b	[0.005,0.1]
Θ_s	[0.5,10]
τ	[0.01,0.8]
n_s	[0.8,1.2]
$\ln [10^{10} A_s]$	[2,4]
$\sum m_\nu$ (eV)	[0,5]
r	[0,1]
w_0	[-3, -0.33]
w_a	[-2, 2]

Table 2.1: Flat priors on cosmological parameters included in this work. For the NPDDE model, hard priors according to Eq. (2.7) are also implemented so as to exclude the parameter space region corresponding to phantom dark energy.

[42] as the Boltzmann solver and the Gelman and Rubin statistics [102] to quantify the convergence of chains. All our MCMC runs achieved a convergence criterion of $R - 1 < 0.01$, except for the analyses including the SPT-SZ dataset where we had $R - 1 < 0.03$. We use the Halofit model [103, 104] included in CAMB to take care of any non-linear corrections required.

2.2 Datasets

Below, we provide a description of the datasets used in our analyses. We have used different combinations of these datasets.

Cosmic Microwave Background: Planck 2015: Measurements of the CMB temperature, polarization, and temperature-polarization cross-correlation spectra from the publicly available Planck 2015 data release [105] are used. We consider a

combination of the high- l ($30 \leq l \leq 2508$) TT likelihood, as well as the low- l ($2 \leq l \leq 29$) TT likelihood. We call this combination simply as TT. Along with that, we include the Planck polarization data in the low- l ($2 \leq l \leq 29$) likelihood, and refer to this as lowP. We also consider the high- l ($30 \leq l \leq 1996$) EE and TE likelihood. This dataset and TT together are referred to as TTTEEE. The Planck 2015 high- l polarization data might have remained contaminated with residual systematics [106], so bounds obtained without the use of high- l polarization likelihoods can be considered slightly more reliable.

Baryon Acoustic Oscillations (BAO) Measurements and Related Galaxy

Cluster data: In this work, we include BAO measurements obtained from various galaxy surveys. We make use of the SDSS-III BOSS DR12 Consensus sample (as described in [107]; uses galaxy samples at $z_{\text{eff}} = 0.38, 0.51$ and 0.61), the DR7 MGS at $z_{\text{eff}} = 0.15$ [108], and 6dFGS survey at $z_{\text{eff}} = 0.106$ [109]. We refer to this combination as BAO. Here z_{eff} is the effective redshift of the particular survey. In some cases, we have also used the full shape measurements of the correlation function and galaxy power spectrum (refer to [107] for details) from the SDSS-III BOSS DR12. We denote this as FS. The full shape of these measurements reveal additional information other than the BAO signal.

Type Ia Supernovae (SNe Ia) Luminosity Distance Measurements: We also include measurements of the luminosity distance from Type-Ia Supernovae (SNe Ia) from the Pantheon Sample [110] which has data from 279 Pan-STARRS1 (PS1) Medium Deep Survey SNe Ia ($0.03 < z < 0.68$) and combines it with distance estimates of SNe Ia from SDSS, SNLS, various low- z and HST samples. This combined

sample of SNe Ia is largest till date and consists of data from a total of 1048 SNe Ia with $0.01 < z < 2.3$. We denote this dataset as PAN hereafter. This dataset replaces the Joint Light-curve Analysis (JLA) SNe Ia sample which consists of 740 spectroscopically confirmed type Ia supernovae [111].

Galaxy Cluster Data from South Pole Telescope: In this work, we use data from the SPT-SZ survey [61] which provides data from a sample of 377 clusters (identified at $z > 0.25$). SPT-SZ is a survey of 2500 deg² of the southern sky conducted with the South Pole Telescope (SPT, [112]). These galaxy clusters are recognized by their Sunyaev-Zel’dovich (SZ) effect [113] signature. We call this dataset as SZ from now on.

Optical Depth to Reionization: The optical depth is proportional to the electron number density integrated along the line of sight, and thus most of the contribution to it comes from the time when the universe re-ionizes. We impose a Gaussian prior of $\tau = 0.055 \pm 0.009$, taken from [114], in which Planck collaboration has identified, modeled and removed previously unexplained systematic effects in the polarization data of the Planck High Frequency Instrument (HFI) on large angular scales (low- l) (the data was not made publicly available). It was the most recent and reliable measurement of τ from Planck data available at the time of inception of this work. Also, this prior is very close to the $\tau = 0.0544^{+0.0070}_{-0.0081}$ (68%) bound reported by Planck 2018 collaboration [33]. As we shall see, use of this prior ($\tau = 0.055 \pm 0.009$) ensures that the results on $\sum m_\nu$ presented in this chapter are very close to the results that can be obtained with Planck 2018 likelihoods, since the improvement in measurement of τ is one of the key changes from Planck 2015 to Planck 2018 [33].

We shall hereafter refer to this prior as $\tau 0p055$. We use $\tau 0p055$ as a substitute for low- l polarization data, and hence we exclude the lowP data whenever we apply the $\tau 0p055$ prior, to avoid any double counting.

Hubble Parameter Measurements: We used a Gaussian prior of 73.24 ± 1.74 km/sec/Mpc (68%) on H_0 measured by [115]. We shall refer to this prior as R16. It is to be noted that different datasets prefer different values of H_0 and there is no clear consensus. For instance, strong lensing observations [116] of the H0LiCOW program gave a slightly lower value of $H_0 = 71.9^{+2.4}_{-3.0}$ km/sec/Mpc, whereas another measurement [117] prefers a much lower value of $H_0 = 68.3^{+2.7}_{-2.6}$ km/sec/Mpc. The recent SDSS DR12 BAO data prefers an even lower value of 67.6 ± 0.5 km/sec/Mpc [107]. We chose the R16 value as it is in 3.4σ tension with Planck 2016 intermediate results [114], whose measured value of H_0 is 66.93 ± 0.62 km/sec/Mpc assuming Λ CDM with 3 active neutrinos of total mass fixed at $\sum m_\nu = 0.06$ eV. Using the R16 prior we get an idea of how the parameter bounds will change if cosmology has to accommodate such a large value of Hubble constant. However the large tension between Planck 2015 and R16 leads to a considerably worse fit to the data when the R16 prior is included and thus makes the bounds on $\sum m_\nu$ much less reliable. The situation has become even worse recently (after the work in presented this thesis was completed) with the current best local measurement of H_0 being 74.03 ± 1.42 km/sec/Mpc (68%) [118], with a 4.4σ with Planck 2018 in the Λ CDM model.

B Mode Polarization data of CMB: For the BB mode spectrum of CMB, we use the dataset available from BICEP2/Keck collaboration which includes all data (spanning the range: $20 < l < 330$) taken up to and including 2014 [95]. This

dataset is referred to as BK14.

2.3 Results on $\sum m_\nu$

For clarity, we have presented and explained the results on the sum of three active neutrino masses separately for each model (see Section 2.1 for a description of models) in different subsections. All the quoted upper bounds are at 95% C.L. The main results are summarized in Tables 2.2 – 2.9. Details about models and datasets are given in Section 2.1 and Section 2.2 respectively.

2.3.1 Results for the Λ CDM + $\sum m_\nu$ Model

In this subsection, we present the 2σ (95% C.L.) upper bounds on $\sum m_\nu$ for the Λ CDM + $\sum m_\nu$ model for various combinations of datasets. Upper bounds on $\sum m_\nu$ are given at 2σ (95% C.L.) while marginalized limits for any other parameter mentioned in the text are given at 1σ (68% C.L.). We have divided these results in two separate sections for convenience of analyzing and presenting. First we present results obtained without using any priors on the optical depth to reionization (τ) and Hubble constant (H_0) and discuss the effects of different datasets on the bounds. Next we summarize the results obtained using the said priors.

Results without τ and H_0 priors

In Tables 2.2 and 2.3 we present the bounds without applying any Gaussian prior to the low redshift parameters τ and H_0 . In Table 2.2 bounds are obtained without the

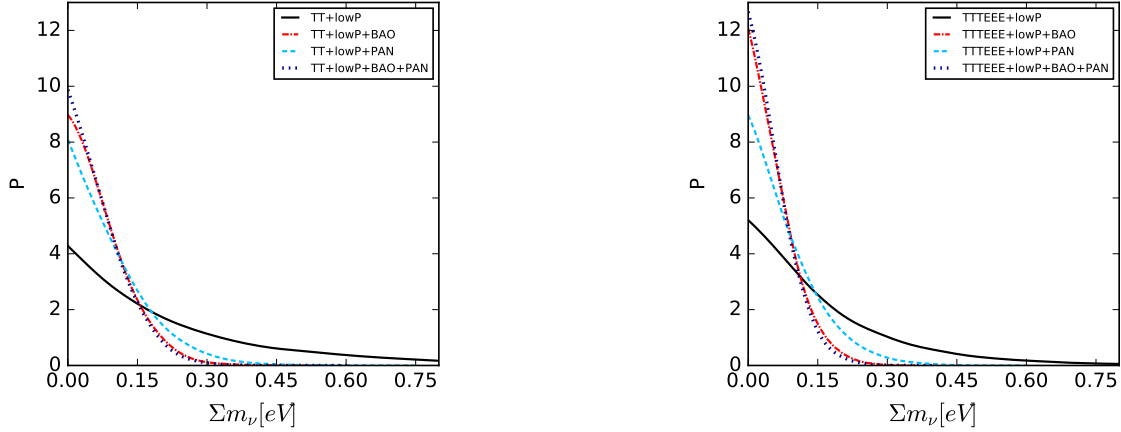


Figure 2.1: Comparison of 1-D marginalized posterior distributions for $\sum m_\nu$ for various data combinations in Λ CDM + $\sum m_\nu$, without τ and H_0 priors. The plots are normalized in the sense that area under the curve is same for all curves.

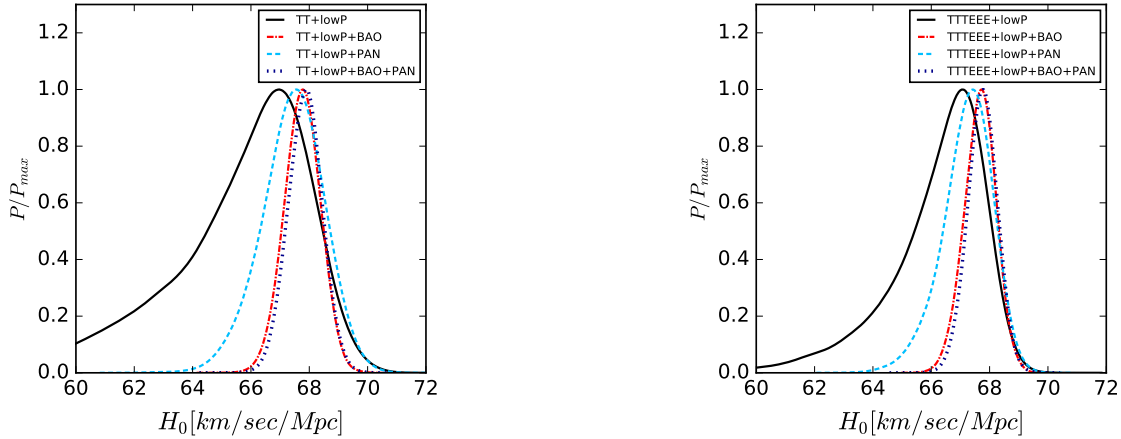


Figure 2.2: Comparison of 1-D marginalized posterior distributions for H_0 for various data combinations in Λ CDM + $\sum m_\nu$, without τ and H_0 priors.

Model: Λ CDM + $\sum m_\nu$	
Dataset	$\sum m_\nu$ (95% C.L.)
TT	< 1.064 eV
TT + lowP	<0.724 eV
TT + BAO	<0.311 eV
TT + lowP + BAO	<0.200 eV
TT + PAN	<0.383 eV
TT + lowP + PAN	<0.260 eV
TT + BAO + PAN	<0.299 eV
TT + lowP + BAO + PAN	<0.190 eV

Table 2.2: Upper bounds at 95% C.L. on $\sum m_\nu$ (degenerate case), in Λ CDM+ $\sum m_\nu$ model for the given datasets. Details about models and datasets are given in Section 2.1 and Section 2.2 respectively.

Model: Λ CDM + $\sum m_\nu$	
Dataset	$\sum m_\nu$ (95% C.L.)
TTTEEE	<0.833 eV
TTTEEE + lowP	<0.508 eV
TTTEEE + BAO	<0.204 eV
TTTEEE + lowP + BAO	<0.158 eV
TTTEEE + PAN	<0.306 eV
TTTEEE + lowP + PAN	<0.230 eV
TTTEEE + BAO + PAN	<0.196 eV
TTTEEE + lowP + BAO + PAN	<0.145 eV

Table 2.3: Upper bounds at 95% C.L. on $\sum m_\nu$ (degenerate case), in Λ CDM+ $\sum m_\nu$ model for the given datasets. This is same as Table 2.2 but including the high- l polarization data of Planck 2015. Details about models and datasets are given in Sections 2.1 and 2.2 respectively.

use of the high- l polarization data from Planck 2015, while in Table 2.3 it is included. Figure 2.1 and 2.2 shows 1-D marginalized posterior distributions for $\sum m_\nu$ and H_0 respectively, for various data combinations. As mentioned in Chapter 1, CMB TT data alone is not particularly sensitive to masses much lower than 1 eV. This is clearly reflected in the results. The TT data alone can only constrain $\sum m_\nu < 1.064$ eV at 95% C.L. Addition of the high- l E mode polarization auto-correlation and temperature-polarization cross-correlation data leads to a higher constraining capability, reducing the bound to $\sum m_\nu < 0.833$ eV. This phenomenon of mass bounds getting stronger with addition of high- l polarization data is seen throughout all the analyses we have done, and corroborates well with previous studies [78, 87].

Addition of the lowP data makes the bounds significantly stronger, i.e., $\sum m_\nu < 0.724$ eV for TT+lowP and $\sum m_\nu < 0.508$ eV for TTTEEE+lowP. This can be attributed to lowP data being able to partially do away with degeneracies present with $\sum m_\nu$ and other parameters like τ and A_s . If we consider TT data only, an increase in $\sum m_\nu$ reduces the smearing of the damping tail [119, 120], which can be compensated by an increase in τ . The value of A_s also needs to increase, as the Planck TT data severely constrains the quantity $A_s e^{-2\tau}$, which leads to a degeneracy between these two parameters; variations approximately following the relation $\delta A_s / A_s \sim 2 \delta \tau$. Effects of A_s and $\sum m_\nu$ are also not independent in cosmology. The value of A_s determines the overall amplitude of matter power spectrum. Increase in A_s increases the amplitude, whereas an increase $\sum m_\nu$ suppresses matter power spectrum in small scales. The low- l polarization data can in principle break this degeneracy between A_s and τ , and consequently the three-way degeneracy between

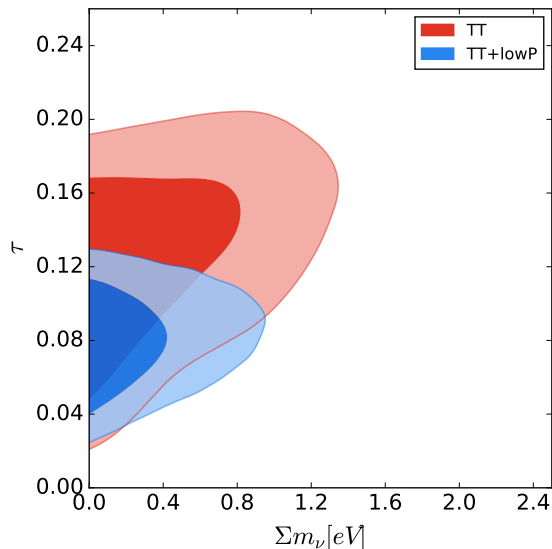


Figure 2.3: 1σ and 2σ marginalised contours for τ vs. $\sum m_\nu$ for TT and TT+lowP datasets in the Λ CDM + $\sum m_\nu$ model, showing the reduction in correlation between τ and $\sum m_\nu$ due to addition of lowP data, leading to a stronger bound on $\sum m_\nu$.

A_s , τ and $\sum m_\nu$. This is possible through the appearance of the well known “reionization bump” in the $l < 20$ range in the polarization spectra whose amplitude is $\propto \tau^2$ in the EE spectra and $\propto \tau$ in the TE spectra [121], and the bump cannot be reproduced by varying other parameters, thus breaking the degeneracy. Indeed, while the TT data alone prefers a $\tau = 0.127^{+0.037}_{-0.033}$, the TT+lowP data prefers a much lower $\tau = 0.080 \pm 0.019$; a smaller value of τ leading to a stronger upper bound of $\sum m_\nu$. Refer to Figure 2.3 for a visualization of this effect. Similar inference can be made for TTTEEE and TTTEEE+lowP. However this degeneracy breaking is only partial. A very precise measurement of low- l polarization is needed to completely break the degeneracy.

While $\sum m_\nu$ and τ are strongly correlated in the Planck TT, $\sum m_\nu$ and H_0 are

strongly anti-correlated. As in Chapter 1, defining $\omega_i \equiv \Omega_i h^2$ (where $i \equiv \gamma, c, b, \Lambda$ with $\gamma \equiv$ photons, $c \equiv$ CDM, $b \equiv$ baryons, and $\Lambda \equiv$ cosmological constant) the comoving distance to the last scattering surface at redshift z_{dec} in a flat Λ CDM + $\sum m_\nu$ universe is given by,

$$\chi(z_{dec}) = \int_0^{z_{dec}} \frac{dz}{H(z)} \propto \int_0^{z_{dec}} \frac{dz}{\sqrt{\omega_\gamma(1+z)^4 + (\omega_c + \omega_b)(1+z)^3 + \omega_\Lambda + \frac{\rho_\nu(z)h^2}{\rho_{cr,0}}}}, \quad (2.8)$$

where $\rho_\nu(z)$ is the neutrino energy density at a redshift z , and $\rho_{cr,0} = 3H_0^2/8\pi G$ is the critical density today as defined in Eq. 1.6. $\rho_\nu(z)$ scales differently with redshift, depending on whether neutrinos can be considered as radiation or matter. At late times, when neutrinos become non-relativistic, $\rho_\nu(z)$ scales as matter (i.e. $\rho_\nu(z) \propto (1+z)^3$) and depends on $\sum m_\nu$. Since in a flat universe, $\Omega_\Lambda = 1 - (\Omega_c + \Omega_b) - \Omega_\gamma - \Omega_\nu$, at late times, the last two terms within the square root in the denominator in Eq. 2.8 give:

$$\omega_\Lambda + \frac{\rho_\nu(z)h^2}{\rho_{cr,0}} = (1 - \Omega_\gamma)h^2 - (\omega_c + \omega_b) + \omega_\nu((1+z)^3 - 1). \quad (2.9)$$

Now, $(\omega_c + \omega_b)$ is well constrained by CMB acoustic peaks. Since $\omega_\nu \propto \sum m_\nu$, any change to $\chi(z_{dec})$ due to increase in $\sum m_\nu$ can be compensated by decreasing h , i.e., H_0 , and hence the anti-correlation. This corroborates with what we have already discussed in Section 1.7.

Addition of the BAO data improves the mass bounds significantly by partially breaking the degeneracy between $\sum m_\nu$ and H_0 . We find that addition of the BAO data to TT + lowP reduces the bound to $\sum m_\nu < 0.200$ eV from $\sum m_\nu < 0.724$ eV.

For the TTTEEE+lowP+BAO case, we get $\sum m_\nu < 0.158$ eV, which is also much stronger than the bound without BAO data. One can understand such important changes in bounds by understanding the impact of neutrino masses on the quantity $D_\nu(z_{\text{eff}})/r_s(z_{\text{drag}})$ which is measured by BAO using spatial correlation of galaxies. Here $r_s(z_{\text{drag}})$ is the comoving sound horizon at the end of the baryon drag epoch (the epoch at which baryons decouple from photons, slightly after recombination) and changes in $\sum m_\nu$ has a small effect on it. On the other hand, the dilation scale $D_\nu(z_{\text{eff}})$ at the effective redshift z_{eff} of the survey, is a combination of the angular diameter distance $D_A(z)$ and the Hubble parameter $H(z)$,

$$D_\nu(z) = \left[(1+z)^2 D_A^2(z) \frac{cz}{H(z)} \right]^{1/3} \quad (c \equiv \text{speed of light}), \quad (2.10)$$

and it is the quantity which is affected by $\sum m_\nu$ most. If $\sum m_\nu$ is increased while $\omega_c + \omega_b$ is kept fixed, the expansion rate at early times increases. This requires Ω_Λ to decrease to keep Θ_s fixed, which is very well constrained by the CMB power spectra. Decrease in Ω_Λ leads to a increase in $D_\nu(z_{\text{eff}})$, which in turn leads to a decrease in both $r_s(z_{\text{drag}})/D_\nu(z_{\text{eff}})$ and H_0 . BAO data prefers a higher value of H_0 than the CMB spectra, and by rejecting the lower H_0 values removes the regions with higher $\sum m_\nu$ values. See [61] for a detailed discussion on this topic. In our analysis we found that TT+lowP data prefers a value of $H_0 = 65.53^{+3.01}_{-1.26}$ km/sec/Mpc, whereas TT+lowP+BAO prefers $H_0 = 67.76 \pm 0.62$ km/sec/Mpc, confirming the above. For TTTEEE+lowP and TTTEEE+lowP+BAO these bounds are $H_0 = 66.17^{+1.96}_{-0.81}$ km/sec/Mpc and $H_0 = 67.67^{+0.54}_{-0.51}$ km/sec/Mpc respectively. This effect of BAO

data rejecting lower H_0 values is evident from Figure 2.2.

As stated before, the Pantheon Sample (PAN) is the newest dataset available on Supernovae type Ia luminosity distance measurements, replacing its predecessor, the Joint Light-curve Analysis (JLA) sample. Observations of SNe Ia at a range of redshifts ($0.01 < z < 2.3$ for the Pantheon Sample) can be used to measure the evolution of luminosity distance as a function of redshift, and thereby determining the evolution of the scale factor [122]. This information can be used to constraint cosmological parameters like dark energy equation of state w , and Ω_m . The PAN dataset also provides substantially stronger mass bound when added to the CMB data, albeit not as strong as BAO data. In particular, TT+lowP+PAN gives a bound of $\sum m_\nu < 0.260$ eV, whereas for TTTEEE+lowP+PAN we get $\sum m_\nu < 0.230$ eV. The 1σ constraints on the Hubble constant are $H_0 = 67.43^{+1.16}_{-0.96}$ and $H_0 = 67.22^{+0.98}_{-0.70}$ km/sec/Mpc respectively. These are higher than that of CMB only data but lower than that of CMB+BAO data, which explains the weaker bounds from the Pantheon Sample compared to BAO. On the other hand, inclusion of both BAO and PAN data with CMB produces bounds slightly stronger than CMB+BAO. The bound with TT+lowP+BAO+PAN is $\sum m_\nu < 0.190$ eV whereas, for TTTEEE+lowP+BAO+PAN, it is $\sum m_\nu < 0.145$ eV, both of which far below the $\sum m_\nu < 0.23$ eV bound quoted in [87]. Figure 2.1 depicts this effect of addition of BAO, PAN and BAO+PAN to the Planck data. Also from Figure 2.2 we see that the CMB+BAO+PAN combination prefers a slightly higher value of H_0 than CMB+BAO. The degeneracy breaking between H_0 and $\sum m_\nu$ due to BAO and PAN can be visualized in Figure 2.4.

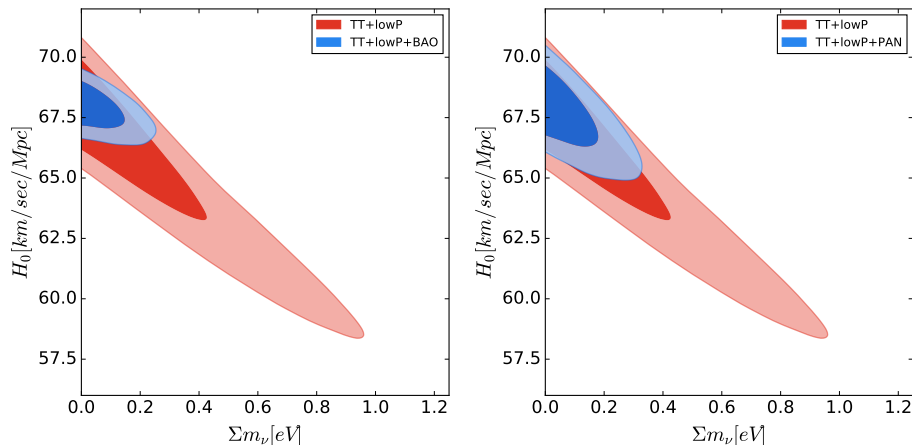


Figure 2.4: 1σ and 2σ marginalised contours for H_0 vs. $\sum m_\nu$ for TT+lowP, TT+lowP+BAO and TT+lowP+PAN datasets in Λ CDM + $\sum m_\nu$ model, showing the degeneracy breaking effect of BAO and PAN datasets separately. Evidently the BAO data is more effective in breaking the degeneracy between the two parameters.

Results with τ and H_0 priors

In the previous section (2.3.1) we described how lower values of τ and higher values of H_0 help in constraining $\sum m_\nu$. Thus precise measurement of these two parameters are instrumental in obtaining meaningful bounds on the sum of neutrino masses. Figures 2.5 and 2.6 shows 1-D marginalized posterior distributions for $\sum m_\nu$ and H_0 respectively, for various data combinations. In Tables 2.4 and 2.5 we have presented the 95% C.L. bounds on $\sum m_\nu$ where we have utilized the τ_{0p055} and R16 priors, along with bounds where we have included the FS and SZ datasets.

The addition of the Gaussian prior $\tau = 0.055 \pm 0.009$ significantly improves the bound by strongly breaking the degeneracy between τ and $\sum m_\nu$, which is depicted in Figure 2.7 Compared to the bound of $\sum m_\nu < 0.311$ eV from TT+BAO, TT+BAO+ τ_{0p055} yields a bound of $\sum m_\nu < 0.159$ eV. This change in mass bound

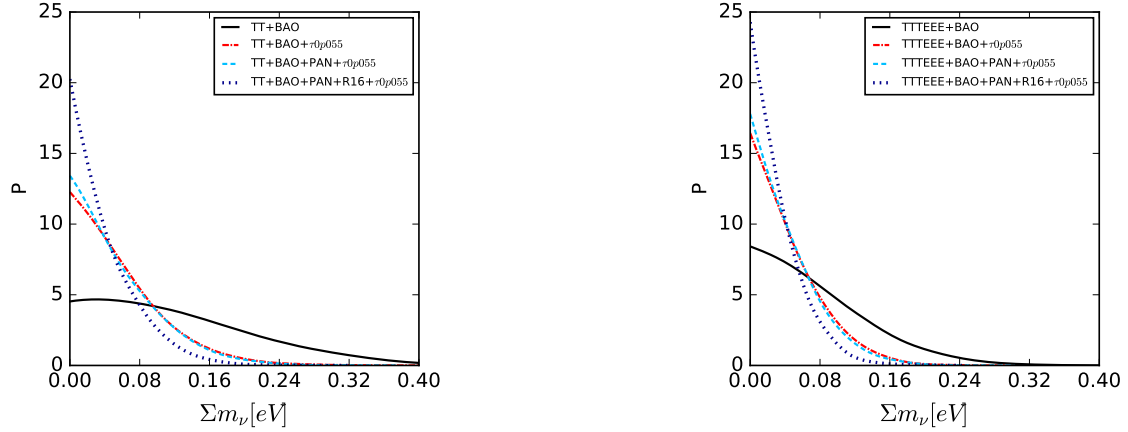


Figure 2.5: Comparison of 1-D marginalized posterior distributions for $\sum m_\nu$ for various data combinations in Λ CDM + $\sum m_\nu$, with τ and H_0 priors. The plots are normalized in the sense that area under the curve is same for all curves.

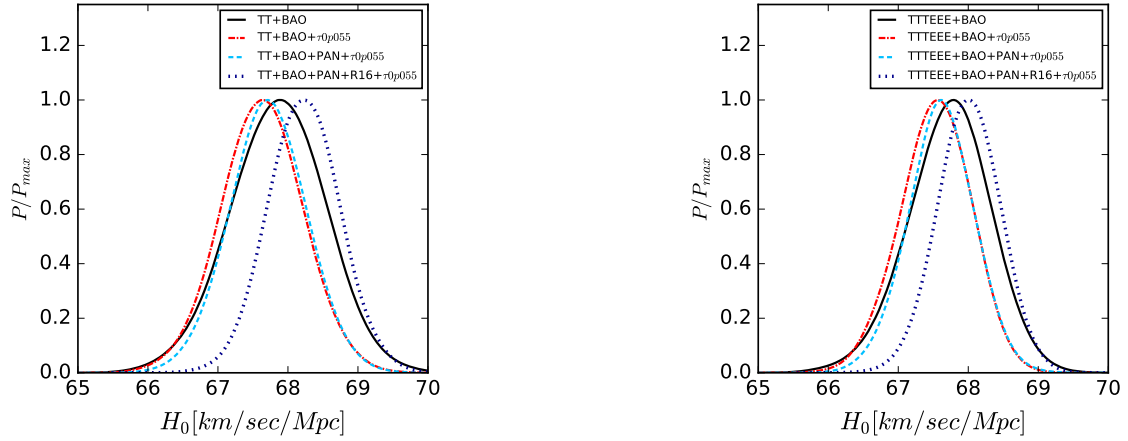


Figure 2.6: Comparison of 1-D marginalized posterior distributions for H_0 for various data combinations in Λ CDM + $\sum m_\nu$, with τ and H_0 priors.

Model: Λ CDM + $\sum m_\nu$	
Dataset	$\sum m_\nu$ (95% C.L.)
TT + BAO + $\tau 0p055$	< 0.159 eV
TT + BAO + FS + $\tau 0p055$	< 0.159 eV
TT + BAO + PAN + $\tau 0p055$	< 0.152 eV
TT + BAO - MGS + PAN + $\tau 0p055$	< 0.141 eV
TT + BAO + FS + PAN + $\tau 0p055$	< 0.160 eV
TT + BAO + SZ + $\tau 0p055$	< 0.175 eV
TT + BAO + PAN + SZ + $\tau 0p055$	< 0.168 eV
TT + lowP + R16	< 0.134 eV
TT + R16 + $\tau 0p055$	< 0.121 eV
TT + BAO + PAN + R16 + $\tau 0p055$	< 0.117 eV
TT + BAO - MGS + PAN + R16 + $\tau 0p055$	< 0.109 eV
TT + BAO + FS + PAN + R16 + $\tau 0p055$	< 0.122 eV

Table 2.4: Upper bounds at 95% C.L. on $\sum m_\nu$ (degenerate case), in Λ CDM + $\sum m_\nu$ model for the given datasets. Details about models and datasets are given in Section 2.1 and Section 2.2 respectively.

Model: Λ CDM + $\sum m_\nu$	
Dataset	$\sum m_\nu$ (95% C.L.)
TTTEEE + BAO + $\tau 0p055$	< 0.124 eV
TTTEEE + BAO + FS + $\tau 0p055$	< 0.133 eV
TTTEEE + BAO + PAN + $\tau 0p055$	< 0.118 eV
TTTEEE + BAO - MGS + PAN + $\tau 0p055$	< 0.113 eV
TTTEEE + BAO + FS + PAN + $\tau 0p055$	< 0.123 eV
TTTEEE + BAO + SZ + $\tau 0p055$	< 0.136 eV
TTTEEE + BAO + PAN + SZ + $\tau 0p055$	< 0.131 eV
TTTEEE + lowP + R16	< 0.125 eV
TTTEEE + BAO + PAN + R16 + $\tau 0p055$	< 0.091 eV
TTTEEE + BAO - MGS + PAN + R16 + $\tau 0p055$	< 0.089 eV
TTTEEE + BAO + FS + PAN + R16 + $\tau 0p055$	< 0.098 eV

Table 2.5: Upper bounds at 95% C.L. on $\sum m_\nu$ (degenerate case), in Λ CDM + $\sum m_\nu$ model for the given datasets. This is same as Table 2.4 but including the high- l polarization data of Planck 2015. Details about models and datasets are given in Section 2.1 and Section 2.2 respectively.

can be attributed to a large change in the preferred value of τ , mostly driven by the prior on τ (and albeit preferring a slightly lower value of H_0 as depicted in Figure 2.6). For TT+BAO we have the 1σ bound of $\tau = 0.123 \pm 0.031$, whereas for TT+BAO+ $\tau 0p055$ we have $\tau = 0.060 \pm 0.009$. Similarly for TTTEEE+BAO, we have $\sum m_\nu < 0.204$ eV and $\tau = 0.105 \pm 0.023$, and it improves to $\sum m_\nu < 0.124$ eV and $\tau = 0.060^{+0.08}_{-0.09}$ for TTTEEE+BAO+ $\tau 0p055$. We emphasize here again that this use of the prior $\tau 0p055$ is well motivated in the sense that, as Planck Collaboration [114] has mentioned in their paper that such a small value of τ also fully agrees with other astrophysical measurements of reionization from high redshift sources. Also Planck 2018 measurements agree with this value of τ [33]. For Λ CDM + $\sum m_\nu$, our tightest bound (except when we remove the MGS data from BAO) without any H_0 prior comes from addition of the PAN data. TTTEEE+BAO+PAN+ $\tau 0p055$ gives a bound of $\sum m_\nu < 0.118$ eV, whereas without the high- l polarization data, we achieved $\sum m_\nu < 0.152$ eV. This is one of our main results in this chapter, and one of the strongest bounds in literature available presently without the use of any H_0 prior. In fact, after the completion of our work, Planck 2018 results [33] reported a bound of $\sum m_\nu < 0.120$ eV (95%; Planck 2018 TT,TE,EE+lowE+lensing+BAO) in this Λ CDM + $\sum m_\nu$ model. Thus we can see that the use of the τ -prior with Planck 2015 data (combined with BAO) actually helped us in getting bounds which we can expect with the use of Planck 2018 and BAO.

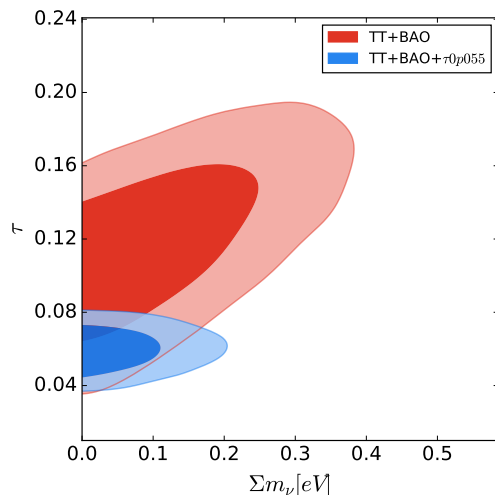


Figure 2.7: 1σ and 2σ marginalized contours for τ vs. $\sum m_\nu$ for TT+BAO and TT+BAO+ $\tau 0p055$ datasets in Λ CDM + $\sum m_\nu$ model, showing the reduction in correlation between τ and $\sum m_\nu$ due to addition of $\tau 0p055$, leading to a stronger bound on $\sum m_\nu$.

$$\sum m_\nu < 0.152 \text{ eV (95\%)} \text{ (TT+BAO + PAN + } \tau 0p055), \quad (2.11a)$$

$$\sum m_\nu < 0.118 \text{ eV (95\%)} \text{ (TTTEEE+BAO + PAN + } \tau 0p055). \quad (2.11b)$$

A prior on H_0 helps to break the degeneracy between $\sum m_\nu$ and H_0 in the Planck data. In Figure 2.8 we demonstrate the same. Addition of the R16 prior ($H_0 = 73.24 \pm 1.74$ km/sec/Mpc) leads to even stronger bounds than BAO data; TT+lowP+R16 yields $\sum m_\nu < 0.134$ eV at 95% C.L., whereas with TTTEEE + lowP + R16 it is $\sum m_\nu < 0.125$ eV. A very aggressive bound of $\sum m_\nu < 0.091$ eV

for $\Lambda\text{CDM} + \sum m_\nu$ is obtained with TTTEEE+BAO+PAN+R16+ $\tau 0p055$, while the bound with TT+BAO+PAN+R16+ $\tau 0p055$ is a bit relaxed at $\sum m_\nu < 0.117$ eV. These might be the most stringent bounds ever reported in literature within the minimal $\Lambda\text{CDM} + \sum m_\nu$ model. However, note that in Table 2.4, TT + R16 + $\tau 0p055$ yields a bound of $\sum m_\nu < 0.121$ eV, which shows us that BAO and PAN do not contribute significantly above the combination of CMB+R16. One can visualize from Figure 2.5 that the R16 data prefers neutrinos with lower mass much more, due to the preference of significantly higher values of H_0 as shown in Figure 2.6 and the strong anti-correlation present between H_0 and $\sum m_\nu$. However, as stated before, we need to be cautious with the interpretation of such tight mass bounds, since they are driven by the large 3.4σ tension between Planck and R16 measurements of the Hubble constant and since there seems to be no agreement among datasets on the value of H_0 .

We notice the bounds can be strengthened further by removal of the DR7 Main Galaxy Sample (MGS) from the BAO data, as can be seen in Tables 2.4 and 2.5. We have denoted the MGS removed dataset simply as BAO – MGS. We find that TT + BAO – MGS + PAN + $\tau 0p055$ prefers an $H_0 = 67.88^{+0.55}_{-0.56}$ km/sec/Mpc which is a bit higher than TT + BAO + PAN + $\tau 0p055$, which prefers $H_0 = 67.71 \pm 0.55$ km/sec/Mpc. The preference of MGS sample for lower H_0 values has been discussed in [108]. The lack of MGS data improves the mass bounds to $\sum m_\nu < 0.141$ eV for TT + BAO – MGS + PAN + $\tau 0p055$, and $\sum m_\nu < 0.113$ eV for TTTEEE + BAO – MGS + PAN + $\tau 0p055$. Adding the R16 prior, we get $\sum m_\nu < 0.109$ eV and $\sum m_\nu < 0.089$ eV respectively.

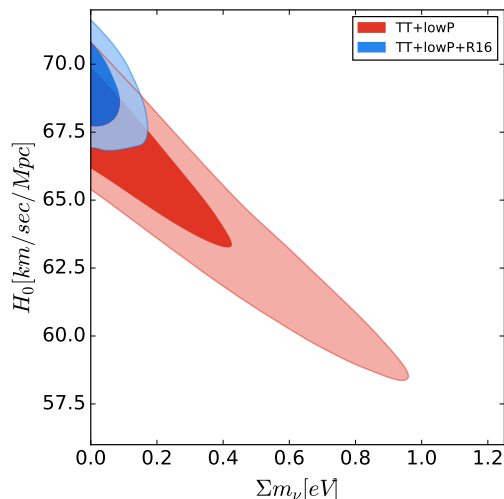


Figure 2.8: 1σ and 2σ marginalized contours for H_0 vs. $\sum m_\nu$ for TT+lowP and TT+lowP+R16 datasets in Λ CDM + $\sum m_\nu$ model, showing the reduction in correlation between H_0 and $\sum m_\nu$ due to addition of the R16 prior, leading to a very strong bound on $\sum m_\nu$.

Inclusion of the galaxy cluster data from full spectrum measurements (FS) from the SDSS-III BOSS DR12 either worsened or did not help the bounds, as can be seen in Tables 2.4 and 2.5. Previous studies [78, 123, 124] have shown that the constraining power of the BAO measurements is higher than that of the full shape measurements in the minimal Λ CDM + $\sum m_\nu$ model, and we find that still to be true for the latest data. Addition of the galaxy cluster data (SZ) from the SPT-SZ survey also worsened the neutrino mass bounds slightly. As shown in Figure 2.9, both FS and SZ data prefer a slightly lower value of σ_8 (the normalization of linear matter power spectrum on scales of $8h^{-1}$ Mpc) and thereby favouring slightly larger values of $\sum m_\nu$; as more suppression of matter power spectrum allows for a larger neutrino mass sum, i.e., σ_8 and $\sum m_\nu$ are strongly anti-correlated.

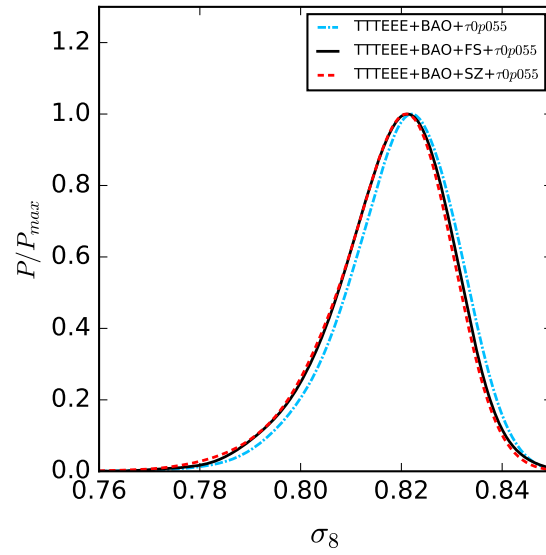


Figure 2.9: Comparison of 1-D marginalized posterior distributions for σ_8 for various data combinations in Λ CDM + $\sum m_\nu$ model. Data combinations with FS and SZ prefer a slightly lower value of σ_8 , due to which slightly less stringent upper bounds on $\sum m_\nu$ are obtained.

Model: Λ CDM + r + $\sum m_\nu$	
Dataset	$\sum m_\nu$ (95% C.L.)
TT + BAO + PAN + $\tau 0p055$	<0.161 eV
TT + BAO + PAN + BK14 + $\tau 0p055$	<0.133 eV
TT + BAO + PAN + BK14 + R16 + $\tau 0p055$	<0.107 eV
TTTEEE + BAO + PAN + $\tau 0p055$	<0.122 eV
TTTEEE + BAO + PAN + BK14 + $\tau 0p055$	<0.110 eV
TTTEEE + BAO + PAN + BK14 + R16 + $\tau 0p055$	<0.085 eV

Table 2.6: Upper bounds at 95% C.L. on $\sum m_\nu$ (degenerate case), Λ CDM + r + $\sum m_\nu$ model for the given datasets. Details about models and datasets are given in Section 2.1 and Section 2.2 respectively.

2.3.2 Results for the Λ CDM + r + $\sum m_\nu$ Model

In this section we present results in the Λ CDM + r + $\sum m_\nu$ model in Table 2.6. For the TT+BAO+PAN+ $\tau 0p055$ dataset, we see that in the Λ CDM + r + $\sum m_\nu$ model $\sum m_\nu < 0.161$ eV, which is a bit relaxed than the $\sum m_\nu < 0.152$ eV in the minimal Λ CDM + $\sum m_\nu$ model. This is simply due to added degeneracies in an extended parameter space with an extra parameter, r , which is the tensor-to-scalar ratio defined at a pivot scale of $k = 0.005$ Mpc⁻¹. The TT+BAO+PAN+ $\tau 0p055$ combination constrains the tensor-to-scalar ratio at $r < 0.13$ (95% C.L.), whereas for TTTEEE+BAO+PAN+ $\tau 0p055$, we have $r < 0.12$ (95% C.L.). Addition of the BK14 data from BICEP2/Keck collaboration, which contains information about the CMB BB spectra, strengthens this bound to $r < 0.07$ for both the data combinations. It also strengthens the sum of neutrino mass bounds to $\sum m_\nu < 0.133$ eV and $\sum m_\nu < 0.110$ eV for TT+BAO+PAN+BK14+ $\tau 0p055$ and TTTEEE + BAO + PAN + BK14 + $\tau 0p055$ respectively, which are actually lower than the ones quoted in Eq. 2.11.

CMB B-mode polarization has two well-known sources [125]. The first part comes from the inflationary gravitational waves (IGW), i.e., tensors, which is supposed to produce a bump peaked around $l \simeq 80$ (the so called ‘recombination bump’) in the BB-mode CMB spectra due to induction of quadrupole anisotropies in the CMB within the last scattering surface. The IGW signature cannot be reproduced by scalar perturbations, and the amplitude of the bump depends on the tensor-to-scalar ratio, r . The other part comes from the deflection of CMB photons due to gravitational lensing produced by large scale structure at considerably late times, which converts a small fraction of the E mode power into B mode. This lensing BB spectra peaks at around $l \simeq 1000$. The ‘reionization bump’ is also expected to be present as in the EE spectra, in the $l < 10$ region. However, the BK14 data contains information only in the $20 < l < 330$ and cannot constrain τ through the reionization bump.

While the bound on r is stronger due to BK14, this does not seem to be the main effect in tightening of the mass bounds. We found that the correlation coefficient (defined as $R_{ij} = C_{ij} / \sqrt{C_{ii}C_{jj}}$, where i and j are the two parameters being considered and C is the covariance matrix of cosmological parameters) between r and $\sum m_\nu$ to be $R_{r,\Sigma m_\nu} = +0.056$ in case of TT+BAO+PAN+ τ 0p055, and $R_{r,\Sigma m_\nu} = +0.051$ in case of TT+BAO+PAN+BK14+ τ 0p055, which implies that the correlation is very small before addition of BK14, and there is also no big enough change in the correlation with the addition of BK14 dataset to account for the change in mass bound. The main effect might be coming from lensing BB spectra. Quantitatively, the correlation coefficient between σ_8 and $\sum m_\nu$ in TT+BAO+PAN+ τ 0p055 is $R_{\sigma_8,\Sigma m_\nu} = -0.828$,

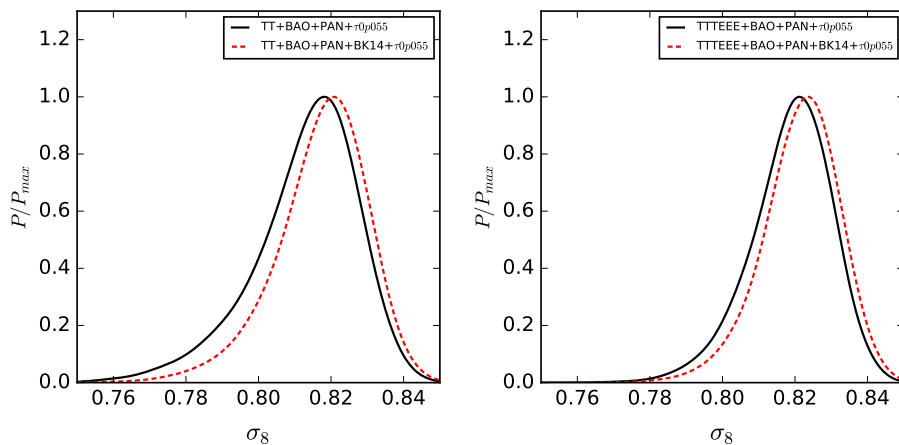


Figure 2.10: Comparison of 1-D marginalized posterior distributions for σ_8 for various data combinations in Λ CDM + r + $\sum m_\nu$ model. Addition of BK14 data seems to prefer a higher σ_8 , due to which slightly more stringent upper bounds on $\sum m_\nu$ are obtained.

and in TT+BAO+PAN+BK14+ $\tau 0p055$ it is $R_{\sigma_8, \sum m_\nu} = -0.780$. We find that BK14 data prefers a slightly larger value of σ_8 (see in Figure 2.10), and due to the strong anti-correlation present between σ_8 and $\sum m_\nu$ in the data, the mass bounds improve a bit. Similar inference can be made for the results including the high- l polarization from Planck. As before, inclusion of the R16 prior improves the bounds even more. For TT+BAO+PAN+BK14+R16+ $\tau 0p055$, we have a bound of $\sum m_\nu < 0.107$ eV and for TTTEEE+BAO+PAN+BK14+R16+ $\tau 0p055$ it is $\sum m_\nu < 0.085$ eV, both of which are tighter than the corresponding bounds in minimal Λ CDM + $\sum m_\nu$ model without the BK14 data.

Model: $w_0w_a\text{CDM} + \sum m_\nu$ (DDE)	
Dataset	$\sum m_\nu$ (95% C.L.)
TT + BAO + PAN + $\tau 0p055$	<0.305 eV
TT + BAO + PAN + R16 + $\tau 0p055$	<0.284 eV
TTTEEE + BAO + PAN + $\tau 0p055$	<0.276 eV
TTTEEE + BAO + PAN + R16 + $\tau 0p055$	<0.247 eV

Table 2.7: Upper bounds at 95% C.L. on $\sum m_\nu$ (degenerate case), in $w_0w_a\text{CDM} + \sum m_\nu$ model (DDE), for the given datasets. Details about models and datasets are given in Section 2.1 and Section 2.2 respectively.

2.3.3 Results for the $w_0w_a\text{CDM} + \sum m_\nu$ Model (DDE)

In this section we present results for the $w_0w_a\text{CDM} + \sum m_\nu$ (DDE) model. The mass bounds are presented in Table 2.7. For the DDE model we let the dark energy parameters vary in both the phantom and non-phantom range. There is a well-known strong degeneracy between the dark energy equation of state, w and sum of neutrino masses, $\sum m_\nu$ [126]. An increase in $\sum m_\nu$ can be compensated by a decrease in w , due to the mutual degeneracy with Ω_m . This degeneracy leads to a large degradation of the mass bounds, as can be seen from Table 2.7 and comparing with the results from the $\Lambda\text{CDM} + \sum m_\nu$ model for the same datasets (see Tables 2.4 and 2.5). Figures 2.11 and 2.12 provide the 1-D marginalized posterior distributions for $\sum m_\nu$ and H_0 respectively. From Figure 2.11 we can clearly observe that for the same dataset, the DDE model allows much larger values of $\sum m_\nu$ than $\Lambda\text{CDM} + \sum m_\nu$. For TT+BAO+PAN+ $\tau 0p055$ we obtain a bound of $\sum m_\nu < 0.305$ eV, whereas for TTTEEE+BAO+PAN+ $\tau 0p055$ the bound is slightly tighter at $\sum m_\nu < 0.276$ eV. The dynamical dark energy model also helps to reduce the tension between Planck 2015 and R16, by allowing higher values of H_0 along with

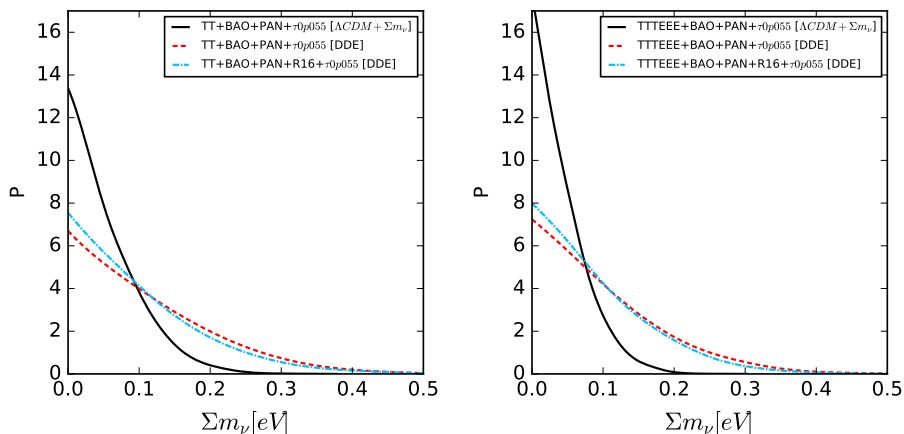


Figure 2.11: Comparison of 1-D marginalised posterior distributions for $\sum m_\nu$ comparing the Λ CDM + $\sum m_\nu$ and DDE models. The plots are normalized in the sense that area under the curve is same for all curves.

a broader distribution. (see Figure 2.12). Imposition of the R16 prior improves the mass bounds. However, the magnitude of this effect is less than what we saw in Λ CDM + $\sum m_\nu$. This is because H_0 and w are also degenerate, i.e., a change in H_0 can be compensated by a change in w instead of $\sum m_\nu$. This decreases the magnitude of correlation coefficient between H_0 and $\sum m_\nu$. This phenomenon of changing correlation across these two models can be looked upon in Figure 2.13. Quantitatively, for TT+BAO+PAN+ $\tau_0 p055$, the correlation coefficient between H_0 and $\sum m_\nu$ changes from $R_{H_0, \sum m_\nu} = -0.40$ in Λ CDM + $\sum m_\nu$ to $R_{H_0, \sum m_\nu} = -0.15$ in $w_0 w_a$ CDM + $\sum m_\nu$. Also, in the DDE model, Planck 2015 and the R16 prior have a much smaller tension than in Λ CDM + $\sum m_\nu$.

The w_0 - w_a diagram in Figure 2.14 shows that for CMB+BAO+PAN+ $\tau_0 p055$ only a very small region which corresponds to completely non-phantom dark energy is allowed. Rest of the allowed region in the parameter space crosses the phantom

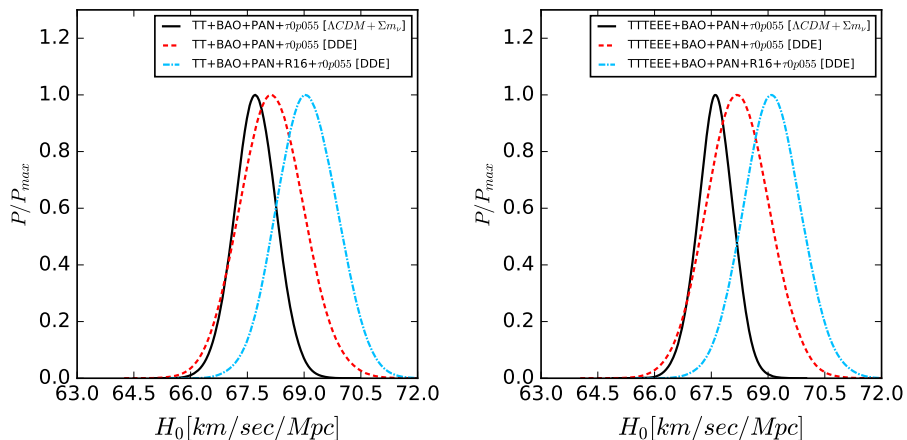


Figure 2.12: Comparison of 1-D marginalised posterior distributions for H_0 comparing the $\Lambda\text{CDM} + \sum m_\nu$ and DDE models. The DDE model prefers a broader distribution for H_0 and also the mean value of H_0 is higher, thereby reducing the tension between Planck 2015 and R16. Adding the R16 prior in the DDE model leads to even larger H_0 values.

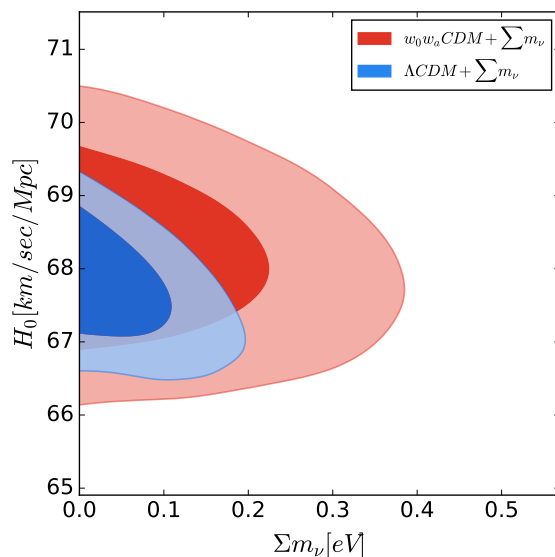


Figure 2.13: 1σ and 2σ marginalised contours in the $\sum m_\nu - H_0$ plane for TT + BAO + PAN + τ_{0p055} , comparing their correlation in the $w_0w_a\text{CDM} + \sum m_\nu$ (DDE) and $\Lambda\text{CDM} + \sum m_\nu$ models.

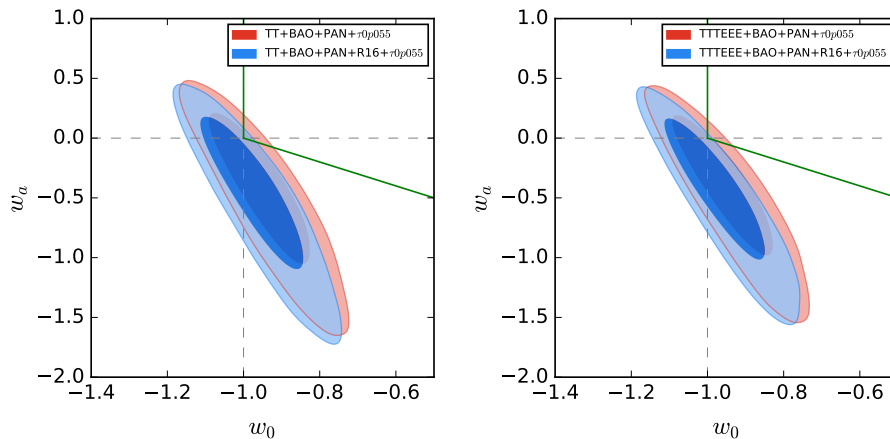


Figure 2.14: 1σ and 2σ marginalized contours for w_0 vs. w_a for TT + BAO + PAN + $\tau 0p055$ and TTTEEE + BAO + PAN + R16 + $\tau 0p055$ datasets in the $w_0 w_a$ CDM + $\sum m_\nu$ (DDE) model. The dashed lines are at $w_0 = -1$ and $w_a = 0$ respectively. The two green lines originating from $(-1, 0)$ separate the non-phantom region from the rest. The region above the slanted green line and at the right of the vertical green line is the non-phantom region.

barrier ($w = -1$ line) at some point in the evolution of the universe. We also find that the datasets are compatible with a cosmological constant ($w_0 = -1$, $w_a = 0$). Imposing the R16 prior leads to shifting of the contours towards the phantom region. Thus, the allowed non-phantom region shrinks even more. A recent study [127] showed that the disfavouring of the non-phantom region even persists in a 12 parameter extended space. Our results are also in agreement with Planck collaboration [87] which reported similar contours for the given combination of similar but older datasets (see Figure 28 in that paper, for the combination of TT+lowP+ext, where 'ext' implies combination of BAO, JLA and a H_0 prior). In the next two sections we present our results on neutrino mass bounds in a cosmology with only non-phantom dynamical dark energy.

Model: $w_0w_a\text{CDM} + \sum m_\nu$ with $w(z) \geq -1$ (NPDDE)	
Dataset	$\sum m_\nu$ (95% C.L.)
TT + BAO + PAN + $\tau 0p055$	<0.129 eV
TT + BAO + PAN + R16 + $\tau 0p055$	<0.106 eV
TTTEEE + BAO + PAN + $\tau 0p055$	<0.101 eV
TTTEEE + BAO + PAN + R16 + $\tau 0p055$	<0.082 eV

Table 2.8: Upper bounds at 95% C.L. on $\sum m_\nu$ (degenerate), in $w_0w_a\text{CDM} + \sum m_\nu$ model with $w(z) \geq -1$ (NPDDE), for the given datasets. Details about models and datasets are given in Section 2.1 and Section 2.2 respectively.

χ^2 -values: Previous studies [128, 129] reported a improvement in fit with DDE models compared to ΛCDM . We found similar improvement in our analysis. We compare the best-fit χ^2 values of the $w_0w_a\text{CDM} + \sum m_\nu$ and $\Lambda\text{CDM} + \sum m_\nu$ models. We define, $\Delta\chi_{\text{DDE}}^2 \equiv \chi_{\text{min}}^2(\text{DDE}) - \chi_{\text{min}}^2(\Lambda\text{CDM} + \sum m_\nu)$, when used for the same dataset. For TT+BAO+PAN+ $\tau 0p055$, we find $\Delta\chi_{\text{DDE}}^2 = -0.40$; for TTTEEE+BAO+PAN+ $\tau 0p055$ it is $\Delta\chi_{\text{DDE}}^2 = -0.34$. The $\Delta\chi^2$ is better with the R16 prior. For TT+BAO+PAN+R16+ $\tau 0p055$, we find $\Delta\chi_{\text{DDE}}^2 = -1.48$, whereas for TTTEEE+BAO+PAN+R16+ $\tau 0p055$ it is $\Delta\chi_{\text{DDE}}^2 = -3.27$.

See also [130–135] for previous studies on massive neutrinos and dynamic dark energy together.

2.3.4 Results for the $w_0w_a\text{CDM} + \sum m_\nu$ Model with $w(z) \geq -1$ (NPDDE)

While the current data prefers the phantom region of the dark energy parameter space, it is also important to look at the non-phantom side of the things, since phantom dark energy is somewhat unphysical [136]. Dark energy models with a single

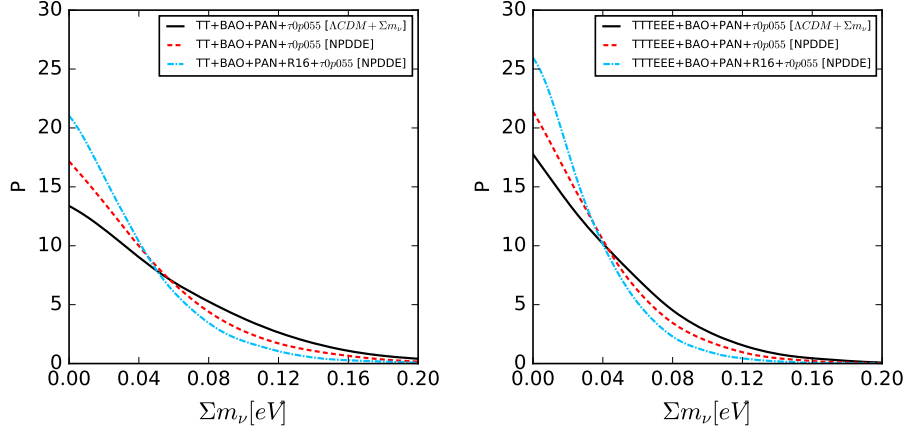


Figure 2.15: Comparison of 1-D marginalized posterior distributions for $\sum m_\nu$ comparing the Λ CDM + $\sum m_\nu$ and NPDDE models. The plots are normalized in the sense that area under the curve is same for all curves.

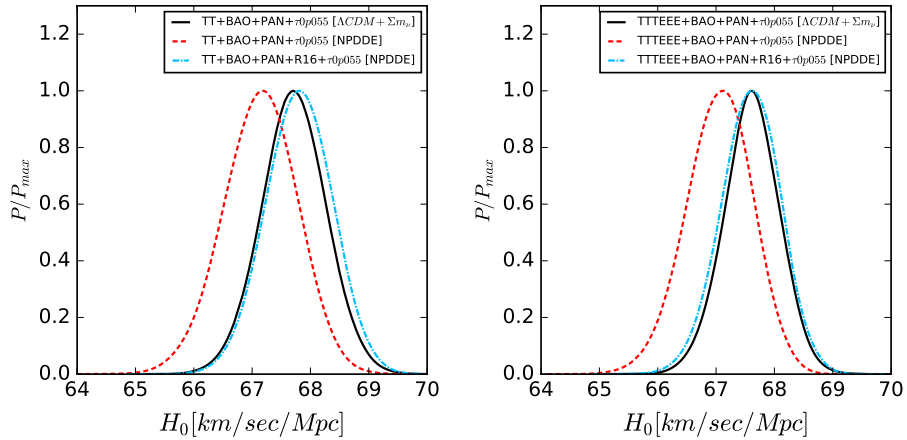


Figure 2.16: Comparison of 1-D marginalized posterior distributions for H_0 comparing the Λ CDM + $\sum m_\nu$ and NPDDE models. The NPDDE model prefers smaller values for H_0 , thereby increasing the tension between Planck 2015 and R16. Adding the R16 prior in the NPDDE model leads to H_0 values which are somewhat similar to Λ CDM + $\sum m_\nu$ without R16.

scalar field cannot cross the phantom barrier ($w = -1$) and more general models that permit the crossing require extra degrees of freedom to provide gravitational stability [137]. Field theories allowing phantom dark energy are fraught with one or more of the following problems like unstable vacuum, Lorentz violation, ghosts, superluminal modes, non-locality, or instability to quantum corrections. There, however, have also been theories where the field theory does not have any such issues but other effects like photon-axion conversion or modified gravity leads to an apparent $w < -1$ (see [138] for a brief review). Nonetheless, there are wide class of theories like quintessence [139, 140] which are non-phantom in nature and it is important to consider situations where we do not allow the phantom crossing.

The constraints on $\sum m_\nu$ are shown in Table 2.8. We find that the restricting ourselves to only the non-phantom sector yields bounds which are even stronger than the minimal Λ CDM + $\sum m_\nu$ model for the same datasets, even though it is an extended parameter space (also previously confirmed in [100]). For TT + BAO + PAN + $\tau 0p055$, we have $\sum m_\nu < 0.129$ eV in the NPDDE model, whereas for Λ CDM + $\sum m_\nu$ model, using the same dataset, we had $\sum m_\nu < 0.152$ eV. For TTTEEE + BAO + PAN + $\tau 0p055$, in NPDDE, we have $\sum m_\nu < 0.101$ eV, compared to $\sum m_\nu < 0.118$ eV for Λ CDM + $\sum m_\nu$. Adding the R16 prior further reduces the allowable mass region, as we have seen throughout this chapter. TT + BAO + R16 + PAN + $\tau 0p055$ prefers a $\sum m_\nu < 0.106$ eV, and TTTEEE + BAO + PAN + R16 + $\tau 0p055$ prefers $\sum m_\nu < 0.082$ eV, which is below the minimum sum required by the inverted hierarchy.

However this substantial strengthening of neutrino mass bound in NPDDE model

compared to DDE model is not surprising when we consider the degeneracy between w and $\sum m_\nu$. As depicted in Figure 2 of [126], due to strong anti-correlation between w and $\sum m_\nu$, higher mass sum values prefer a lower value of w and on the other hand higher values of w for $w \geq -1$ are dominated by very low mass sum values. In NPDDE, what happens is we remove the phantom region, i.e., the portion of the parameter space which likes larger values of neutrino mass sum. Stronger bounds in an NPDDE model compared to Λ CDM + $\sum m_\nu$ is also confirmed in a recent study [100], which also confirmed the phenomenon that as we go away from the $w = -1$ line in the non-phantom region of the parameter space the mass bounds get stronger, whereas in the phantom region going away from the $w = -1$ line leads to weaker bounds, by running MCMC with separate fixed values of w_0 and w_a . A similar effect is seen in the bounds on H_0 . Higher values of H_0 prefer a lower w , and removal of the phantom region of the parameter space leads to a preference towards lower values of H_0 . Consequently, an NPDDE model actually increases the tension between Planck CMB data and R16. The alleviation of tension between Planck and R16 in DDE models comes from the phantom region of the $w_0 - w_a$ plane. One of the consequences of such strong mass bounds is that, if in future neutrino hierarchy is found to be inverted by experiments, a universe with non-phantom dark energy will be less likely than a cosmological constant Λ or phantom dark energy [100]. The 1-D marginalized posteriors for $\sum m_\nu$ and H_0 for the NPDDE model are shown in Figures 2.15 and 2.16 respectively.

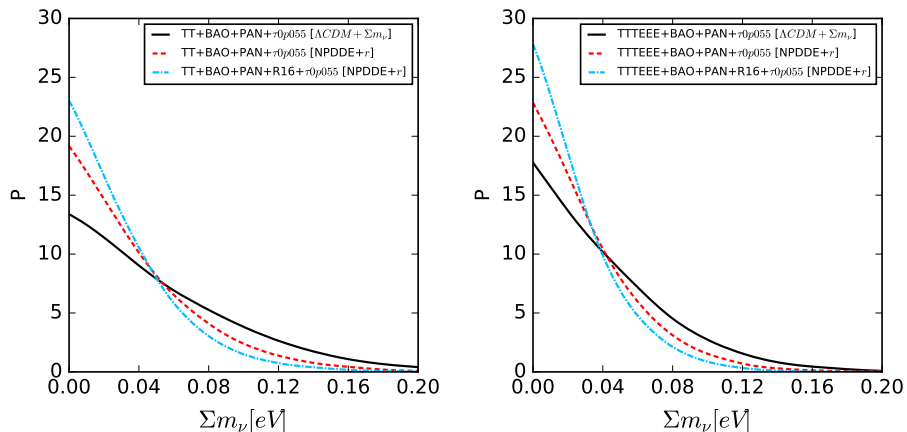


Figure 2.17: Comparison of 1-D marginalized posterior distributions for $\sum m_\nu$ comparing the Λ CDM + $\sum m_\nu$ and NPDDE+r models. The plots are normalized in the sense that area under the curve is same for all curves.

Model: $w_0 w_a$ CDM + r + $\sum m_\nu$ with $w(z) \geq -1$ (NPDDE+r)	
Dataset	$\sum m_\nu$ (95% C.L.)
TT + BAO + PAN + BK14 + $\tau 0p055$	<0.116 eV
TT + BAO + PAN + BK14 + R16 + $\tau 0p055$	<0.095 eV
TTTEEE + BAO + PAN + BK14 + $\tau 0p055$	<0.093 eV
TTTEEE + BAO + PAN + BK14 + R16 + $\tau 0p055$	<0.078 eV

Table 2.9: Upper bounds at 95% C.L. on $\sum m_\nu$ (degenerate), in $w_0 w_a$ CDM + r + $\sum m_\nu$ model with $w(z) \geq -1$ (NPDDE with tensors), for the given datasets. Details about models and datasets are given in Section 2.1 and Section 2.2 respectively.

2.3.5 Results for the $w_0 w_a$ CDM+r+ $\sum m_\nu$ Model with $w(z) \geq -1$ (NPDDE+r)

In this section we report results for the $w_0 w_a$ CDM+r+ $\sum m_\nu$ model with $w(z) \geq -1$. We denote this model as "NPDDE+r". The main motivation behind studying this model was to see if we can further strengthen the mass bounds by adding the tensor-to-scalar ratio as a free parameter and adding the BK14 dataset, as in Section 2.3.2.

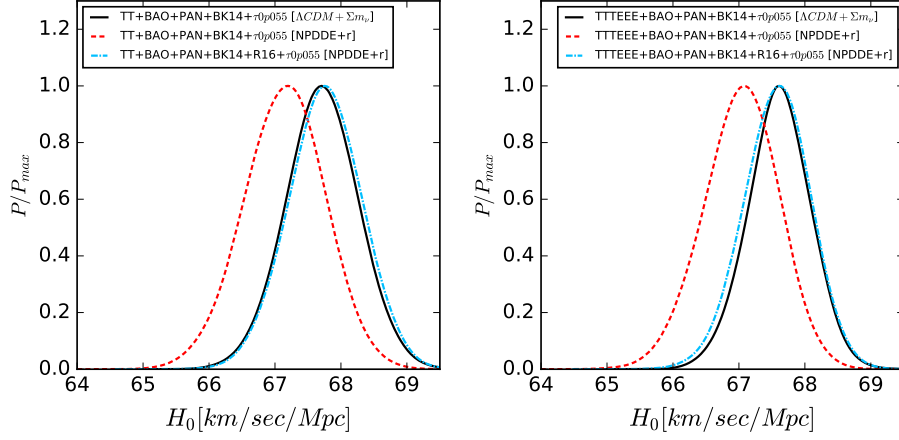


Figure 2.18: Comparison of 1-D marginalized posterior distributions for H_0 comparing the Λ CDM + $\sum m_\nu$ and NPDDE+ r models.

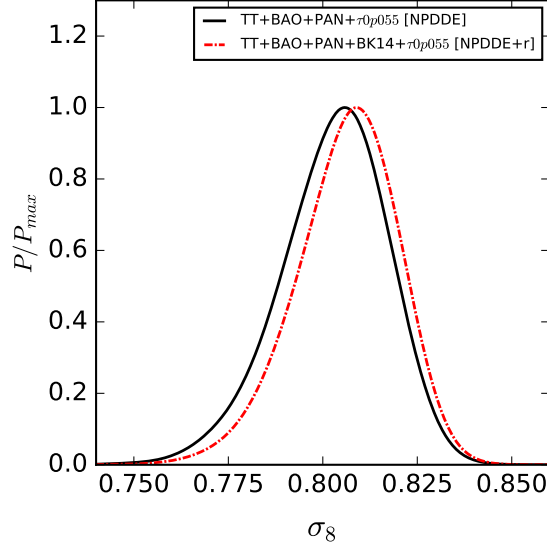


Figure 2.19: Comparison of 1-D marginalized posterior distributions for σ_8 for NPDDE and NPDDE+ r models. Addition of BK14 data seems to prefer a higher σ_8 , due to which slightly more stringent upper bound on $\sum m_\nu$ is obtained.

We find that it is still possible. Once again, the BK14 data prefers a slightly larger value of σ_8 , as can be observed from Figure 2.19, which leads to slightly stronger bounds. The 1-D marginalized posterior distributions for $\sum m_\nu$ and H_0 are given in Figures 2.17 and 2.18 respectively. The 95% C.L. bounds on $\sum m_\nu$ are shown in Table 2.9. Albeit the fact that we don't know for sure if we live in a universe with non-phantom dark energy or if the debatable R16 prior should be used, the $\sum m_\nu < 0.078$ eV bound for TTTEEE + BAO + PAN + BK14 + R16 + $\tau_0 p055$ dataset for this NPDDE+r model was possibly the strongest bound on $\sum m_\nu$ ever reported in literature for any kind of cosmological scenario, at the time of completion of this work.

2.4 Discussion and Summary

Neutrino oscillation experiments have confirmed that neutrinos are massive with three distinct species. However, still, certain neutrino properties including the sum of the three neutrino masses ($\sum m_\nu$) have not been precisely determined. Cosmology can put bounds on $\sum m_\nu$ and in reality, tightest bounds on $\sum m_\nu$ are obtained from cosmological data. Massive neutrinos leave distinct imprints in the CMB and can be constrained with CMB data. However since neutrinos with masses $\ll 1$ eV are relativistic during decoupling of photons, CMB data is not particularly sensitive to low values of $\sum m_\nu$. Since massive neutrinos also cause suppression in the matter power spectrum, tighter bounds are obtained with large scale structure data. In this work we have used latest cosmological datasets and likelihoods available at that

time and provided very strong bounds on the sum of the masses of three active neutrinos in five different cosmological models: Λ CDM + $\sum m_\nu$, Λ CDM + r + $\sum m_\nu$, $w_0 w_a$ CDM + $\sum m_\nu$ (DDE), $w_0 w_a$ CDM + $\sum m_\nu$ with $w(z) \geq -1$ (NPDDE), and $w_0 w_a$ CDM + r + $\sum m_\nu$ with $w(z) \geq -1$ (NPDDE+ r). Among datasets, along with CMB data from Planck 2015, we have used BAO measurements from SDSS-III DR12, MGS and 6dFGS; full shape (FS) measurements from SDSS-III DR12, SNe Ia luminosity distance measurements from Pantheon Sample (PAN); the BK14 data from the BICEP2/Keck Collaboration; the galaxy cluster data from the SPT-SZ survey and suitable Gaussian priors on H_0 (R16) and τ ($\tau 0p055$). The priors help in breaking the mutual degeneracies of H_0 and τ with $\sum m_\nu$ present in the Planck data. In the minimal Λ CDM + $\sum m_\nu$ model, we obtained a robust bound of $\sum m_\nu < 0.152$ eV at 95% C.L. with the use of TT + BAO + PAN + $\tau 0p055$. Adding the high- l polarization data tightens the bound to $\sum m_\nu < 0.118$ eV. The use of the H_0 prior further improves these bounds to $\sum m_\nu < 0.117$ eV and $\sum m_\nu < 0.091$ eV respectively, showing a weak preference for normal hierarchy. The low bounds obtained with the R16 prior, $H_0 = 73.24 \pm 1.74$ km/sec/Mpc are debatable since they are driven by the 3.4σ tension between Planck data and R16 over the value of H_0 . Currently there seem to be no agreement over datasets on the value of H_0 . The R16 prior itself is obtained from combining geometric distance calibrations of Cepheids, each of which separately give constraints on H_0 : 72.25 ± 2.51 , 72.04 ± 2.67 , 76.18 ± 2.37 , and 74.50 ± 3.27 km/sec/Mpc [115]. Removing the third constraint (obtained from Milkyway cepheids) can reduce the H_0 tension and thereby worsen the bounds. While there is no reason to discard the data from Milkyway cepheids we should be

cautious while looking at results obtained with the R16 prior. On the other hand, however, there is a possibility that both Planck and R16 might be correct and the discrepancy has to be explained by some new physics, like say, some dark radiation species which contributes to N_{eff} .

In the dynamical dark energy model $w_0w_a\text{CDM} + \sum m_\nu$ (DDE) we find that the degeneracy between the dark energy equation of state, w and $\sum m_\nu$ significantly relaxes the bounds. Our most conservative bound for this model is $\sum m_\nu < 0.305$ eV with TT + BAO + PAN + $\tau 0p055$, while the most aggressive bound of $\sum m_\nu < 0.247$ eV has been obtained with TTTEEE + BAO + PAN + R16 + $\tau 0p055$, which is very close to the $\sum m_\nu < 0.23$ eV set by Planck collaboration in $\Lambda\text{CDM} + \sum m_\nu$ with similar datasets. This shows the superior constraining power of the new datasets and priors. The DDE model also provides marginally better χ^2 fit to the data compared to $\Lambda\text{CDM} + \sum m_\nu$ and partially alleviates the H_0 tension between Planck data and R16. While we find that the DDE model is compatible with a cosmological constant for the combination of CMB+BAO+PAN+ $\tau 0p055$, the 68% and 95% contours in the $w_0 - w_a$ plane mostly allow phantom dark energy ($w < -1$) and only a very small region of non-phantom dark energy, which shrinks even more with the inclusion of the R16 prior. Also due to the strong degeneracy between $\sum m_\nu$ and w , larger $\sum m_\nu$ is preferred for lower w (i.e. phantom region), while the deeper we go into the non-phantom region smaller the preferred $\sum m_\nu$. So in the NPDDE model ($w_0w_a\text{CDM} + \sum m_\nu$ with $w(z) \geq -1$) when we vary the dark energy parameters only in the non-phantom region, we end up with $\sum m_\nu$ bounds which are even tighter than $\Lambda\text{CDM} + \sum m_\nu$ (also confirmed by a recent study [100]). In NPDDE,

without R16, we obtained a very strong bound of $\sum m_\nu < 0.101$ eV with TTTEEE + BAO + PAN + $\tau 0p055$. Adding the R16 prior leads to an even more aggressive bound of $\sum m_\nu < 0.082$ eV. Allowing for tensors in the Λ CDM + r + $\sum m_\nu$ model and including the BK14 data leads to slightly stronger bounds, which seems to be stemming from BK14 preferring a slightly larger value of σ_8 . This phenomenon persists even when we consider the NPDDE model with tensors (i.e., NPDDE+ r model). In the NPDDE+ r model, without R16, for TTTEEE + BAO + PAN + BK14 + $\tau 0p055$, we found $\sum m_\nu < 0.093$ eV. Such strong bounds in the NPDDE and NPDDE+ r models imply that if future experiments discover that neutrino hierarchy is inverted, the nature of dark energy is more likely to be phantom than non-phantom ((as previously inferred in [100])). In NPDDE+ r , with the R16 prior, we find our most aggressive bound of $\sum m_\nu < 0.078$ eV.

The fact that in the $w_0 w_a$ CDM + $\sum m_\nu$ model (with $w(z) \geq -1$) the neutrino mass bounds are tighter than Λ CDM + $\sum m_\nu$ piqued our interest in cosmologies with massive neutrinos and non-phantom dynamical dark energy. The non-phantom ($w(z) \geq -1$) part of the $w_0 - w_a$ parameter space corresponds to single field dark energy models like Quintessence, which are of great theoretical interest. We thus wanted to study this scenario further in an even more extended parameter space to see if the mass bounds are still tighter than Λ CDM + $\sum m_\nu$. This is the topic of the next chapter.

Neutrino masses and non-phantom dark energy in a 12 parameter extended scenario

This chapter is based on our paper titled “Strong Bounds on Sum of Neutrino Masses in a 12 Parameter Extended Scenario with Non-Phantom Dynamical Dark Energy ($w(z) \geq -1$)” (arXiv: 1807.02860) [141].

In this work we have first considered a 12 parameter extended scenario with 6 usual Λ CDM parameters, two dynamical dark energy parameters ($w_0 - w_a$ approach, CPL parametrization) with $w(z) \geq -1$, two neutrino parameters (N_{eff} and $\sum m_\nu$), and two inflationary parameters (r and the running of the spectral index, $n_{run} \equiv dn_s/d\ln k$). We performed Bayesian analyses to constrain parameters using different combinations of datasets quite similar to as in Chapter 2: (1) Cosmic Microwave Background temperature, polarization, and lensing data from Planck 2015; (2) the data released from the BICEP2/Keck Collaboration for the BB mode of the CMB spectrum up to and including 2014 (BK14); (3) Baryon Acoustic Oscillation

Measurements from SDSS III BOSS DR12, MGS and 6dFGS; (4) Supernovae Type Ia Luminosity Distance Measurements from the newly released Pantheon Sample, and (5) the HST Gaussian prior ($H_0 = 73.24 \pm 1.74$ km/sec/Mpc (68% C.L.)) on Hubble constant. Next we turned off the tensor perturbations (i.e., removed r) and constrained this 11 parameter scenario with the same datasets except BK14. Finally we add a new parameter A_{lens} (scaling of the lensing amplitude) and again constrain this 12 parameter extended space with the mentioned datasets. We emphasize here that this is the first time someone has evaluated the non-phantom dark energy scenario in a 12 parameter extended space. Our main focus in this chapter is on sum of neutrino masses, however we provide the constraints on all the varying parameters.

The main motivation behind this work is the fact that the neutrino mass bounds from cosmology improve greatly in a non-phantom dynamical dark energy (NPDDE) scenario, and are stronger even compared to the minimal $\Lambda\text{CDM} + \sum m_\nu$ as we saw in the previous chapter. Main goal of this work is to see, with NPDDE, if the bounds remain stronger than $\Lambda\text{CDM} + \sum m_\nu$ even in a 12 parameter extended space. Also, in the previous chapter, we had not touched upon issues like the possibility of extra radiation species ($N_{\text{eff}} > 3.045$) and the A_{lens} -problem [142, 143], which we do now.

In a particular model, we set $A_{\text{lens}} = 1$ for the theoretically predicted value of the gravitational potential (which generates weak lensing of the CMB photons). When A_{lens} is varied, the weak lensing is uncoupled from the primary anisotropies which produce it, and then multiplied by the value of A_{lens} [143]. As we have mentioned in Chapter 1, lensing causes smoothing of the CMB acoustic peaks. In a particular model, if the data prefers $A_{\text{lens}} > 1$, it means it prefers more smoothing than what

theoretically should be. Thus A_{lens} serves as a consistency check parameter. A puzzling inconsistency in ΛCDM with Planck data is that the latest measurement by Planck 2018 gives $A_{\text{lens}} = 1.180 \pm 0.065$ (68% C.L.) in a $\Lambda\text{CDM} + A_{\text{lens}}$ model [33] is 2.8σ level higher than the theoretical prediction of $A_{\text{lens}} = 1$. If there is any physical reason for this extra smoothing (i.e. if this is not some statistical fluctuation in the data), it may not be extra lensing but may be any new effect that mimics lensing [33], though currently the cause of this discrepancy is unknown.

Apart from the A_{lens} inconsistency issue and the H_0 tension (discussed in the previous chapter), CMB data also has $\sim 2\sigma$ tension in the measurements of Ω_m and σ_8 with x-ray galaxy cluster measurements [144] or cosmic shear surveys like CFHTLenS [145] and KiDS-450 [146]. For instance, the KiDS-450 survey measures a combined quantity $S_8 \equiv \sigma_8 \sqrt{\Omega_m/0.3} = 0.745 \pm 0.039$ (68% C.L.) which has a more than 2σ tension with Planck 2018, which prefers a much higher value of $S_8 = 0.834 \pm 0.016$ (68% C.L.; TT,TE,EE + lowE). These inconsistencies in ΛCDM model and different datasets have motivated several studies of cosmological scenarios in largely extended parameter spaces [127, 147–149].

In this work, we have, for the first time, shown that neutrino mass bounds can indeed be stronger than the minimal $\Lambda\text{CDM} + \sum m_\nu$ model even in a 12 parameter extended scenario if one considers non-phantom dark energy, even though one expects the bounds to relax in such a large extended space. We have also shown that it is possible to effectively constrain cosmological parameters with some reasonable $1-\sigma$ ranges with current cosmological data, in a 12 parameter extended scenario with non-phantom dark energy. The mass bound however relaxes considerably when we

include A_{lens} , since A_{lens} is strongly correlated with $\sum m_\nu$.

Here we would also like to emphasize that we take the datasets at face value, i.e., any discrepancy or tension between datasets in our model is assumed to have a physical reason and not due to unknown systematics involved in the experiments. Also, it is imperative to point out that the best bounds on sum of neutrino masses that we have presented, are strong and comparable or better to the bounds provided by the recently released Planck 2018 results [33] in the $\Lambda\text{CDM} + \sum m_\nu$ model. Hence our results remain very much relevant although we have used the Planck 2015 data.

This chapter is arranged as follows: in section 3.1 we describe the cosmological models used in this chapter and the prior ranges of parameters used. In section 3.2 we briefly describe the datasets used in this work. In section 3.3 we present our analysis results. In section 3.4, we further discuss how the neutrino mass bounds will change in the three models with new values of τ and A_{lens} obtained by the new Planck 2018 collaboration [33]. We provide a discussion and summary in section 3.5. The main results are in tables 3.2, 3.4, and 3.5.

3.1 Models

In this work we have considered 3 different cosmological scenarios to obtain bounds on the cosmological parameters. Below we list the vector of parameters to vary in each of these cosmological scenarios.

- For NPDDE11+r model with 12 parameters:

$$\theta \equiv \left[\omega_c, \omega_b, \Theta_s, \tau, n_s, \ln[10^{10} A_s], w_0, w_a, N_{\text{eff}}, \sum m_\nu, r, n_{run} \right]. \quad (3.1)$$

- For NPDDE11 model with 11 parameters:

$$\theta \equiv \left[\omega_c, \omega_b, \Theta_s, \tau, n_s, \ln[10^{10} A_s], w_0, w_a, N_{\text{eff}}, \sum m_\nu, n_{run} \right]. \quad (3.2)$$

- For NPDDE11+A_{lens} model with 12 parameters :

$$\theta \equiv \left[\omega_c, \omega_b, \Theta_s, \tau, n_s, \ln[10^{10} A_s], w_0, w_a, N_{\text{eff}}, \sum m_\nu, n_{run}, A_{\text{lens}} \right]. \quad (3.3)$$

In this analysis, the first model, NPDDE11+r, comprises of six additional parameters on top of Λ CDM model. For our analysis we are adding the following additional parameters: two dark energy parameters w_0 and w_a , effective number of relativistic species at recombination N_{eff} , total neutrino mass $\sum m_\nu$, the tensor-to-scalar ratio r (evaluated at pivot scale $k_* = 0.05 h Mpc^{-1}$) and the running of spectral index of primordial power spectrum $n_{run} (\equiv dn_s/d\ln k)$. In this model, the scaling of the lensing amplitude, A_{lens} is fixed at the theoretically predicted value of unity.

We also consider two other scenarios. In the NPDDE11 model, we do not run the tensor perturbations and constrain the parameter space considering scalar only perturbations. In the NPDDE11+A_{lens} model we also allow the A_{lens} parameter to vary. This is since the cause of the A_{lens} -anomaly is unknown and therefore it is

Parameter	Prior
$\Omega_b h^2$	[0.005,0.1]
$\Omega_c h^2$	[0.001,0.99]
τ	[0.01,0.8]
n_s	[0.8, 1.2]
$\log[10^{10} A_s]$	[2,4]
Θ_s	[0.5,10]
w_0	[-1,-0.33]
w_a	[-2,2]
N_{eff}	[0.05,10]
$\sum m_\nu$ (eV)	[0,5]
r	[0,1]
n_{run}	[-1,1]
A_{lens}	[0,10]

Table 3.1: Flat priors on the main cosmological parameters constrained in this chapter.

important to look into the effect of varying A_{lens} on the constraints of rest of the parameter space.

For the cosmological parameters mentioned in eqs. 3.1–3.3, we have assumed flat priors which are listed in table 3.1, along with hard priors given in eq. 2.7. Once again, we obtain the constraints using the Markov Chain Monte Carlo (MCMC) sampler CosmoMC [84] which uses CAMB [42] as the Boltzmann code and the Gelman and Rubin statistics [102] to estimate the convergence of chains. All our chains reached the convergence criterion of $R - 1 < 0.01$.

3.2 Datasets

In this chapter we use similar datasets as in Chapter 2 with some small changes in naming. Firstly, we use the Planck 2015 high- l and low- l temperature and E mode polarization power spectra and their cross-correlation, TTTEEE+lowP, but here we refer to it simply as “Planck” for convenience. We also use the lensing potential measurements via reconstruction through the four point functions of Planck 2015 measurements of CMB anisotropies [87]. We simply refer to this data as “lensing.”

Other than Planck and lensing, we also use BK14, BAO, PAN, and R16, as detailed in Section 2.2 in previous chapter. While we use R16 in most cases, we also provide some results with a prior with a lower value of $H_0 = 71.6 \pm 2.7$ km/sec/Mpc, which is based on the determination of the Hubble constant from the H0LiCOW programme [116]. We call this prior $H071p6$. This is to compare what happens when we use a H_0 prior that has less tension with Planck than R16.

3.3 Results

We have split the results in the three smaller sections for the three different models we have studied. The description of models and datasets are given at section 3.1 and section 3.2 respectively. We have presented the results in the following order: first the NPDDE11+ r model, then the NPDDE11 model and lastly the NPDDE11+ A_{lens} model. All the marginalized limits quoted in the text or tables are at 68% C.L. whereas upper limits are quoted at 95% C.L.

3 Neutrino masses and non-phantom dark energy in a 12 parameter extended scenario

Parameter	Planck+BK14 +BAO	Planck+BK14 +BAO+PAN	Planck+BK14 +R16	Planck+BK14 +R16+lensing
$\Omega_b h^2$	0.02243 ± 0.00021	0.02244 ± 0.00020	0.02265 ± 0.00020	0.02262 ± 0.00020
$\Omega_c h^2$	$0.1189^{+0.0033}_{-0.0034}$	0.1190 ± 0.0033	0.1233 ± 0.0030	$0.1228^{+0.0029}_{-0.0032}$
τ	$0.096^{+0.017}_{-0.018}$	$0.095^{+0.017}_{-0.018}$	0.099 ± 0.018	0.079 ± 0.015
n_s	0.969 ± 0.010	0.969 ± 0.009	0.981 ± 0.008	0.982 ± 0.009
$\ln(10^{10} A_s)$	$3.126^{+0.036}_{-0.037}$	$3.125^{+0.036}_{-0.037}$	3.142 ± 0.036	3.099 ± 0.030
Θ_s	1.041 ± 0.0005	1.041 ± 0.0005	1.040 ± 0.0004	1.041 ± 0.0004
r	< 0.075	< 0.074	< 0.070	< 0.075
H_0 (km/s/Mpc)	$66.64^{+1.38}_{-1.37}$	$67.37^{+1.26}_{-1.25}$	$69.14^{+1.36}_{-1.35}$	69.15 ± 1.38
σ_8	0.827 ± 0.018	0.833 ± 0.018	0.847 ± 0.018	0.825 ± 0.015
$\sum m_\nu$ (eV)	< 0.123	< 0.126	< 0.143	< 0.186
w_0	< -0.859	< -0.933	< -0.915	< -0.914
w_a	$0.013^{+0.065}_{-0.077}$	$0.033^{+0.036}_{-0.063}$	$0.031^{+0.041}_{-0.064}$	$0.035^{+0.043}_{-0.070}$
N_{eff}	$3.082^{+0.209}_{-0.211}$	3.089 ± 0.208	3.391 ± 0.185	$3.393^{+0.181}_{-0.197}$
n_{run}	$-0.00756^{+0.00793}_{-0.00797}$	$-0.00743^{+0.00811}_{-0.00815}$	$-0.00232^{+0.00783}_{-0.00788}$	$0.00173^{+0.00754}_{-0.00750}$

Table 3.2: Bounds on cosmological parameters in the NPDDE11+ r model. Marginalized limits are given at 68% C.L. whereas upper limits are given at 95% C.L. Note that H_0 and σ_8 are derived parameters.

3.3.1 NPDDE11+ r model

Bounds on the NPDDE11+ r model parameters are presented in table 3.2 while the bounds on the Λ CDM model parameters are presented in table 3.3. We do not include the bounds from CMB only data as the bounds are not strong enough in the NPDDE11+ r model, a finding that corroborates with a recent study [127] which had varied the dark energy EoS in both phantom and non-phantom regions. However adding either BAO or R16 with CMB data seems to provide strong bounds on cosmological parameters. Comparing with the bounds on the parameters in

3 Neutrino masses and non-phantom dark energy in a 12 parameter extended scenario

Parameter	Planck +BAO	Planck +BAO+PAN	Planck +R16	Planck +R16+lensing
$\Omega_b h^2$	0.02230 ± 0.00014	0.02230 ± 0.00014	0.02236 ± 0.00015	0.02237 ± 0.00015
$\Omega_c h^2$	0.1190 ± 0.0010	0.1188 ± 0.0010	0.1183 ± 0.0013	0.1179 ± 0.0013
τ	0.083 ± 0.016	0.084 ± 0.017	0.086 ± 0.017	0.071 ± 0.013
n_s	0.967 ± 0.004	0.967 ± 0.004	0.968 ± 0.004	0.969 ± 0.004
$\ln(10^{10} A_s)$	3.098 ± 0.032	$3.100^{+0.033}_{-0.032}$	3.104 ± 0.033	3.073 ± 0.025
Θ_s	1.041 ± 0.0003	1.041 ± 0.0003	1.041 ± 0.0003	1.041 ± 0.0003
H_0 (km/s/Mpc)	67.63 ± 0.47	67.69 ± 0.47	$67.94^{+0.62}_{-0.63}$	$68.13^{+0.62}_{-0.61}$
σ_8	0.831 ± 0.013	0.831 ± 0.013	0.831 ± 0.013	0.817 ± 0.008

Table 3.3: Bounds on cosmological parameters in the Λ CDM model. Marginalized limits are given at 68% C.L. whereas upper limits are given at 95% C.L. Note that H_0 and σ_8 are derived parameters.

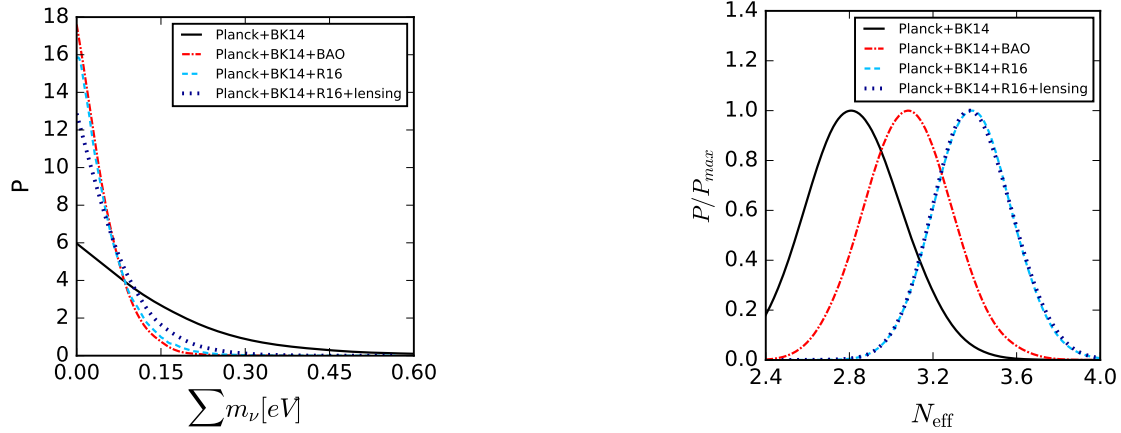


Figure 3.1: Comparison of 1-D marginalized posterior distributions for $\sum m_\nu$ (eV) and N_{eff} for various data combinations in NPDDE11+r.

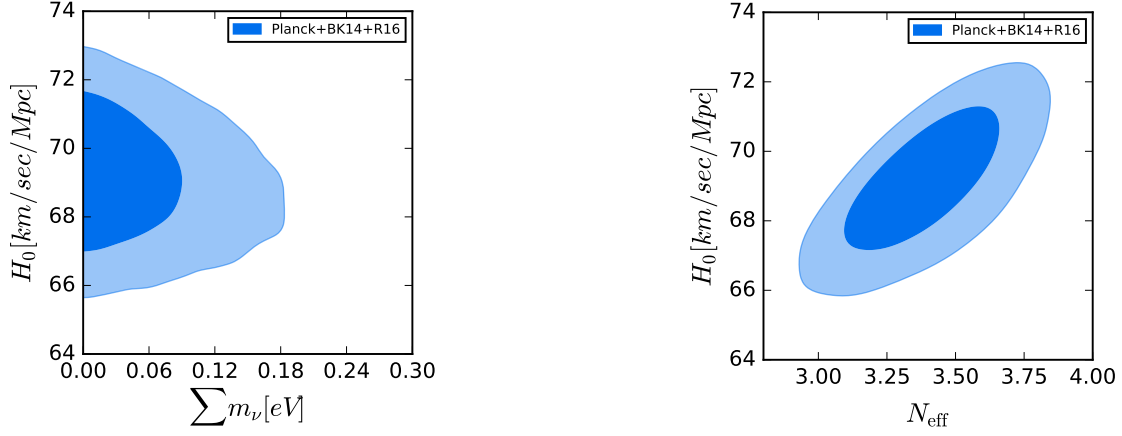


Figure 3.2: 1σ and 2σ marginalized contours for H_0 (km/sec/Mpc) vs. $\sum m_\nu$ (eV) and H_0 (km/sec/Mpc) vs. N_{eff} for Planck+BK14+R16 in the NPDDE11+r model, showing only a small correlation between H_0 and $\sum m_\nu$ whereas a strong positive correlation between H_0 vs. N_{eff} .

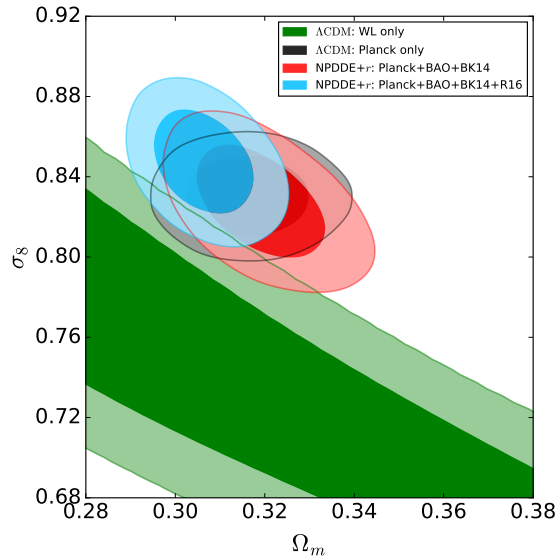


Figure 3.3: 1σ and 2σ marginalized contours in the $\sigma_8 - \Omega_m$ plane showing that the NPDDE+r model is ineffective in reducing the tension between CFHTLenS and Planck 2015.

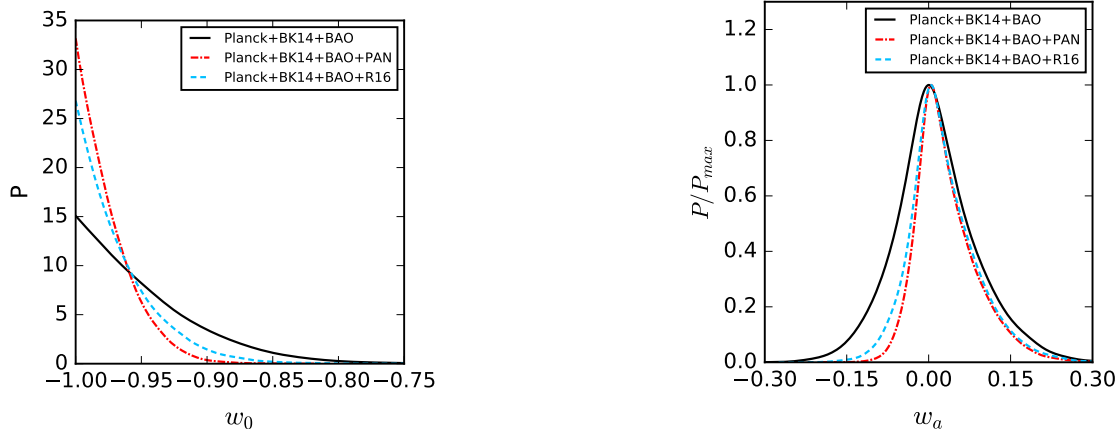


Figure 3.4: Comparison of 1-D marginalized posterior distributions for w_0 and w_a for different data combinations in NPDDE11+r.

the Λ CDM model however we can see that the 68% C.L. spreads of the relevant parameters have increased to different degrees for different parameters. This is an expected phenomenon given the number of parameters has been doubled. Overall the six Λ CDM parameters have been estimated in the NPDDE11+r model with reasonable spreads, showing that it is possible to constrain cosmology with NPDDE effectively in a large parameter space, with current datasets.

We also find tight bounds on $\sum m_\nu$ in this model. The 1-D posteriors for $\sum m_\nu$ and N_{eff} are given in figure 3.1. Our most aggressive bound in this chapter is found in this model with Planck+BAO dataset: $\sum m_\nu < 0.123$ eV (95% C.L.) which is very close to the minimum mass of $\sum m_\nu \simeq 0.1$ eV (95% C.L.) required for inverted hierarchy of neutrinos. Although we are in such an extended parameter space, this bound is stronger than a bound of $\sum m_\nu < 0.158$ eV (95% C.L.) obtained in Λ CDM + $\sum m_\nu$ with Planck+BAO [85]. Without the BAO data, only Planck

and BK14 together provide a bound of $\sum m_\nu < 0.414$ eV (95% C.L.) whereas only using Planck in the same model gives us a bound of $\sum m_\nu < 0.509$ eV (95% C.L.) which is incidentally very close to the bound of $\sum m_\nu < 0.49$ eV (95% C.L.) reported by Planck collaboration [87] using the same data in the minimal Λ CDM + $\sum m_\nu$ model. We saw in Chapter 2, in smaller parameter spaces, that the models comprising of NPDDE provide stronger bounds on $\sum m_\nu$ than Λ CDM + $\sum m_\nu$, because of a degeneracy present between the dark energy EoS w and $\sum m_\nu$ [126] which leads to the phantom region of the dark energy parameter space preferring larger masses and the non-phantom region preferring smaller masses. However, cosmological datasets usually prefer the phantom region more when the dark energy EoS is allowed to vary both in the phantom and non-phantom regions, which usually leads to weaker bounds on $\sum m_\nu$. This work shows that even in a 12 parameter model like NPDDE11+r the data is effective in constraining $\sum m_\nu$, unlike in the 12 parameter model in [127] (with both phantom and non-phantom regions allowed), where the bounds on neutrino mass sum loosens up considerably. Contrary to what happens in lower dimensional parameter spaces, the R16 prior does not lead to stronger bounds on $\sum m_\nu$, as the magnitude of correlation between H_0 and $\sum m_\nu$ is very small in this model. Again, as in Chapter 2 this small correlation can be explained with the mutual degeneracies between H_0 , $\sum m_\nu$, and w . As we saw in Chapter 2 when w is kept constant in a flat Λ CDM + $\sum m_\nu$ universe, H_0 and $\sum m_\nu$ are strongly anti-correlated, to keep the distance to the last scattering surface, $\chi(z_{dec})$ unchanged. On the other hand, when the DE EoS is varied, H_0 and w are also degenerate, as both of them control the late time expansion rate of the universe.

Thus, when we consider a varying DE EoS, a change in H_0 now can be compensated by a change in w , instead of $\sum m_\nu$. This leads to the decreased degeneracy between H_0 and $\sum m_\nu$ in our NPDDE models.

However we found a strong positive correlation still present with N_{eff} , which leads to a large increase in the value of N_{eff} with the use of R16 prior (the correlations can be visualized in figure 3.2). Indeed, while Planck+BK14+BAO prefers a $H_0 = 66.64^{+1.38}_{-1.37}$ km/sec/Mpc (68% C.L.), and $N_{\text{eff}} = 3.082^{+0.209}_{-0.211}$ (68% C.L.), the inclusion of the R16 prior to this data combination leads to higher values of $H_0 = 69.13^{+1.09}_{-1.08}$ km/sec/Mpc (68% C.L.), and $N_{\text{eff}} = 3.392^{+0.188}_{-0.186}$ (68% C.L.) both. The standard value of $N_{\text{eff}} = 3.045$ is excluded at 68% C.L., and favours a dark radiation component, but only very mildly, since $N_{\text{eff}} = 3.045$ is included in 95% C.L. Thus this exclusion of $N_{\text{eff}} = 3.045$ at 68% C.L. happens solely due the large tension present between Planck and R16 regarding the value of H_0 . The R16 prior also prefers higher values of σ_8 . This model does not help the conflict between Planck and CFHTLenS regarding the value of σ_8 . Visual depiction of this can be found in figure 3.3 in the $\sigma_8 - \Omega_m$ plane. Inclusion of the Planck lensing data lead to worsening of the mass bounds whereas bounds on N_{eff} are almost unaffected. Lensing data however lowers the preferred σ_8 value.

The use of the *H071p6* prior, which has a lower value of H_0 than R16, however, leads to lower values of N_{eff} , due to a smaller tension between Planck and *H071p6*. In particular, with Planck + BK14 + BAO + *H07106*, we get a bound of $N_{\text{eff}} = 3.202^{+0.200}_{-0.202}$ (68%). Thus, $N_{\text{eff}} = 3.045$ is no longer excluded at 68% in this

case.

As discussed in Chapter 2 the SNe Ia luminosity distance measurements provide information about evolution of luminosity distance as a function of redshift ($0.01 < z < 2.3$ for the Pantheon sample). This can be used to measure the evolution of the scale factor [122] and is helpful in constraining the dark energy EoS. We found that addition of the PAN data did help in constraining the dark energy parameters more tightly. For Planck+BK14+BAO, we have a bound of $w_0 < -0.859$ (95% C.L.), which shrinks to $w_0 < -0.933$ (95% C.L.) with the addition of PAN. On the other hand, Planck+BK14+BAO produces a bound of $w_a = 0.013_{-0.077}^{+0.065}$ (68% C.L.), whereas Planck+BK14+BAO+PAN leads to $w_a = 0.033_{-0.063}^{+0.036}$ (68% C.L.). We see that the 68% spreads of w_a have shrunk. This has also been depicted in figure 3.4. The R16 prior also has similar but less strong effect. With Planck+BK14+BAO+R16 we have $w_0 < -0.908$ (95% C.L.) and $w_a = 0.028_{-0.065}^{+0.046}$ (68% C.L.). In all cases we found that the cosmology is compatible with a cosmological constant (i.e., $w_0 = -1$, $w_a = 0$).

As far as values of the tensor-to-scalar ratio is concerned, we find that if we run the chains without the BK14 data, we get a bound of $r < 0.155$ (95% C.L.) with Planck+BAO, which is higher than the bound of $r < 0.12$ (95% C.L.) set by Planck collaboration [87]. However, inclusion of the BK14 data leads to a bound of $r < 0.075$ (95% C.L.), which is close to the $r < 0.07$ (95% C.L.) limit set by the BICEP2/Keck collaboration [95]. This value of r remains almost unchanged across all the datasets as long as the BK14 data is included.

3 Neutrino masses and non-phantom dark energy in a 12 parameter extended scenario

Parameter	Planck +BAO	Planck +BAO+PAN	Planck +R16	Planck +R16+lensing
$\Omega_b h^2$	0.02241 ± 0.00021	0.02242 ± 0.00020	0.02264 ± 0.00020	0.02261 ± 0.00020
$\Omega_c h^2$	0.1187 ± 0.0033	0.1188 ± 0.0034	0.1232 ± 0.0031	0.1226 ± 0.0031
τ	0.092 ± 0.018	0.091 ± 0.018	0.095 ± 0.018	$0.077^{+0.014}_{-0.016}$
n_s	0.969 ± 0.009	0.969 ± 0.009	0.981 ± 0.009	0.982 ± 0.009
$\ln(10^{10} A_s)$	$3.117^{+0.037}_{-0.038}$	3.116 ± 0.038	3.133 ± 0.037	$3.095^{+0.031}_{-0.028}$
Θ_s	1.041 ± 0.0005	1.041 ± 0.0005	1.040 ± 0.0004	1.041 ± 0.0004
H_0 (km/s/Mpc)	$66.53^{+1.37}_{-1.36}$	$67.32^{+1.27}_{-1.28}$	$69.07^{+1.39}_{-1.38}$	69.05 ± 1.39
σ_8	0.822 ± 0.019	0.829 ± 0.018	0.843 ± 0.019	$0.823^{+0.015}_{-0.014}$
$\sum m_\nu$ (eV)	< 0.126	< 0.128	< 0.151	< 0.191
w_0	< -0.851	< -0.934	< -0.912	< -0.914
w_a	$0.011^{+0.069}_{-0.079}$	$0.035^{+0.035}_{-0.064}$	$0.030^{+0.043}_{-0.064}$	$0.035^{+0.042}_{-0.069}$
N_{eff}	$3.073^{+0.209}_{-0.211}$	$3.081^{+0.212}_{-0.211}$	3.385 ± 0.190	3.382 ± 0.191
n_{run}	$-0.00511^{+0.00775}_{-0.00780}$	$-0.00477^{+0.00785}_{-0.00784}$	$-0.00016^{+0.00775}_{-0.00777}$	0.00356 ± 0.00742

Table 3.4: Bounds on cosmological parameters in the NPDDE11 model. Marginalized limits are given at 68% C.L. whereas upper limits are given at 95% C.L.. Note that H_0 and σ_8 are derived parameters.

3.3.2 NPDDE11 model

In this section we consider the NPDDE11 model where we turn off the tensor perturbations and also do not include the BK14 data. This does not affect the bounds much as can be seen from table 3.4 and comparing with table 3.2, which verifies the stability of the results in a smaller parameter space.

The 1-D posteriors for $\sum m_\nu$ and N_{eff} for selected datasets are given in figure 3.5. We again find strong bounds on the sum of neutrino masses. We notice that the removal of BK14 data has a small effect on $\sum m_\nu$ which persists over different datasets. For instance, in NPDDE11+r, for Planck+BAO, we find a $\sum m_\nu < 0.131$

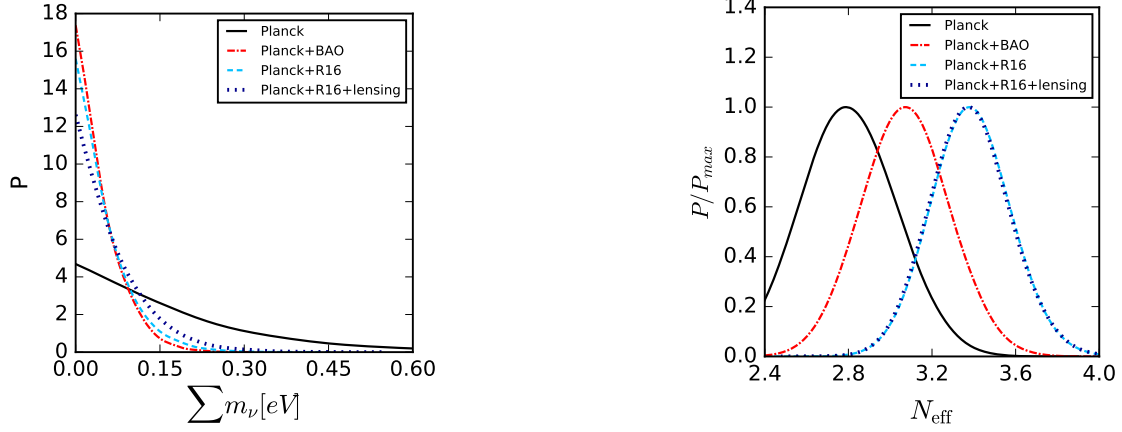


Figure 3.5: Comparison of 1-D marginalized posterior distributions for $\sum m_\nu$ (eV) and N_{eff} for various data combinations in NPDDE11.

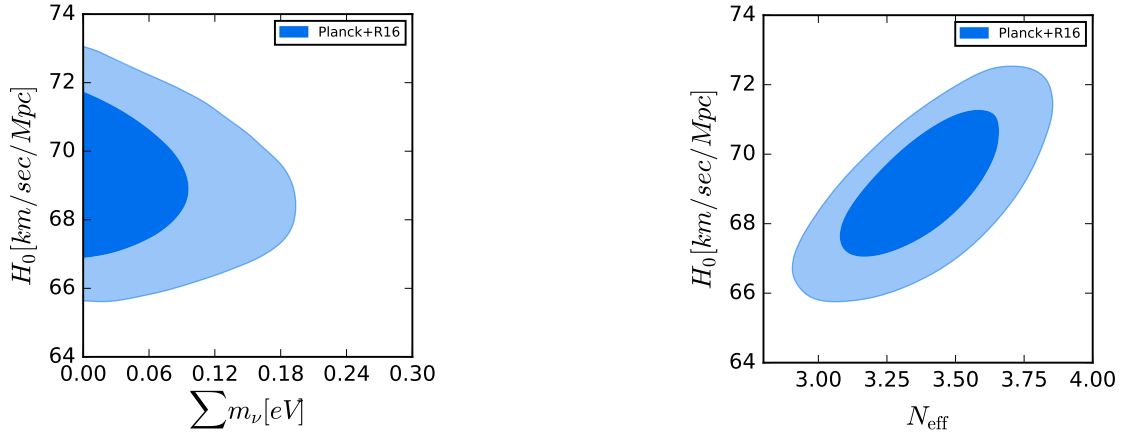


Figure 3.6: 1σ and 2σ marginalized contours for H_0 (km/sec/Mpc) vs. $\sum m_\nu$ (eV) and H_0 (km/sec/Mpc) vs. N_{eff} for Planck+R16 in the NPDDE11 model, showing negligible correlation between H_0 and $\sum m_\nu$ whereas a strong positive correlation between H_0 vs. N_{eff} .

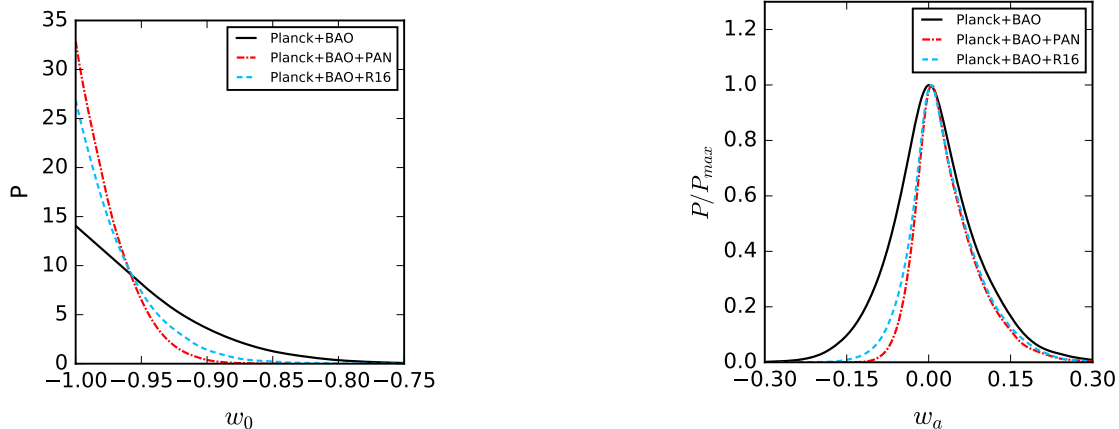


Figure 3.7: Comparison of 1-D marginalized posterior distributions for w_0 and w_a for different data combinations in NPDDE11.

eV (95% C.L.), which is reduced to $\sum m_\nu < 0.123$ eV (95% C.L.) when we add the BK14 data. In the NPDDE11, this bound is $\sum m_\nu < 0.126$ eV (95% C.L.) with Planck+BAO, which is our best bound in this model. This is also stronger than the bound obtained in Λ CDM + $\sum m_\nu$ with Planck+BAO, as in the previous NPDDE11+ r model, and a large improvement compared to the ones presented in [127], which varied dark energy parameters in both in phantom and non-phantom range.

The strengthening of the bound from NPDDE11+ r to NPDDE11 with Planck + BAO might simply be due to reduction in the parameter space volume. On the other hand, as we saw in Chapter 2, it seems BK14 prefers a lower $\sum m_\nu$. However even then the changes are small. Again, BK14 data seems to prefer slightly larger values of σ_8 , thereby increasing the tension with CFHTLenS. Also, the inclusion of R16 prior again seems to discard the standard value of $N_{\text{eff}} = 3.045$ at 68% C.L.

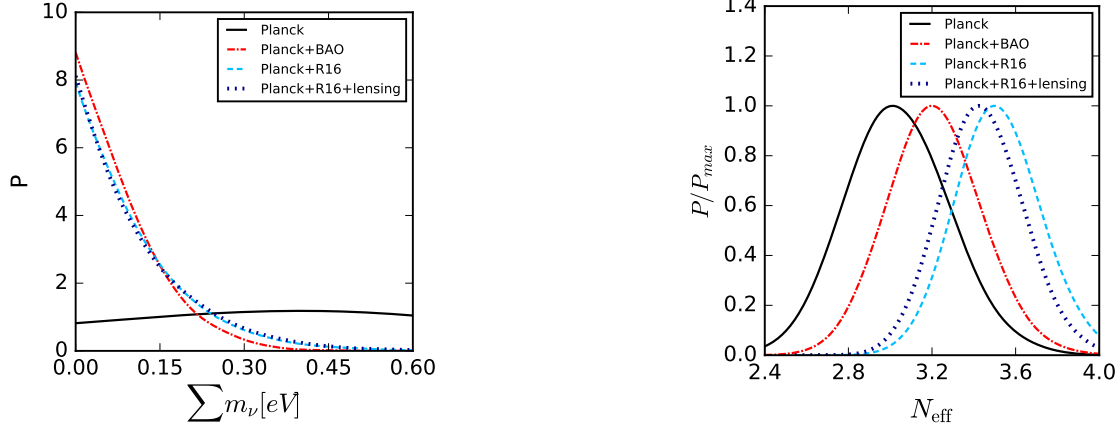


Figure 3.8: Comparison of 1-D marginalized posterior distributions for $\sum m_\nu$ (eV) and N_{eff} for various data combinations in NPDDE11+ A_{lens} .

but again, not at 95% C.L., and also it doesn't lead to stronger $\sum m_\nu$, as before in the NPDDE+ r model, due to a large positive correlation between H_0 and N_{eff} but a only small correlation between H_0 and $\sum m_\nu$. This can be visualized in figure 3.6. The PAN dataset provides stricter bounds on w_0 and w_a , as before. We depict that in figure 3.7.

The use of the $H071p6$ prior instead of R16, here again, leads to lower values of N_{eff} . For instance, with Planck+BAO+ $H07106$, we get a bound of $N_{\text{eff}} = 3.193^{+0.197}_{-0.199}$ (68%). Thus, $N_{\text{eff}} = 3.045$ is no longer excluded at 68% in this model also.

3 Neutrino masses and non-phantom dark energy in a 12 parameter extended scenario

Parameter	Planck +BAO	Planck +BAO+PAN	Planck +R16	Planck +R16+lensing
$\Omega_b h^2$	0.02265 ± 0.00024	0.02263 ± 0.00023	0.02289 ± 0.00023	0.02270 ± 0.00021
$\Omega_c h^2$	0.1192 ± 0.0034	$0.1192^{+0.0034}_{-0.0033}$	0.1232 ± 0.0032	$0.1226^{+0.0030}_{-0.0033}$
τ	$0.059^{+0.021}_{-0.022}$	$0.059^{+0.021}_{-0.022}$	0.059 ± 0.022	$0.058^{+0.021}_{-0.022}$
n_s	0.978 ± 0.011	0.978 ± 0.010	0.991 ± 0.010	0.986 ± 0.009
$\ln(10^{10} A_s)$	3.052 ± 0.044	$3.052^{+0.044}_{-0.045}$	$3.060^{+0.044}_{-0.045}$	$3.055^{+0.043}_{-0.044}$
Θ_s	1.041 ± 0.0005	1.041 ± 0.0005	1.040 ± 0.0004	1.041 ± 0.0004
H_0 (km/s/Mpc)	$66.99^{+1.45}_{-1.46}$	67.94 ± 1.30	69.80 ± 1.48	$69.23^{+1.44}_{-1.45}$
σ_8	0.781 ± 0.025	$0.791^{+0.025}_{-0.023}$	$0.796^{+0.030}_{-0.024}$	$0.795^{+0.030}_{-0.023}$
$\sum m_\nu$ (eV)	< 0.239	< 0.246	< 0.312	< 0.321
w_0	< -0.812	< -0.923	< -0.890	< -0.903
w_a	$0.020^{+0.089}_{-0.114}$	$0.056^{+0.048}_{-0.089}$	$0.048^{+0.056}_{-0.092}$	$0.043^{+0.047}_{-0.083}$
N_{eff}	$3.212^{+0.227}_{-0.228}$	3.201 ± 0.223	$3.517^{+0.196}_{-0.216}$	$3.440^{+0.192}_{-0.210}$
n_{run}	$0.00136^{+0.00806}_{-0.00807}$	$0.00123^{+0.00805}_{-0.00809}$	$0.00685^{+0.00794}_{-0.00803}$	0.00718 ± 0.00788
A_{lens}	$1.21^{+0.08}_{-0.09}$	$1.20^{+0.08}_{-0.09}$	$1.24^{+0.08}_{-0.10}$	$1.08^{+0.06}_{-0.07}$

Table 3.5: Bounds on cosmological parameters in the NPDDE11+ A_{lens} model. Marginalized limits are given at 68% C.L. whereas upper limits are given at 95% C.L. Note that H_0 and σ_8 are derived parameters.

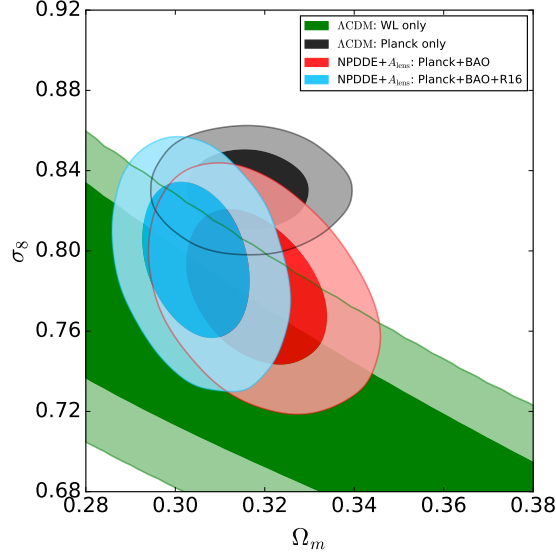


Figure 3.9: 1σ and 2σ marginalized contours in the $\sigma_8 - \Omega_m$ plane showing that the NPDDE11+ A_{lens} model is effective in reducing the tension between CFHTLenS and Planck 2015.

3.3.3 NPDDE11+ A_{lens} model

We present the limits on the cosmological parameters in table 3.5. A number of important changes happen with the introduction of the new varying parameter A_{lens} . Considering that our main goal in this chapter is to constrain neutrino masses, we see a substantial relaxation in the bounds on $\sum m_\nu$. In previous cases we had fixed $A_{\text{lens}} = 1$. However now that A_{lens} is varied we find that the data prefers a large A_{lens} and discards the Λ CDM value of $A_{\text{lens}} = 1$ at more than 95% C.L. (except in case of inclusion of Planck lensing data, which prefers a much lower A_{lens} , implying a tension between Planck and lensing). The increasing of the lensing amplitude with increasing A_{lens} has the same effect as the decreasing of $\sum m_\nu$ [119]. Increasing A_{lens} leads to more smearing of high- l peaks in the CMB temperature and polariza-

tion angular power spectra (C_l^{TT} , C_l^{TE} , C_l^{EE} , C_l^{BB}), due to increased gravitational lensing of CMB photons. On the other hand, massive neutrinos help in reducing this smearing, because it decreases the gravitational lensing of the CMB photons, by suppressing the matter power spectrum in small scales, due to neutrinos having large thermal velocities which prevents them from clustering. As described in Chapter 1 increasing the $\sum m_\nu$ parameter causes increasing suppression of matter power in the small scales [44], which leads to decreasing gravitational lensing of the CMB photons. This leads to a strong positive correlation between A_{lens} and $\sum m_\nu$, such as, to compensate for the increase in A_{lens} , the neutrino masses are also increased. The 1-D plots for $\sum m_\nu$ and N_{eff} for selected datasets are given in figure 3.8. In this model, the Planck only data is almost insensitive to neutrino masses < 0.6 eV. Our tightest bound of $\sum m_\nu < 0.239$ eV (95% C.L.) again comes with Planck+BAO data. This bound, while weaker than the previous models we have discussed, is still close to the $\sum m_\nu < 0.23$ eV (95% C.L.) bound provided by Planck 2015 collaboration [87], and still a large improvement compared to the ones presented in [127], which varied dark energy parameters in both in phantom and non-phantom range and had found a bound of $\sum m_\nu < 0.557$ eV (95% C.L.) with Planck+BAO, demonstrating the large difference between phantom and non-phantom dark energies as far as neutrino masses are concerned. The preferred N_{eff} values are also higher in NPDDE11+ A_{lens} compared to the previous cases. The addition of the R16 data leads to even higher N_{eff} which leads to the $N_{\text{eff}} = 3.045$ value being disallowed even at 95% C.L. with Planck+R16, for which the 68% and 95% limits are $N_{\text{eff}} = 3.517^{+0.196}_{-0.216}$ and $N_{\text{eff}} = 3.517^{+0.424}_{-0.396}$ respectively. This signifies

the presence of tension between Planck and R16 in this model, as it was in previous models.

The use of the *H071p6* prior, again leads to lower values of N_{eff} . In particular, with Planck + BAO + *H07106*, we get a bound of $N_{\text{eff}} = 3.329^{+0.207}_{-0.227}$ (68%). Thus, $N_{\text{eff}} = 3.045$ is not excluded at 95% in this model, but excluded only at 68%.

Another important change is the change in bounds on the optical depth to reionization, τ . With Planck+BAO, the NPDDE11 model preferred a value of $\tau = 0.092 \pm 0.018$ (68% C.L.), whereas this model prefers $\tau = 0.059^{+0.21}_{-0.22}$ (68% C.L.), which is actually closer to the bound of $\tau = 0.055 \pm 0.009$ (68% C.L.) given by Planck 2016 intermediate results [114]. This was previously observed in [127] which did the analysis with varying the dark energy parameters in both the phantom and non-phantom sector. This implies that the main effect is through the degeneracy between τ and A_{lens} and has not much to do with dark energy. Again, while the NPDDE11+ r and NPDDE11 models failed to reconcile Planck with weak lensing measurements like CFHTLenS, the NPDDE11+ A_{lens} model prefers lower values of σ_8 and the agreement with CFHTLenS is considerable. This can be visualized in figure 3.9. This was also previously seen in [127] and hence, again we can infer that this happens because of varying A_{lens} . The bounds on the dynamical dark energy parameters are however weaker than in the other two models we have studied in this chapter. The cosmological constant is however compatible with the data even in this model.

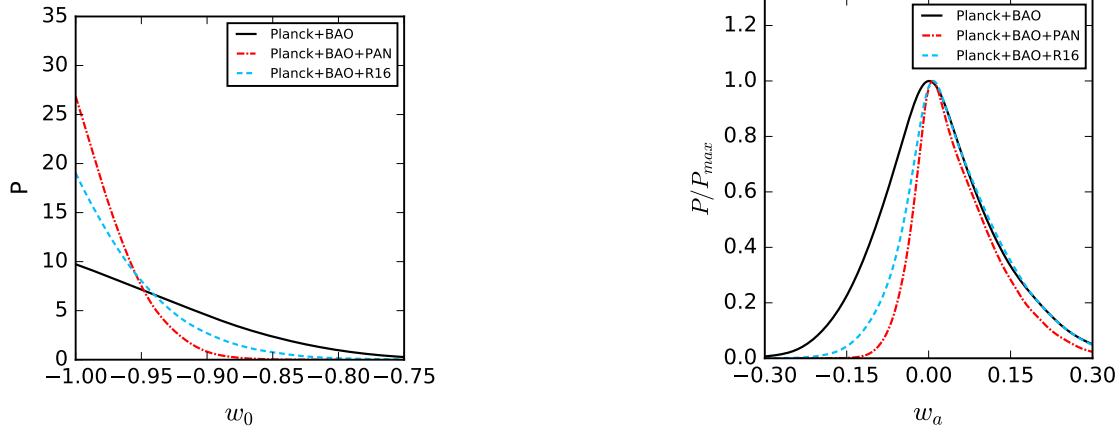


Figure 3.10: Comparison of 1-D marginalized posterior distributions for w_0 and w_a for different data combinations in NPDDE11+ A_{lens} .

3.4 τ and A_{lens} : Implications for Planck 2018

Both τ and A_{lens} are correlated with $\sum m_\nu$, and with each other. As we saw in Chapter 2, when A_{lens} is fixed, increase in $\sum m_\nu$ reduces smearing in the damping tail of the CMB power spectra, and it can be compensated by increasing τ [78, 85]. Hence they have a positive correlation. On the other hand, increasing A_{lens} increases the smearing of the damping tail, i.e., negative correlation with τ . Since the value of τ has been significantly improved from Planck 2015 to Planck 2018, as in Chapter 2 we consider a prior of $\tau = 0.055 \pm 0.009$ (denoted with τ_{0p055}) from Planck 2016 intermediate results [150] to understand how the bounds reported in this chapter might change with the use of Planck 2018 likelihoods. Again, we note here that we

use $\tau 0p055$ as a substitute for low- l polarization data, and thus we discard the lowP data whenever we apply the $\tau 0p055$ prior, to avoid any double counting.

We find that in the NPDDE11+ r model, with Planck + BK14 + BAO + $\tau 0p055$, we get $\sum m_\nu < 0.097$ eV (95%) (i.e. improvement over the $\sum m_\nu < 0.123$ eV limit as in Table 3.2, with Planck + BK14 + BAO). This bound is actually lower than the $\sum m_\nu \simeq 0.1$ eV, i.e. minimum mass required for inverted mass hierarchy of neutrinos. At the same time, in the NPDDE11 model, with Planck + BAO + $\tau 0p055$ we get $\sum m_\nu < 0.107$ eV (95%), which is also an improvement from the result: $\sum m_\nu < 0.126$ eV (95%) with Planck + BAO (see Table 3.5. This happens, since in both of these models, for the datasets considered in Tables 3.2 and 3.5, the mean value of τ hovers around 0.09-0.1. The $\tau 0p055$ prior partially breaks the degeneracy between τ and $\sum m_\nu$, and produces lower values of $\sum m_\nu$ by lowering the preferred τ values.

On the other hand, in the NPDDE11+ A_{lens} model with Planck + BAO + $\tau 0p055$, we found $\sum m_\nu < 0.237$ eV, which is almost similar to the bound $\sum m_\nu < 0.239$ eV (95%) with Planck + BAO (see table 3.3). This happens since all the three parameters, τ , A_{lens} , and $\sum m_\nu$ are varied together. Now, as the data prefers A_{lens} values higher than the theoretical prediction of $A_{\text{lens}} = 1$ in this model, the degeneracy between A_{lens} and τ leads to a much lowered value of τ , and thus the correlation between τ and $\sum m_\nu$ is already much smaller in this model, than the other two. Thus $\tau 0p055$ has little effect on the neutrino mass bounds in this model.

Also, we obtained limits of A_{lens} in a $\Lambda\text{CDM} + A_{\text{lens}}$ model with Planck 2015

full temperature and polarization data. The value we got is $A_{\text{lens}} = 1.15_{-0.082}^{+0.072}$ (68% C.L.). In the Planck 2018 Cosmological Parameters chapter [33], for similar data and same model, given value of A_{lens} is: $A_{\text{lens}} = 1.18 \pm 0.065$ (68%) (see equation 36b in the Planck 2018 paper). This shows that there is only a small change in A_{lens} from Planck 2015 to Planck 2018. Thus, it is likely that there will not be any considerable changes in the limits of other cosmological parameters with the Planck 2018 data, in the context of the value of A_{lens} .

3.5 Summary

In this work we have studied three different extended cosmological scenarios with non-phantom dynamical dark energy (NPDDE) with a focus on constraining sum of neutrino masses. We have presented bounds on all the varying parameters in these extended scenarios and described the main effects we observed. In the first model, NPDDE11+r, we consider 12 parameters: the 6 Λ CDM parameters, two dynamical dark energy parameters with CPL parametrization (w_0 and w_a) with hard priors to satisfy the non-phantom requirement, number of effective relativistic neutrino species at recombination (N_{eff} and sum of neutrino masses ($\sum m_\nu$), and the running of the inflation spectral index (n_{run}) and the tensor-to-scalar ratio (r). We used different combinations of recent datasets including Planck 2015 temperature and polarization data, CMB B-mode spectrum data from BICEP2/Keck collaboration (BK14), BAO SDSS III BOSS DR12, MGS and 6dFS data, SNe Ia Pantheon sample (PAN), the R16 prior ($H_0 = 73.24 \pm 1.74$ km/sec/Mpc (68% C.L.)). We found that

CMB only data is not very effective in constraining the cosmological parameters. The 1σ spreads for the parameters were however increased in this model compared to Λ CDM due to the doubling of number of parameters. Our best bound on neutrino masses in this model came from Planck+BK14+BAO: $\sum m_\nu < 0.123$ eV (95% C.L.) which is a strong bound close to the minimum mass of $\simeq 0.1$ eV (95% C.L.) required for inverted hierarchy of neutrino masses and is stronger than a bound of $\sum m_\nu < 0.158$ eV (95% C.L.) obtained in Λ CDM + $\sum m_\nu$ with Planck+BAO [85] (see also [100] for a similar conclusion in a smaller parameter space). We also found that inclusion of the R16 prior leads to a preference for dark radiation at 68% C.L. but not at 95%, while without the R16 prior the data is completely consistent with the standard value of $N_{\text{eff}} = 3.045$. Although this is driven by the more than 3σ tension present between Planck and R16 regarding the value of H_0 and should be interpreted cautiously. This model did not improve the σ_8 tension present in the $\sigma_8 - \Omega_m$ plane between Planck and CFHTLenS. The Pantheon sample improved the bounds on the dark energy parameters. All combinations of data are also compatible with a cosmological constant ($w_0 = -1, w_a = 0$). However, this is mostly because we are restricting the parameter space to $w(z) \geq -1$ and [127] had found that the data mostly prefers the phantom region in such an extended parameter space when both phantom and non-phantom regions are allowed.

We tested the stability of these results in a lower parameter space (model: NPDDE11) where we turned off the tensor perturbations and also did not use the BK14 data. We found that the general conclusions made for NPDDE11+r were

also true in this model. The tightest bound of $\sum m_\nu < 0.126$ eV (95% C.L.) in this model also came from Planck + BAO.

Finally we studied the NPDDE11+ A_{lens} model where we also varied the lensing amplitude. We found that except when Planck lensing data is included, the $A_{\text{lens}} = 1$ value predicted by Λ CDM was rejected at more than 95% C.L. by the datasets. Due to this, the $\sum m_\nu$ bounds also worsened with our best result in this model: $\sum m_\nu < 0.239$ eV (95% C.L.) coming from Planck+BAO again. This result is, however, still close to the $\sum m_\nu < 0.23$ eV (95% C.L.) bound by Planck collaboration [87], showing that the cosmological data is effective in constraining neutrino masses in a cosmology with NPDDE. The R16 prior also preferred a dark radiation component but this time also at 95% C.L. level, as this model also prefers higher values of N_{eff} . On the other hand, we found that this model helps relieve the σ_8 tension between Planck and CFHTLenS considerably.

The recent Planck 2018 results [33] put the bound of $\sum m_\nu < 0.13$ eV (95% C.L.) in Λ CDM + $\sum m_\nu$ with Planck+BAO. Thus, the aggressive bound of $\sum m_\nu < 0.123$ eV (95% C.L.) (Planck + BK14 + BAO) is still stronger than this bound by Planck 2018 and hence, our results are very much relevant albeit the analysis is with Planck 2015 dataset. In fact, when we use the following Gaussian prior on optical depth to reionization: $\tau = 0.055 \pm 0.009$ from 2016 Planck intermediate results, and discard the low- l polarization data, the bound on neutrino masses improves to $\sum m_\nu < 0.097$ eV (95%), which is less than the 0.1 eV mass sum required for

inverted hierarchy of active neutrino masses.

While we have used the CPL parametrization in our work, it is not the only parametrization that can be used for non-phantom dark energy. Any change in parametrization can lead to change in bounds obtained on the sum of neutrino masses. For instance, if we set the w_a parameter to zero, i.e., if we consider only a simple $w(z) = w_0$ parametrization, we find that bounds on $\sum m_\nu$ relax slightly. In the NPDDE11 model, with $w_a = 0$ and $w(z) = w_0$, and using Planck + BAO data, we found $\sum m_\nu < 0.141$ eV (95%), instead of $\sum m_\nu < 0.126$ eV (95%) when we vary both w_0 and w_a . In the NPDDE11+ A_{lens} model also, with $w_a = 0$ and $w(z) = w_0$, and using Planck + BAO, we obtained $\sum m_\nu < 0.261$ eV (95%), instead of $\sum m_\nu < 0.239$ eV (95%). Some other parametrizations that can be considered include Logarithmic parametrization [151] ($w(a) = w_0 - w_a \ln(a)$), Jassal-Bagla-Padmanabhan (JBP) parametrization [152] ($w(a) = w_0 + w_a a(1 - a)$) etc. Analysis involving these parametrizations is beyond the scope of this thesis. However, we would like to point the reader to [130], where the authors found similar limits, with CPL and Logarithmic parametrizations, on $\sum m_\nu$ for the case of degenerate hierarchy. However, in case of JBP, bound on $\sum m_\nu$ was found to be significantly stronger. While [130] does not discard the phantom region, it is possible that results from analyses with only non-phantom dark energy will also vary depending on the parametrization used, as far as neutrino masses are concerned.

We would like to add a final remark that we have obtained the bounds while

taking the datasets at face value. However unresolved systematics present in the dataset could have affected our results and conclusions. Thus there is still a lot to learn about robustness of datasets and also about dynamics of dark energy.

Constraints on light sterile neutrino mass from cosmology

This chapter uses parts of the preprint “Constraining light sterile neutrino mass with the BICEP2/Keck Array 2014 B-mode polarization data” (arXiv: 1807.10294) [153]. Leaving aside active neutrinos, we now move to sterile neutrinos. Sterile neutrinos still remain nothing short of an enigma in neutrino physics. Presence of anomalies in some short-baseline oscillation experiments [154–156] have been explained with an extra species of neutrino, namely a sterile neutrino, of mass $\simeq 1$ eV, which amply mixes with the active neutrinos but is uncharged under the standard model gauge group. Again, there are analyses [157–161] which indicate that all the results cannot be explained comfortably with the sterile neutrino hypothesis. A recent result [162] from the MiniBooNE collaboration finds present electron neutrino and anti-neutrino appearance data still consistent with an extra sterile neutrino.

In a situation where standard model (SM) of particle physics is augmented with

only an extra sterile neutrino species, from a cosmological perspective there are two parameters of utmost importance. One is the effective number of relativistic neutrino species, N_{eff} , whose theoretically predicted value $N_{\text{eff}}^{\text{SM}} = 3.046$ is supposed to increase when contribution from the sterile neutrino is counted. The other is the effective mass of the sterile neutrino, $m_s^{\text{eff}} = \Delta N_{\text{eff}}^{3/4} m_s^{\text{ph}}$, where $\Delta N_{\text{eff}} = N_{\text{eff}} - 3.046$ and m_s^{ph} is the physical mass of the sterile neutrino. Cosmology can provide strong constraints on these two parameters. N_{eff} , in general, can have contribution from any relativistic species which is not a photon, and hence it is not restricted only to the neutrino sector. Also, in certain scenarios like very low-reheating scenarios with sterile neutrinos [163] or self-interacting sterile neutrinos [164], ΔN_{eff} can be negative. However, we do not consider such scenarios in this work, and consider only a non-interacting extra species of sterile neutrino.

Provided we are only considering an extension to standard model with neutrino oscillations in a 3+1 scenario, as long as the sterile neutrino is of similar mass to an active neutrino and amply mixes with the active ones, its cosmological implications are identical to the active neutrino. Sufficient mixing will lead to almost complete thermalization [165, 166]. However, even if there is partial thermalization, it will, in general, increase N_{eff} , leading to a delayed matter-radiation equality and a higher value of the Hubble parameter, $H(z_{\text{dec}})$, at the CMB decoupling (given other parameters are kept fixed). This has two main consequences [167] on the CMB anisotropy power spectrum, first being an increase in the first peak of the spectrum because of early Integrated Sachs Wolfe (ISW) effect, and the second being a horizontal shift of the peaks towards higher multipoles. Along with a horizontal shift, there will also

be a vertical shift which will decrease the amplitude of the peaks at high multipoles, a phenomenon related to Silk damping. These effects of an additional relativistic sterile neutrino can be partially compensated if other cosmological parameters are simultaneously varied. For example, if the total matter density ω_m is also increased without altering the baryon density, the redshift of matter-radiation equality can be kept fixed. These degeneracies tend to degrade the constraints on N_{eff} . However, the CMB power spectra won't be exactly the same even after such adjustments with other parameters, especially because of the neutrino anisotropic stress arising from the quadrupole moment of the cosmic neutrino background temperature anisotropies which alters the gravitational potentials [168, 169]. Hence constraints can be put on N_{eff} from CMB power spectra data. In Chapter 3 we have already seen bounds on N_{eff} in case of massive active neutrinos.

If a light sterile neutrino has a mass $\simeq 1$ eV, it only starts to become non-relativistic during CMB, and hence the effect of the mass is not strong on CMB power spectra. Sterile neutrinos with masses much smaller than 1 eV will have a small effect on CMB temperature and polarization power spectra. However, when CMB power spectra data is used with other cosmological observations like constraining the Hubble parameter from direct measurements via a Gaussian prior or using the Baryon Acoustic Oscillation (BAO) data or both, better bounds on the mass of the sterile neutrino can be obtained [55], similar to the $\sum m_\nu$ case. Current bounds on sterile neutrinos from cosmological data imply that fully thermalized sterile neutrinos of mass $\simeq 1$ eV are disfavoured and can only be accommodated with partial thermalization. See previous analyses on constraining sterile neutrino properties

with cosmological data [170–181].

In this paper, we have, for the first time, used the BK14 data to constrain the parameters associated with sterile neutrinos in an extended Λ CDM model, which can be simply denoted with Λ CDM + r + N_{eff} + m_s^{eff} . BK14 constrains the tensor-to-scalar ratio and also contains information on gravitational lensing. In previous two chapters we have noticed that BK14 data makes the bounds on $\sum m_\nu$ slightly stronger. Thus we expect this data to affect the constraints on the sterile neutrino mass as well. We also provide results with N_{eff} fixed at 4.046 and 3.5 separately, i.e., assuming full and partial thermalization of the sterile neutrinos respectively, and these models are denoted as Λ CDM + r + m_s^{eff} .

4.1 Cosmological Analysis: Models and Datasets

Below we list the vector of parameters we have varied in this work in two cosmological models.

- For Λ CDM + r + N_{eff} + m_s^{eff} model:

$$\theta \equiv [\omega_c, \omega_b, \Theta_s, \tau, n_s, \ln[10^{10} A_s], r, N_{\text{eff}}, m_s^{\text{eff}}]. \quad (4.1)$$

- For Λ CDM + r + m_s^{eff} model:

$$\theta \equiv [\omega_c, \omega_b, \Theta_s, \tau, n_s, \ln[10^{10} A_s], r, m_s^{\text{eff}}]. \quad (4.2)$$

with i) N_{eff} fixed to the value 4.046, which corresponds to full thermalization of the sterile neutrino with active neutrinos and, ii) N_{eff} fixed to the value 3.5, which corresponds to partial thermalization.

In our work, we have fixed the active neutrino sector to give a contribution of $N_{\text{eff}}^{\text{SM}} = 3.046$ to N_{eff} , with two massless and one massive neutrino with mass of 0.06 eV. Thus the contribution to N_{eff} from the sterile species is simply $\Delta N_{\text{eff}} = N_{\text{eff}} - 3.046$.

When the sterile neutrino is relativistic at early times, assuming the only radiation species are photons and neutrinos, contribution of a light sterile neutrino to N_{eff} is given by [182],

$$\Delta N_{\text{eff}} = \left[\frac{7}{8} \frac{\pi^2}{15} T_\nu^4 \right]^{-1} \frac{1}{\pi^2} \int dp p^3 f_s(p), \quad (4.3)$$

where T_ν is active neutrino temperature, p is the neutrino momentum, and $f_s(p)$ is momentum distribution function of the sterile neutrino. At late times its energy density is parametrized as an effective mass [182, 183]:

$$\omega_s \equiv \Omega_s h^2 = \frac{m_s^{\text{eff}}}{94.1 \text{eV}} = \frac{h^2 m_s^{\text{ph}}}{\pi^2 \rho_{\text{cr},0}} \int dp p^2 f_s(p), \quad (4.4)$$

where $\rho_{\text{cr},0}$ is the critical density as defined in Eq. 1.6, $\Omega_s h^2$ is the sterile neutrino energy density. Since sterile neutrinos don't have electroweak interactions and they have mixing with the active neutrinos, they cannot decouple after the decoupling of active neutrinos. Active neutrinos decouple at a temperature $T \sim 1$ MeV, when all of them are relativistic. Hence $f_s(p)$ doesn't depend on the physical mass of the

sterile neutrino, m_s^{ph} . However $f_s(p)$ depends on the production mechanism of the light sterile neutrino. If the production is through a thermal process, one can simply write $f_s(p) = (e^{p/T_s} + 1)^{-1}$, the usual Fermi-Dirac distribution function, where T_s is the sterile neutrino temperature. In this case, it can be shown that,

$$m_s^{\text{eff}} = \Delta N_{\text{eff}}^{3/4} m_s^{\text{ph}}; \quad \Delta N_{\text{eff}} = \left(\frac{T_s}{T_\nu}\right)^4. \quad (4.5)$$

Non-thermal production, on the other hand, can lead to various possible scenarios. One of the popular scenarios is the Dodelson-Widrow (DW) mechanism [184], for which $f_s(p) = \beta(e^{p/T_\nu} + 1)^{-1}$, where β is a normalization factor. In this case, one gets [182],

$$m_s^{\text{eff}} = \Delta N_{\text{eff}} m_s^{\text{ph}}; \quad \Delta N_{\text{eff}} = \beta. \quad (4.6)$$

So, the m_s^{eff} parametrization can accommodate two different scenarios of sterile neutrino production. Also notice that in the $\Lambda\text{CDM} + r + m_s^{\text{eff}}$ model, fixing $N_{\text{eff}} = 4.046$ leads to m_s^{eff} being same as m_s^{ph} .

In our work, we conduct a Bayesian analysis to derive constraints on the sterile neutrino parameters. For all the parameters listed in Eq. (4.1), and Eq. (4.2), we impose flat priors. We also limit the physical mass of the sterile neutrino to $m_s^{\text{ph}} \leq 10$ eV. The prior ranges are provided on the Table 4.1. We run chains using CosmoMC [84] which incorporates CAMB [42] as the Boltzmann code and the Gelman and Rubin statistics [102] to estimate the convergence of chains.

We use separate combinations of the following datasets: Planck 2015 TT+lowP,

Parameter	Prior
ω_c	[0.001,0.99]
ω_b	[0.005,0.1]
Θ_s	[0.5,10]
τ	[0.01,0.8]
n_s	[0.8,1.2]
$\ln [10^{10} A_s]$	[2,4]
r	[0,2]
N_{eff}	[3.046,7]
m_s^{eff}	[0,3]

Table 4.1: Flat priors on cosmological parameters included in this work.

lensing, BK14, BAO and R16. The datasets are described in Chapter 2.

4.2 Results

For convenience, we have separated the results in two subsections for the the two different models. The description of models and datasets are given in Section 4.1. We have presented the results, first in the $\Lambda\text{CDM} + r + N_{\text{eff}} + m_s^{\text{eff}}$ model, and then in the $\Lambda\text{CDM} + r + m_s^{\text{eff}}$ model. All the marginalized limits quoted in the text or tables are at 68% C.L. whereas upper limits are quoted at 95% C.L., unless otherwise specified.

4.2.1 Results for $\Lambda\text{CDM} + r + N_{\text{eff}} + m_s^{\text{eff}}$ model

In this section, we present the results for the $\Lambda\text{CDM} + r + N_{\text{eff}} + m_s^{\text{eff}}$ model. In Table 4.2 we have provided results without BK14 data, whereas, in Table 4.3, the results are with BK14, to compare. We have presented constraints on the three

4 Constraints on light sterile neutrino mass from cosmology

Parameter	TT+lowP	TT+lowP +BAO	TT+lowP +R16	TT+lowP +R16+BAO	TT+lowP +R16+BAO+lensing
m_s^{eff} (eV)	< 0.78	< 0.53	< 0.34	< 0.36	< 0.40
N_{eff}	< 3.78	< 3.75	3.63 ± 0.21	3.59 ± 0.22	$3.60^{+0.21}_{-0.24}$
r	< 0.127	< 0.129	< 0.151	< 0.148	< 0.155
H_0 (km/sec/Mpc)	$68.35^{+1.23}_{-2.50}$	$69.14^{+0.89}_{-1.59}$	$71.77^{+1.63}_{-1.64}$	$70.79^{+1.19}_{-1.20}$	70.78 ± 1.21
σ_8	$0.802^{+0.040}_{-0.029}$	$0.815^{+0.029}_{-0.023}$	$0.836^{+0.029}_{-0.021}$	$0.828^{+0.029}_{-0.023}$	$0.816^{+0.020}_{-0.016}$

Table 4.2: Bounds on cosmological parameters in the $\Lambda\text{CDM} + r + N_{\text{eff}} + m_s^{\text{eff}}$ model without BK14 data. Marginalized limits are given at 68% C.L. whereas upper limits are given at 95% C.L. Note that H_0 and σ_8 are derived parameters.

Parameter	TT+lowP +BK14	TT+lowP +BK14+BAO	TT+lowP +BK14+R16	TT+lowP +BK14+R16+BAO	TT+lowP+BK14 +R16+BAO+lensing
m_s^{eff} (eV)	< 0.68	< 0.46	< 0.28	< 0.30	< 0.35
N_{eff}	< 3.76	< 3.74	3.63 ± 0.21	3.59 ± 0.21	$3.59^{+0.21}_{-0.23}$
r	< 0.068	< 0.070	< 0.073	< 0.072	< 0.078
H_0 (km/sec/Mpc)	$68.31^{+1.25}_{-2.48}$	$69.16^{+0.95}_{-1.61}$	71.73 ± 1.62	70.84 ± 1.20	$70.75^{+1.17}_{-1.18}$
σ_8	$0.814^{+0.036}_{-0.027}$	$0.825^{+0.027}_{-0.021}$	$0.846^{+0.026}_{-0.020}$	$0.841^{+0.025}_{-0.021}$	$0.820^{+0.019}_{-0.015}$

Table 4.3: Bounds on cosmological parameters in the $\Lambda\text{CDM} + r + N_{\text{eff}} + m_s^{\text{eff}}$ model with BK14 data. Marginalized limits are given at 68% C.L. whereas upper limits are given at 95% C.L.. Note that H_0 and σ_8 are derived parameters.

parameters r , N_{eff} , and m_s^{eff} . with which we have extended the Λ CDM model, and also two derived parameters H_0 and σ_8 , which are important in constraining the sterile neutrino mass.

With only TT+lowP, we see that the bound on the sterile mass is relaxed at $m_s^{\text{eff}} < 0.78$ eV. The bound gets tightened with BAO data, which partially breaks the degeneracy between m_s^{eff} and H_0 present in the TT+lowP data, by rejecting lower values of H_0 [61, 85] and leads to a bound of $m_s^{\text{eff}} < 0.53$ eV. This effect can be seen pictorially in Figure 4.1 where addition of BAO data leads to a significantly smaller magnitude of anti-correlation between m_s^{eff} and H_0 . The R16 prior also breaks the degeneracy partially, as can be seen in Figure 4.1. However, the H_0 values preferred by the R16 prior are larger than BAO, which leads to a preference to even smaller masses ($m_s^{\text{eff}} < 0.34$ eV) to keep the comoving distance to the surface of last scattering fixed [85]. Adding R16 and BAO together with CMB however does not provide better bound than CMB+R16. Also, the lensing data degrades the bound on m_s^{eff} . We note that CMB and/or BAO data do not allow full thermalization of sterile neutrinos. However, at 95% C.L., with TT+lowP+R16, we obtained a $N_{\text{eff}} = 3.63^{+0.44}_{-0.42}$. Such high values of N_{eff} disallow the standard model prediction of $N_{\text{eff}}^{SM} = 3.046$ at 95% C.L. but allow $N_{\text{eff}} = 4.046$, i.e., full thermalization. On the other hand, it is also imperative to consider recent constraints on N_{eff} coming from Big Bang Nucleosynthesis (BBN). Planck 2018 results [33] have provided bound of $N_{\text{eff}} = 2.95^{+0.56}_{-0.52}$ (95% C.L.) (which is independent of the details of the CMB spectra at high multipoles) by combining the helium, deuterium, and BAO data with an almost model-independent prior on θ_s derived from Planck data. Another

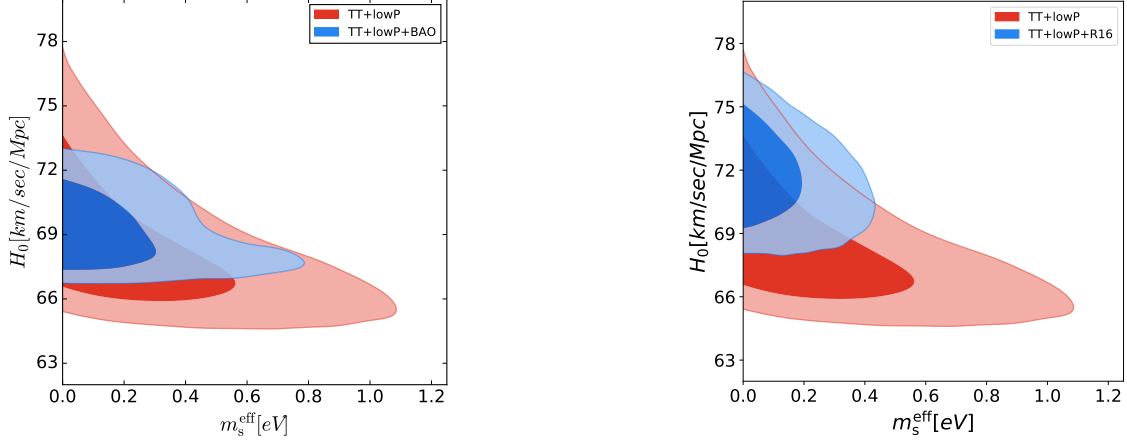


Figure 4.1: 1σ and 2σ marginalized contours for H_0 [km/sec/Mpc] vs. m_s^{eff} [eV] in the $\Lambda\text{CDM} + r + N_{\text{eff}} + m_s^{\text{eff}}$ model with the following combinations: TT+lowP, TT+lowP+BAO, and TT+lowP+R16. Both BAO and R16 data decrease the correlation between the two parameters significantly.

recent study on BBN [185] provide a tight bound of $N_{\text{eff}} = 2.90 \pm 0.22$ (68% C.L.), which means at at 95% C.L., there will be only a small overlap in the values of N_{eff} provided by [185] and TT+lowP+R16. It is also to be noted that addition of the R16 prior leads to a slightly inferior fit to the data, due to the 3.4σ tension present between Planck and R16 regarding the value of H_0 . We find that in this $\Lambda\text{CDM} + r + N_{\text{eff}} + m_s^{\text{eff}}$ model, compared to TT+lowP, the dataset TT+lowP+R16 degrades the χ^2 -fit by an amount of $\Delta\chi^2 = +3.43$.

Akaike information criterion (AIC): To understand the improvement/worsening of the quality of fit with addition of sterile neutrino parameters (N_{eff} and m_s^{eff}) we need to compare the fit to data given by $\Lambda\text{CDM} + r + N_{\text{eff}} + m_s^{\text{eff}}$ with that of $\Lambda\text{CDM} + r$. Since the number of parameters in the two models are not same, a popular method to compare the fit is the Akaike information criterion (AIC) [186].

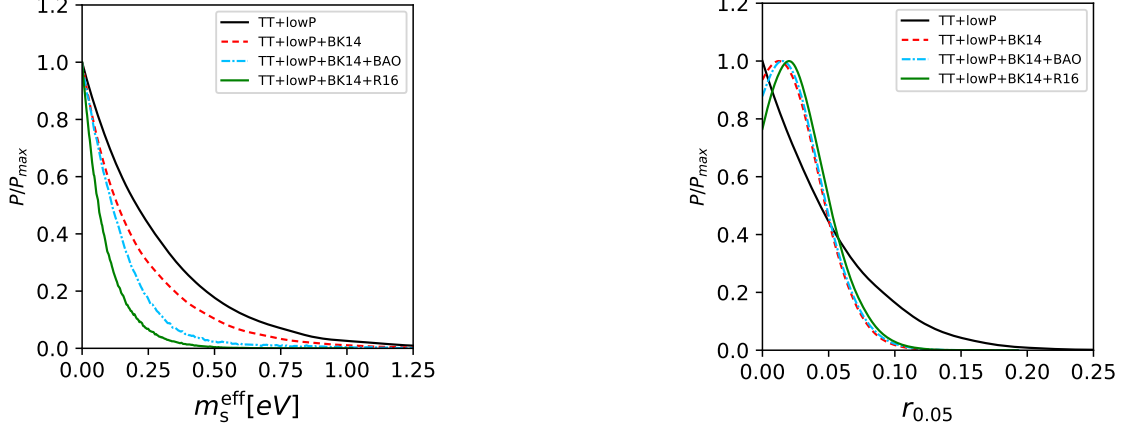


Figure 4.2: 1-D marginalized posteriors for m_s^{eff} [eV] and r in the $\Lambda\text{CDM} + r + N_{\text{eff}} + m_s^{\text{eff}}$ model with various data combinations.

For a particular model and data, AIC is given by,

$$\text{AIC} = \chi_{\text{best-fit}}^2 + 2k \quad (4.7)$$

where k is the number of parameters in the model. The model with lower AIC corresponds to the preferred model.

Thus, comparison with another model (with the same data) can be done with $\Delta\text{AIC} = \Delta\chi^2 + 2\Delta k$. Usually models with extra parameters provide better fit to the data since they have a larger parameter space. The $2\Delta k$ term penalizes models with extra parameters to prevent any over-fitting. Here $2\Delta k = 4$.

We find that for the TT+lowP+R16 data:

$$\Delta\chi^2 = \chi_{\text{best-fit}}^2(\Lambda\text{CDM} + r + N_{\text{eff}} + m_s^{\text{eff}}) - \chi_{\text{best-fit}}^2(\Lambda\text{CDM} + r) = -4.3 \quad (4.8)$$

i.e., the $\Lambda\text{CDM}+r+N_{\text{eff}}+m_s^{\text{eff}}$ model provides a better χ^2 fit compared to $\Lambda\text{CDM}+r$. But due to the 2 extra parameters, $\Delta\text{AIC} = -0.3$. Since this difference is small, it implies that the goodness of fits to the TT+lowP+R16 data for the two models are similar.

Since the main aim of this work is to analyze the role of the BK14 data, Table 4.3 lists the bounds on the cosmological parameters, now with BK14 data included in each combination. The inclusion of the BK14 data seems to have almost no effect on the bounds of N_{eff} and H_0 , as can be seen by comparing the results of Table 4.2 and Table 4.3. However, bounds on m_s^{eff} improve slightly across all data combinations. The 1-D marginalized posteriors for m_s^{eff} and r for various datasets are shown in Figure 4.2. While for TT+lowP, we had $m_s^{\text{eff}} < 0.78$ eV, this bound improves to $m_s^{\text{eff}} < 0.68$ eV with TT+lowP+BK14. Addition of BAO data further improves this bound to $m_s^{\text{eff}} < 0.46$ eV. Our most aggressive bound in this work comes with TT+lowP+BK14+R16: $m_s^{\text{eff}} < 0.28$ eV.

Effect of BK14 data on sum of active neutrino masses ($\sum m_\nu$) was also studied by us in Chapter 2, in the $\Lambda\text{CDM} + r + \sum m_\nu$ model. This is also seen in the recent Planck 2018 results, where they provide a bound of $\sum m_\nu < 0.12$ eV with Planck TT,TE,EE+lowE+lensing+BAO data in $\Lambda\text{CDM} + \sum m_\nu$ model [33], whereas the bound is $\sum m_\nu < 0.11$ eV with Planck TT,TE,EE+lowE+lensing+BK14+BAO data in the $\Lambda\text{CDM}+r+\sum m_\nu$ model [187]. This effect persists even in a 12 parameter extended cosmology with NPDDE, as we saw in Chapter 3. In this work we have shown that such an effect is also present in an extended ΛCDM cosmology with light

sterile neutrinos.

To explain the results, we follow similar arguments as in Chapter 2. As we have seen in previous two chapters, BK14 data significantly constrains the tensor-to-scalar ratio, r . TT+lowP provides $r < 0.127$ whereas TT+lowP+BK14 gives a constraint of $r < 0.068$. However, we found only a very small correlation between r and m_s^{eff} , and that does not explain the decrease in mass. In fact the correlation coefficient between r and m_s^{eff} to be $R_{m_s^{\text{eff}},r} = -0.08$ with TT+lowP and $R_{m_s^{\text{eff}},r} = +0.02$ with TT+lowP+BK14, i.e., there is no significant correlation before addition of BK14 and also no significant change after. However we also find slightly increased values of σ_8 across all data combinations when BK14 is included. For instance, for TT+lowP, we have $\sigma_8 = 0.802_{-0.029}^{+0.040}$, which increases to $\sigma_8 = 0.814_{-0.027}^{+0.036}$ with TT+lowP+BK14. σ_8 and m_s^{eff} , both are strongly anti-correlated, as was the case for σ_8 and $\sum m_\nu$ in Chapter 1. Indeed, we found $R_{\sigma_8, m_s^{\text{eff}}} = -0.84$ with TT+lowP and $R_{\sigma_8, m_s^{\text{eff}}} = -0.81$ with TT+lowP+BK14, and hence, even such small changes in σ_8 should also create small changes in m_s^{eff} , which we find is the case here. This has been depicted in Figure 4.3. Again, notice that the lensing data prefers a lower σ_8 value. As in Table 4.3, TT+lowP+BK14+R16+BAO yields $\sigma_8 = 0.841_{-0.021}^{+0.025}$, whereas adding the lensing data to this combination yields a lower $\sigma_8 = 0.820_{-0.015}^{+0.019}$. Due to the same anti-correlation between σ_8 and m_s^{eff} , we see that inclusion of lensing data degrades the m_s^{eff} bounds.

Overall, we can say that the BK14 data makes the case for fully thermalized eV scale sterile neutrinos slightly worse. The parameter to justify this statement is m_s^{eff} . As we have shown that addition of the BK14 data does not affect the N_{eff} bounds,

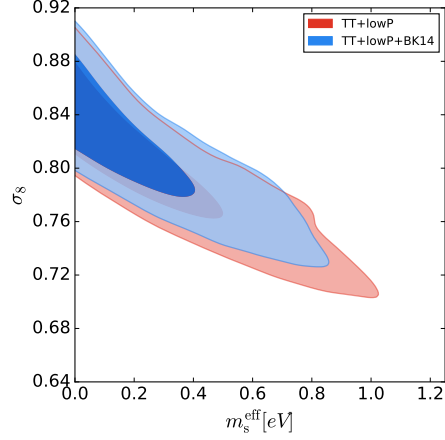


Figure 4.3: 1σ and 2σ marginalized contours for σ_8 vs. m_s^{eff} [eV] in the $\Lambda\text{CDM} + r + N_{\text{eff}} + m_s^{\text{eff}}$ model with the following combinations: TT+lowP and TT+lowP+BK14. Adding BK14 leads to slightly higher σ_8 ; and due to large anti-correlation present between σ_8 and m_s^{eff} , slightly stronger bound on m_s^{eff} is obtained.

BK14 data does not affect the thermalization situation, as far as cosmological data is concerned. However, short baseline oscillation experiments predict a fully thermalised sterile neutrino of mass $\simeq 1$ eV. This requires that both $N_{\text{eff}} = 4.046$ and $m_s^{\text{eff}} \simeq 1$ eV be allowed by the data. Since adding the BK14 data tightens the bounds on m_s^{eff} for all of the cosmological dataset combinations, it also takes the m_s^{eff} value further away from the 1 eV value, while N_{eff} bounds almost remain unchanged. The BICEP2/Keck experiment has a multipole range $20 < l < 330$ aiming to constrain the tensor-to-scalar ratio. However since r and m_s^{eff} are only weakly correlated, the slightly stronger constraints on the neutrino masses is possibly coming from gravitational lensing information encoded in the BK14 data, and not from measurement of r . This conclusion is essentially similar to what we had arrived at in Chapter 2 regarding the slight strengthening of $\sum m_\nu$ bounds with BK14 data.

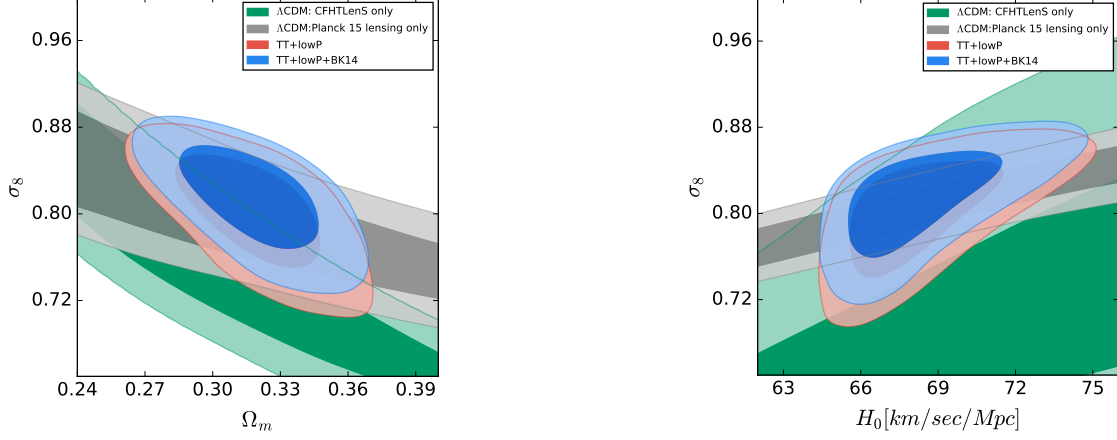


Figure 4.4: 1σ and 2σ marginalized contours for σ_8 vs. Ω_m and σ_8 vs. H_0 in the $\Lambda\text{CDM} + r + N_{\text{eff}} + m_s^{\text{eff}}$ model with the following combinations: TT+lowP and TT+lowP+BK14. We have also presented the contours in the ΛCDM model with Planck 2015 lensing and CFHTLenS data. Adding BK14 leads to slightly higher σ_8 , which worsens the agreement with CFHTLenS and Planck 2015.

H_0 and σ_8 tensions:

It is also worth noting that in ΛCDM model, with TT+lowP, Planck collaboration [87] found that $H_0 = 67.31 \pm 0.96$ km/sec/Mpc, whereas in this $\Lambda\text{CDM} + r + N_{\text{eff}} + m_s^{\text{eff}}$ model we find $H_0 = 68.35^{+1.23}_{-2.50}$ km/sec/Mpc. This preference to larger values of H_0 decreases the more than 3σ tension present in the ΛCDM model, between Planck 2015 and R16. One of the main reasons is that marginalizing over N_{eff} , which allows for $N_{\text{eff}} > 3.046$ and higher N_{eff} values prefer a higher H_0 , to keep the acoustic scale parameter θ_s fixed [87], which is very well constrained by Planck data. Thus H_0 and N_{eff} are strongly correlated.

The $\Lambda\text{CDM} + r + N_{\text{eff}} + m_s^{\text{eff}}$ model also helps in reconciling the σ_8 tension present in the $\sigma_8 - \Omega_m$ plane in ΛCDM model between Planck 2015 and weak lensing survey,

like CFHTLenS [145] and KiDS-450 [146]. As mentioned in Chapter 3, the KiDS-450 survey constrains the quantity $S_8 \equiv \sigma_8 \sqrt{\Omega_m/0.3} = 0.745 \pm 0.039$ which has a 2.3σ tension with Planck 2015 TT+lowP, which prefers a much higher value of $S_8 = 0.851 \pm 0.024$ [87]. Planck data also prefers higher values of σ_8 compared to CFHTLenS. With TT+lowP in base Λ CDM model, one gets $\sigma_8 = 0.829 \pm 0.014$ [87]. However, in this Λ CDM + r + N_{eff} + m_s^{eff} model, with TT+lowP, we get $\sigma_8 = 0.802^{+0.040}_{-0.029}$, which is much lower and thereby the conflict is decreased somewhat. We also get $S_8 = 0.824^{+0.030}_{-0.027}$, which is better agreement with KiDS-450 than Λ CDM. However, the BK14 data prefers slightly higher σ_8 values and thereby increases the tension between Planck and these weak gravitational lensing surveys. This can be visualized in Figure 4.4, where we see that the inclusion of BK14 data drives the 2D contours upwards to a small extent. In Figure 4.4, we have used the CFHTLenS data with conservative cuts as described in [87].

Another important point is that while Λ CDM+ r + N_{eff} + m_s^{eff} helps in relieving the H_0 and σ_8 tensions present in the Λ CDM model, they are not both relieved together in any region of the allowed parameter space. In the right panel of Figure 4.4, we can see that the regions where σ_8 has lower values, H_0 also has lower values (while we need higher values of H_0 to relieve the H_0 tension), and similarly, where H_0 has higher values, σ_8 also has higher values (while we need lower values of σ_8 to relieve the σ_8 tension). This in turn implies that the two conflicts are not resolved together in this model. And BK14 data worsens the conflicts even more. The R16 prior also doesn't help the issue here. As we can see from Tables 4.2 and 4.3, the inclusion of this Gaussian prior leads to a preference for much higher N_{eff} values, and higher σ_8

Parameter	TT+lowP	TT+lowP+BK14
m_s^{eff} (eV)	< 0.66	< 0.50
r	< 0.175	< 0.076
H_0 (km/sec/Mpc)	$73.92^{+2.60}_{-1.37}$	$74.20^{+2.13}_{-1.28}$
σ_8	$0.840^{+0.049}_{-0.020}$	$0.857^{+0.039}_{-0.018}$

Table 4.4: Bounds on a cosmological parameters in the $\Lambda\text{CDM}+r+m_s^{\text{eff}}$ model with $N_{\text{eff}} = 4.046$, assuming complete thermalization of sterile neutrinos. Marginalized limits are given at 68% C.L. whereas upper limits are given at 95% C.L. Note that H_0 and σ_8 are derived parameters.

Parameter	TT+lowP	TT+lowP+BK14
m_s^{eff} (eV)	< 0.83	< 0.63
r	< 0.136	< 0.070
H_0 (km/sec/Mpc)	$69.04^{+2.15}_{-1.59}$	$69.25^{+1.94}_{-1.42}$
σ_8	$0.803^{+0.051}_{-0.025}$	$0.820^{+0.041}_{-0.021}$

Table 4.5: Bounds on a cosmological parameters in the $\Lambda\text{CDM} + r + m_s^{\text{eff}}$ model with $N_{\text{eff}} = 3.5$, assuming partial thermalization of sterile neutrinos. Marginalized limits are given at 68% C.L. whereas upper limits are given at 95% C.L. Note that H_0 and σ_8 are derived parameters.

values as well, increasing the conflict.

4.2.2 Results for $\Lambda\text{CDM} + r + m_s^{\text{eff}}$ model

In this section we verify the stability of the results obtained in the previous section, by going to a smaller parameter space. We stop varying N_{eff} and fix its value to 4.046 and 3.5. The first one corresponds to complete thermalization of sterile neu-

trinos, while the later one corresponds to partial thermalization. We have restricted ourselves to CMB data only. For $N_{\text{eff}} = 4.046$ and $N_{\text{eff}} = 3.5$, the results are given in Tables 4.4 and 4.5 respectively.

We see that BK14 does help in obtaining better constraint on the sterile mass also in this reduced parameter space. For $N_{\text{eff}} = 4.046$, with TT+lowP, we get $m_s^{\text{eff}} < 0.66$ eV, whereas inclusion of BK14 leads to a tighter bound of $m_s^{\text{eff}} < 0.50$ eV. Similar case of strengthening of mass bound is seen with $N_{\text{eff}} = 3.5$, although these bounds are more relaxed compared to the case $N_{\text{eff}} = 4.046$, as a higher N_{eff} prefers a higher H_0 . Again we see that the BK14 data itself does not affect the H_0 constraints much, but heavily constraints the tensor-to-scalar ratio, and also slightly increases the preferred σ_8 values. The main conclusions made in the previous section on the larger parameter space thus remains unchanged in this smaller parameter space.

It is imperative to note that for sterile neutrinos produced by a thermal process and obeying Eq. 4.5, for $N_{\text{eff}} = 4.046$, we have $m_s^{ph} = m_s^{\text{eff}}$, whereas for $N_{\text{eff}} = 3.5$, we have $m_s^{ph} = 1.8m_s^{\text{eff}}$. Hence, for $N_{\text{eff}} = 3.5$ and with TT+lowP+BK14, we have a corresponding bound of $m_s^{ph} < 1.13$ eV. This implies that CMB data allows sterile neutrinos with mass $\simeq 1$ eV, but only with partial thermalization with $N_{\text{eff}} \simeq 3.5$. When we compare the quality of fit to the TT+lowP+BK14 data between the $\Lambda\text{CDM}+r+m_s^{\text{eff}}$ model ($N_{\text{eff}} = 3.5$ and 4.046) and the $\Lambda\text{CDM}+r$ (with $N_{\text{eff}} = N_{\text{eff}}^{\text{SM}}$), we find that,

for the $N_{\text{eff}} = 4.046$ case:

$$\Delta\chi^2 = \chi_{\text{best-fit}}^2(\Lambda\text{CDM} + r + m_s^{\text{eff}}) - \chi_{\text{best-fit}}^2(\Lambda\text{CDM} + r) = +7.03 \quad (4.9)$$

whereas, for the $N_{\text{eff}} = 3.5$ case:

$$\Delta\chi^2 = \chi_{\text{best-fit}}^2(\Lambda\text{CDM} + r + m_s^{\text{eff}}) - \chi_{\text{best-fit}}^2(\Lambda\text{CDM} + r) = -0.22 \quad (4.10)$$

These correspond to $\Delta\text{AIC} = +9.03$ (for $N_{\text{eff}} = 4.046$) and $\Delta\text{AIC} = +1.78$ (for $N_{\text{eff}} = 3.5$). Thus, the model with partial thermalization of $N_{\text{eff}} = 3.5$ provides only a slightly worse fit to the data compared to the $\Lambda\text{CDM} + r$ model (with $N_{\text{eff}} = N_{\text{eff}}^{\text{SM}}$), and is preferred by the data much more than the full-thermalization case. This is not surprising as in the previous section we had seen that CMB data alone did not allow complete thermalization.

4.3 Discussion

Short Baseline (SBL) Oscillation anomalies have hinted towards a fully thermalized sterile neutrino with mass around 1 eV. In this work we have studied, for the first time, the light eV scale sterile neutrino situation in cosmology in light of the BICEP2/Keck array 2014 CMB B-mode polarization data. We call this dataset BK14. We first considered an extended- ΛCDM scenario with tensor perturbations and sterile neutrino parameters: $\Lambda\text{CDM} + r + N_{\text{eff}} + m_s^{\text{eff}}$ model. Apart from BK14, we have used Planck 2015 temperature and low- l polarization data (TT+lowP), latest

BAO data and a Gaussian prior on the Hubble constant (R16) from local measurements. We find that inclusion of the BK14 data has almost no effect on the bounds of N_{eff} and H_0 but it strengthens the bounds on m_s^{eff} to a small extent by preferring slightly higher values of σ_8 , with which m_s^{eff} is strongly anti-correlated. The BK14 data also tightly constraints the tensor-to-scalar ratio, r but we find negligible correlation between r and m_s^{eff} . This makes us think that the effect on mass is coming from the gravitational lensing information encoded in the B-mode polarization and not from the Inflationary Gravitational Waves. The bound of $m_s^{\text{eff}} < 0.46$ eV (95% C.L.) is found for the combination of Planck 2015, BAO and BK14 datasets, whereas the bound is $m_s^{\text{eff}} < 0.53$ eV (95% C.L.) without the BK14 data. Our most aggressive bound of $m_s^{\text{eff}} < 0.28$ eV (95% C.L.) is obtained with Planck 2015, R16 and BK14. The R16 prior also leads to high N_{eff} values which allow full thermalization of the sterile neutrino (at 2σ) but such high values are in conflict with bounds from Big Bang Nucleosynthesis. Also, addition of the R16 prior to the TT+lowP data leads to a slightly worse χ^2 fit to the data. On the other hand, it is to be noted that as per the Akaike information criterion (AIC) the $\Lambda\text{CDM} + r + N_{\text{eff}} + m_s^{\text{eff}}$ model provides equally good fit to the data as the $\Lambda\text{CDM} + r$ model, for the TT+lowP+R16 data combination. Previous studies have indicated that fully thermalized sterile neutrinos with mass ~ 1 eV (as predicted by SBL experiments) are disfavoured by cosmological data. Our analysis indicates that it becomes slightly more disfavoured with the inclusion of BK14 data, due to tighter mass bounds. The BK14 data also seems to make the agreement between Planck 2015 and CFHTLenS (weak gravitational lensing data) worse due to the higher σ_8 values.

We would also like to mention that the Planck 2018 results, released after the above work was completed, indirectly confirmed tightening of bounds on $\sum m_\nu$ with BK14. They provide a bound of $\sum m_\nu < 0.12$ eV with Planck TT,TE,EE + lowE + lensing + BAO data in Λ CDM + $\sum m_\nu$ model [33], whereas the bound is $\sum m_\nu < 0.11$ eV with Planck TT,TE,EE + lowE + lensing + BK14 + BAO data in the Λ CDM + r + $\sum m_\nu$ model [187]. Thus we expect our main conclusion regarding BK14 helping in improving the bound on sterile neutrino mass will remain unchanged if used with the recent Planck 2018 likelihoods instead of Planck 2015 that we have used in this work.

While this work was still being completed, a new B-mode polarization data was released publicly, from the same BICEP2/Keck collaboration. This newly released data includes all the measurements upto and including 2015, and thus we call it BK15 [188]. To understand the effect of the new data, we performed an MCMC analysis with TT+lowP+R16+BK15 in the Λ CDM + r + N_{eff} + m_s^{eff} model (with all other settings remaining unchanged). We found the following bounds: $m_s^{\text{eff}} < 0.27$ eV (95% C.L.), $r < 0.061$, and $\sigma_8 = 0.847^{+0.026}_{-0.021}$. In the same model, when we had used BK14 instead of BK15, we had found (see Table 4.3), $m_s^{\text{eff}} < 0.28$ eV (95% C.L.), $r < 0.073$, and $\sigma_8 = 0.846^{+0.026}_{-0.020}$. As we can see, that while the bound on r changes, the bounds on m_s^{eff} and σ_8 almost remain unchanged. We also checked that other parameters of interest, like H_0 and N_{eff} change negligibly. As before, since r and m_s^{eff} have only a very weak correlation, it doesn't affect the mass bound. On the other hand, since TT+lowP+R16+BK15 almost doesn't change the bound on σ_8 , the mass bound almost remains the same. Thus, we find that reanalysis with

BK15 instead of BK14 will not change the neutrino mass bounds much.

Conclusions and future outlook

Neutrino oscillation experiments have firmly confirmed that the three active neutrinos have 3 distinct mass eigenstates with small but distinct masses, with the option of the lightest neutrino being massless. These mass eigenstates are quantum superpositions of the flavor eigenstates, namely the electron neutrino, muon neutrino, and tau neutrino. While the current oscillation experiments are sensitive to the (squared) mass splittings, they don't say anything about the mass of the lightest neutrino. On the other hand, neutrino masses have non-trivial impact on the evolution of the universe, and we can get a measure of the sum of the masses by observing its impact on CMB and LSS. Due to these reasons, strongest bounds on the sum of these neutrino masses ($\sum m_\nu$) come from cosmological data. However, current cosmological data can only provide an upper bound to $\sum m_\nu$. Detection of the non-zero neutrino mass sum is one of the important goals of near future CMB and LSS surveys. This thesis is a thorough study on the bounds on neutrino masses coming from recent cosmological data in various cosmological models.

In chapter 2, we discuss the first paper which contributes towards this thesis [85]. In this work, using latest datasets publicly available at the time of inception of this work, we provided strong bounds on $\sum m_\nu$ in the backdrop of Λ CDM model and some of its simple extensions with tensor perturbations and dynamical dark energy. We considered five different cosmological models: Λ CDM+ $\sum m_\nu$, Λ CDM+ r + $\sum m_\nu$, w_0w_a CDM + $\sum m_\nu$ (DDE), w_0w_a CDM + $\sum m_\nu$ with $w(z) \geq -1$ (NPDDE), and w_0w_a CDM+ r + $\sum m_\nu$ with $w(z) \geq -1$ (NPDDE+ r). Here $w(z) = w_0 + w_a z / (1+z)$, defined at a redshift z , is the dark energy equation of state with CPL parametrization. r is the tensor to scalar ratio with the pivot scale of $k_* = 0.05 h Mpc^{-1}$. Given a particular cosmological model and dataset combination, we perform a Bayesian analysis using the MCMC sampler CosmoMC that uses CAMB as the Boltzmann solver. Among datasets, along with CMB temperature anisotropy data (TT) from Planck 2015 [87], we have used BAO measurements from various galaxy surveys like SDSS-III BOSS DR12, MGS and 6dFGS; SNe Ia luminosity distance measurements from Pantheon Sample (PAN); the BK14 data (B-mode polarization of CMB) from the BICEP2/Keck Collaboration; and suitable Gaussian prior of $\tau = 0.055 \pm 0.009$ ($\tau 0p055$) on the reionization optical depth. These priors help breaking the mutual degeneracies of H_0 and τ with $\sum m_\nu$ present in the Planck data. The prior on τ was taken from Planck 2016 intermediate results [114] determined from improved analysis of the low- l polarization data (lowP) of Planck. This was a significant improvement in the measurement of τ from Planck 2015 and since τ and $\sum m_\nu$ are strongly correlated in the Planck TT data, we took it into account. We exclude the Planck 2015 lowP data when we include $\tau 0p055$, to avoid any double counting. For

the minimal Λ CDM + $\sum m_\nu$ model we find a robust upper bound of $\sum m_\nu < 0.152$ eV at 95% C.L. with the use of TT + BAO + PAN + τ_{0p055} . Adding the high- l polarization data from Planck strengthens this bound to $\sum m_\nu < 0.118$ eV. This is very close to the $\sum m_\nu \simeq 0.1$ eV, the minimum mass sum allowed for inverted hierarchy. Later, Planck 2018 [33] confirmed the same bound of $\sum m_\nu < 0.120$ eV using Planck 2018 TTTEEE+lowE+lensing+BAO data, thereby confirming that for the Λ CDM + $\sum m_\nu$ model, this τ -prior method works. This bound is strengthened to $\sum m_\nu < 0.110$ eV in Λ CDM + r + $\sum m_\nu$ model with an additional dataset, BK14. This bound becomes better, to $\sum m_\nu < 0.101$ eV in a model with non-phantom dynamical dark energy (NPDDE). Next, considering the NPDDE+ r model and including the BK14 data, the bound can be even further reduced to $\sum m_\nu < 0.093$ eV. So in these models with NPDDE we end up with $\sum m_\nu$ bounds which are even tighter than Λ CDM + $\sum m_\nu$. For the DDE model (without any extra prior on w_0 and w_a), the bound however relaxes to $\sum m_\nu < 0.276$ eV. Including the R16 prior on the Hubble constant ($H_0 = 73.24 \pm 1.74$ km/sec/Mpc) from Hubble Space Telescope (HST), the above bounds get even better, to $\sum m_\nu < 0.117$ eV, 0.091 eV, 0.085 eV, 0.082 eV, 0.078 eV and 0.247 eV respectively. These improvements are mostly due to a greater than 3σ tension between Planck 2015 and Hubble Space Telescope measurements of the Hubble constant in the Λ CDM model, and should be taken cautiously. However, there is a possibility that both Planck and R16 might be correct and the discrepancy has to be explained by some new physics.

The fact that in the non-phantom dynamical dark energy models the neutrino mass bounds are tighter than Λ CDM + $\sum m_\nu$ increased our interest in cosmologies

with massive neutrinos and non-phantom dynamical dark energy. The non-phantom ($w(z) \geq -1$) part of the $w_0 - w_a$ parameter space corresponds to single field dark energy models like Quintessence and these are of considerable theoretical interest. We thus wanted to study this kind of dark energy further in an even more extended parameter space to see if the mass bounds still remain tighter than $\Lambda\text{CDM} + \sum m_\nu$.

In chapter 3, we discuss the second paper which contributes towards this thesis [141]. In this work, we have studied constraints on $\sum m_\nu$ in three different largely extended cosmological scenarios with NPDDE. In the first model, NPDDE11+r, we consider 12 parameters: the 6 ΛCDM parameters, two dynamical dark energy parameters w_0 and w_a , N_{eff} , $\sum m_\nu$, r , and the running of the spectral index (n_{run}). We used various combinations of recent datasets including Planck 2015 temperature and polarization data (Planck), Planck 2015 lensing data (hereafter lensing), and also BK14, BAO, R16, PAN. The most aggressive bound on neutrino masses in this model came from Planck+BK14+BAO: $\sum m_\nu < 0.123$ eV (95% C.L.) which is stronger than a bound of $\sum m_\nu < 0.158$ eV (95% C.L.) obtained in $\Lambda\text{CDM} + \sum m_\nu$ with Planck+BAO. We have tested the stability of these results in a lower parameter space (model: NPDDE11) where we excluded the tensor perturbations (and thus the parameter r) and the results were consistent. The third and final model we studied in this chapter is the NPDDE11+ A_{lens} model, where we also varied the parameter A_{lens} , which is the scaling of the lensing amplitude. We observed that except when Planck lensing data was included, the $A_{\text{lens}} = 1$ was discarded at more than 95% C.L. A_{lens} is strongly correlated with $\sum m_\nu$. Due to this, the $\sum m_\nu$ bounds worsen in this model with our best result being: $\sum m_\nu < 0.239$ eV (95% C.L.; Planck+BAO).

Leaving aside active neutrinos, we now move on to sterile neutrinos. In chapter 4, we discuss the third paper which contributes towards this thesis [153]. In this work, we study the thermal light (eV scale) sterile neutrino situation (3+1 scenario) from cosmological perspective. In this paper, we have, for the first time, used the BK14 data to constrain the effective mass (m_s^{eff}) and energy density parameters associated with sterile neutrinos. We considered an extended- Λ CDM cosmology: Λ CDM + r + N_{eff} + m_s^{eff} . Apart from BK14, we have used Planck 2015 TT+lowP, lensing, BAO and R16. We find that BK14 data makes the constraints on m_s^{eff} stronger to some extent by preferring higher σ_8 values. The bound of $m_s^{\text{eff}} < 0.46$ eV (95% C.L.) is found for the combination of TT+lowP, BAO and BK14 datasets. On the other hand, the bound is $m_s^{\text{eff}} < 0.53$ eV (95% C.L.) without the BK14 data. Our most aggressive bound of $m_s^{\text{eff}} < 0.28$ eV (95% C.L.) is obtained with TT+lowP, R16 and BK14, while without BK14 we get $m_s^{\text{eff}} < 0.34$ eV (95% C.L.). Note that similar effect on $\sum m_\nu$ was seen in previous two chapters. Inclusion of the BK14 data also provides considerably stronger constraints to the tensor-to-scalar ratio, r but we find negligible correlation between r and m_s^{eff} . Thus we conclude that the effect on the neutrino mass is coming from the weak gravitational lensing information encoded in the CMB B-mode polarization spectrum of BK14. Previous cosmological studies have shown that fully thermalized sterile neutrinos with mass ~ 1 eV (as favoured by short baseline experiments) are disfavoured by cosmological data. Our analysis indicates that such light sterile neutrinos become slightly more disfavoured with the inclusion of BK14 data, due to tighter bounds on the effective mass of the sterile neutrino.

This work provides a lot of scope for future work especially in the field of neutrino cosmology. There are a lot of opportunities in determining neutrino properties from future data, a plethora of which will be available within the next few years: DESI [189], Euclid [190], LSST [191], CMB-S4 [192], Simons Observatory [193], LiteBIRD [194], PIXIE [195], CLASS [196], and so on. These future experiments will possibly be able to provide evidence of non-zero neutrino masses, instead of just an upper bound from current experiments, and might even say something conclusive about neutrino mass hierarchy. Currently, as mentioned in Chapter 1, bounds on $\sum m_\nu$ depend greatly on the chosen prior and this is likely to change in the near future. Improvement of measurements on CMB polarization and lensing, optical depth to reionization, galaxy clustering, galaxy-lensing cross-correlation, SZ cluster abundances, cosmic voids etc in the next decade holds a lot of promise in strongly constraining the sum of neutrino masses, and in determining the neutrino mass hierarchy (see [197] for a brief description). See [198–203] for forecasts on neutrino mass from possible future experiments. See also [204–206] for the current status of determination of neutrino mass hierarchy from various experiments.

Apart from neutrino masses, another interesting beyond standard model physics that I would like to work on is non-standard neutrino interactions [207–211] which can partially solve the H_0 and σ_8 tension. In the sterile sector the tension between short baseline neutrino oscillation experiments and cosmological datasets has led to the development of a number of ideas to reconcile the eV-scale sterile neutrinos with cosmology. These include introduction of “secret interactions” among sterile neutrinos which modifies the background potential and blocks thermalization

[164, 171, 178, 179, 212–215], changes to the cosmological expansion rate at the time of production of sterile neutrinos [216] or large lepton asymmetry [217], very low reheating temperature [218] etc. The recent results from the MiniBooNE collaboration [162] have rekindled the interest in the sterile neutrinos. In future, I am particularly interested in working on the case of self interactions in the active or sterile sector.

N-body simulations including massive neutrinos [219–224] is another area that one can work on. Massive neutrinos can greatly affect structure formation and thus it is imperative to do all the non-linear calculations very precisely incorporating neutrino effects, which is possible with an N-body simulation code. Massive neutrinos also induce a scale dependent galaxy bias, even in large scales, which is not important for current galaxy surveys given the sensitivity of current surveys, but will be important to be included in the analysis of data from future galaxy surveys [225–227] for proper estimation of neutrino masses. Thus it is also an important direction I would like to work on.

Apart from neutrinos, one can investigate the viability of various inflationary models in light of future data, especially from the CMB B-mode polarization, whose measurements are predicted to improve largely in the future experiments like LiteBIRD and PIXIE. In case of dark energy, various Dark energy parametrizations for the Equation of State [228], or non-parametric reconstruction using principal component analysis or Gaussian processes [229, 230], will likely be constrained with much narrower limits with data from surveys like DESI and Euclid, and I would like to work in this direction in the future.

Dark energy-dark matter interactions have shown promise in solving both the H_0 and σ_8 tension simultaneously [231, 232]. See also [233–238] for some other recent studies involving dark sector interactions. In future I would like to work in this area. Another interesting research area I am interested in is dark matter self-interactions [239, 240] or interaction with other particle components in cosmology, like neutrinos [241]. These interactions hold potential to solve some anomalies in small scale structure formation, like the core vs cusp issue, and also the σ_8 tension.

References

- [1] S. M. Carroll, *Spacetime and Geometry* (Cambridge University Press, 2019).
- [2] A. Friedmann, “On the Possibility of a world with constant negative curvature of space,” *Z. Phys.* **21**, 326–332 (1924), [Gen. Rel. Grav.31,2001(1999)].
- [3] G. Lemaitre, “A homogeneous universe of constant mass and increasing radius accounting for the radial velocity of extra-galactic nebulae,” *Mon. Not. Roy. Astron. Soc.* **91**, 483–490 (1931).
- [4] H. P. Robertson, “Kinematics and World-Structure,” *Astrophys. J.* **82**, 284–301 (1935).
- [5] K. Abe *et al.* (T2K), “Observation of Electron Neutrino Appearance in a Muon Neutrino Beam,” *Phys. Rev. Lett.* **112**, 061802 (2014), arXiv:1311.4750 [hep-ex] .
- [6] Y. Abe *et al.* (Double Chooz), “Reactor electron antineutrino disappear-

References

- ance in the Double Chooz experiment,” *Phys. Rev.* **D86**, 052008 (2012), [arXiv:1207.6632 \[hep-ex\]](#) .
- [7] F. P. An *et al.* (Daya Bay), “Observation of electron-antineutrino disappearance at Daya Bay,” *Phys. Rev. Lett.* **108**, 171803 (2012), [arXiv:1203.1669 \[hep-ex\]](#) .
- [8] T. Araki *et al.* (KamLAND), “Measurement of neutrino oscillation with KamLAND: Evidence of spectral distortion,” *Phys. Rev. Lett.* **94**, 081801 (2005), [arXiv:hep-ex/0406035 \[hep-ex\]](#) .
- [9] Y. Fukuda *et al.* (Super-Kamiokande), “Evidence for oscillation of atmospheric neutrinos,” *Phys. Rev. Lett.* **81**, 1562–1567 (1998), [arXiv:hep-ex/9807003 \[hep-ex\]](#) .
- [10] B. Pontecorvo, “Inverse beta processes and nonconservation of lepton charge,” *Sov. Phys. JETP* **7**, 172–173 (1958), [*Zh. Eksp. Teor. Fiz.*34,247(1957)].
- [11] Z. Maki, M. Nakagawa, and S. Sakata, “Remarks on the unified model of elementary particles,” *Prog. Theor. Phys.* **28**, 870–880 (1962), [,34(1962)].
- [12] P. Hernandez, “Neutrino physics,” in *High-energy physics. Proceedings, 5th CERN-Latin-American School, Recinto Quirama, Colombia, March 15-28, 2009* (2010) [arXiv:1010.4131 \[hep-ph\]](#) .
- [13] I. Esteban, M. C. Gonzalez-Garcia, A. Hernandez-Cabezudo, M. Maltoni, and T. Schwetz, “Global analysis of three-flavour neutrino oscillations: synergies

References

- and tensions in the determination of θ_{23} , δ_{CP} , and the mass ordering,” [JHEP **01**, 106 \(2019\)](#), [arXiv:1811.05487 \[hep-ph\]](#) .
- [14] A. D. Sakharov, “Violation of CP Invariance, C asymmetry, and baryon asymmetry of the universe,” [Pisma Zh. Eksp. Teor. Fiz. **5**, 32–35 \(1967\)](#), [[Usp. Fiz. Nauk161,no.5,61\(1991\)](#)].
- [15] M. Trodden, “Electroweak baryogenesis,” [Rev. Mod. Phys. **71**, 1463–1500 \(1999\)](#), [arXiv:hep-ph/9803479 \[hep-ph\]](#) .
- [16] A. Riotto, “Theories of baryogenesis,” in *Proceedings, Summer School in High-energy physics and cosmology: Trieste, Italy, June 29-July 17, 1998* (1998) pp. 326–436, [arXiv:hep-ph/9807454 \[hep-ph\]](#) .
- [17] F. Englert and R. Brout, “Broken Symmetry and the Mass of Gauge Vector Mesons,” [Phys. Rev. Lett. **13**, 321–323 \(1964\)](#), [[,157\(1964\)](#)].
- [18] P. W. Higgs, “Broken symmetries, massless particles and gauge fields,” [Phys. Lett. **12**, 132–133 \(1964\)](#).
- [19] P. W. Higgs, “Broken Symmetries and the Masses of Gauge Bosons,” [Phys. Rev. Lett. **13**, 508–509 \(1964\)](#), [[,160\(1964\)](#)].
- [20] P. W. Higgs, “Spontaneous Symmetry Breakdown without Massless Bosons,” [Phys. Rev. **145**, 1156–1163 \(1966\)](#).
- [21] G. S. Guralnik, C. R. Hagen, and T. W. B. Kibble, “Global Conservation Laws and Massless Particles,” [Phys. Rev. Lett. **13**, 585–587 \(1964\)](#), [[,162\(1964\)](#)].

- [22] G. Aad *et al.* (ATLAS), “Observation of a new particle in the search for the Standard Model Higgs boson with the ATLAS detector at the LHC,” *Phys. Lett.* **B716**, 1–29 (2012), [arXiv:1207.7214 \[hep-ex\]](#) .
- [23] S. Chatrchyan *et al.* (CMS), “Observation of a New Boson at a Mass of 125 GeV with the CMS Experiment at the LHC,” *Phys. Lett.* **B716**, 30–61 (2012), [arXiv:1207.7235 \[hep-ex\]](#) .
- [24] D. J. Gross and F. Wilczek, “Asymptotically Free Gauge Theories - I,” *Phys. Rev.* **D8**, 3633–3652 (1973).
- [25] S. Hannestad and J. Madsen, “Neutrino decoupling in the early universe,” *Phys. Rev.* **D52**, 1764–1769 (1995), [arXiv:astro-ph/9506015 \[astro-ph\]](#) .
- [26] G. Mangano, G. Miele, S. Pastor, T. Pinto, O. Pisanti, and P. D. Serpico, “Relic neutrino decoupling including flavor oscillations,” *Nucl. Phys.* **B729**, 221–234 (2005), [arXiv:hep-ph/0506164 \[hep-ph\]](#) .
- [27] P. F. de Salas and S. Pastor, “Relic neutrino decoupling with flavour oscillations revisited,” *JCAP* **1607**, 051 (2016), [arXiv:1606.06986 \[hep-ph\]](#) .
- [28] M. Escudero, “Neutrino decoupling beyond the Standard Model: CMB constraints on the Dark Matter mass with a fast and precise N_{eff} evaluation,” *JCAP* **1902**, 007 (2019), [arXiv:1812.05605 \[hep-ph\]](#) .
- [29] D. Tytler, J. M. O’Meara, N. Suzuki, and D. Lubin, “Review of Big Bang nucleosynthesis and primordial abundances,” *Phys. Scripta* **T85**, 12 (2000), [arXiv:astro-ph/0001318 \[astro-ph\]](#) .

References

- [30] B. Fields and S. Sarkar, “Big-Bang nucleosynthesis (2006 Particle Data Group mini-review),” (2006), [arXiv:astro-ph/0601514 \[astro-ph\]](#) .
- [31] G. Steigman, “Neutrinos And Big Bang Nucleosynthesis,” *Adv. High Energy Phys.* **2012**, 268321 (2012), [arXiv:1208.0032 \[hep-ph\]](#) .
- [32] B. D. Fields, P. Molaro, and S. Sarkar, “Big-Bang Nucleosynthesis,” *Chin. Phys.* **C38**, 339–344 (2014), [arXiv:1412.1408 \[astro-ph.CO\]](#) .
- [33] N. Aghanim *et al.* (Planck), “Planck 2018 results. VI. Cosmological parameters,” (2018), [arXiv:1807.06209 \[astro-ph.CO\]](#) .
- [34] J. Miralda-Escude, “The dark age of the universe,” *Science* **300**, 1904–1909 (2003), [arXiv:astro-ph/0307396 \[astro-ph\]](#) .
- [35] A. Natarajan and N. Yoshida, “The Dark Ages of the Universe and Hydrogen Reionization,” *PTEP* **2014**, 06B112 (2014), [arXiv:1404.7146 \[astro-ph.CO\]](#) .
- [36] S. Furlanetto *et al.*, “Astro 2020 Science White Paper: Fundamental Cosmology in the Dark Ages with 21-cm Line Fluctuations,” (2019), [arXiv:1903.06212 \[astro-ph.CO\]](#) .
- [37] L. Bergstrom and A. Goobar, *Cosmology and particle astrophysics* (1999).
- [38] S. Dodelson, *Modern Cosmology* (Academic Press, Amsterdam, 2003).
- [39] S. Weinberg, *Cosmology* (2008).

References

- [40] J. Lesgourgues, G. Mangano, G. Miele, and S. Pastor, *Neutrino Cosmology* (Cambridge University Press, 2013).
- [41] C.-P. Ma and E. Bertschinger, “Cosmological perturbation theory in the synchronous and conformal Newtonian gauges,” *Astrophys. J.* **455**, 7–25 (1995), [arXiv:astro-ph/9506072 \[astro-ph\]](#) .
- [42] A. Lewis, A. Challinor, and A. Lasenby, “Efficient computation of CMB anisotropies in closed FRW models,” *Astrophys. J.* **538**, 473–476 (2000), [arXiv:astro-ph/9911177 \[astro-ph\]](#) .
- [43] D. Blas, J. Lesgourgues, and T. Tram, “The Cosmic Linear Anisotropy Solving System (CLASS) II: Approximation schemes,” *JCAP* **1107**, 034 (2011), [arXiv:1104.2933 \[astro-ph.CO\]](#) .
- [44] J. Lesgourgues and S. Pastor, “Neutrino mass from Cosmology,” *Adv. High Energy Phys.* **2012**, 608515 (2012), [arXiv:1212.6154 \[hep-ph\]](#) .
- [45] M. Lattanzi and M. Gerbino, “Status of neutrino properties and future prospects - Cosmological and astrophysical constraints,” *Front.in Phys.* **5**, 70 (2018), [arXiv:1712.07109 \[astro-ph.CO\]](#) .
- [46] A. D. Dolgov, “Neutrinos in cosmology,” *Phys. Rept.* **370**, 333–535 (2002), [arXiv:hep-ph/0202122 \[hep-ph\]](#) .
- [47] S. Hannestad, “Neutrinos in cosmology,” *New J. Phys.* **6**, 108 (2004), [arXiv:hep-ph/0404239 \[hep-ph\]](#) .

- [48] M. Fukugita, “Massive neutrinos in cosmology,” *Proceedings, 7th International Workshop on Neutrino factories and superbeams (NuFact05): Frascati, Italy, June 21-26, 2005*, *Nucl. Phys. Proc. Suppl.* **155**, 10–17 (2006), [arXiv:hep-ph/0511068 \[hep-ph\]](#) .
- [49] S. Hannestad, “Introduction to neutrino cosmology,” *Neutrinos in cosmology, in astro, particle and nuclear physics. Proceedings, International School on Nuclear Physics, 27th Course, Erice, Italy, September 16-24, 2005*, *Prog. Part. Nucl. Phys.* **57**, 309–323 (2006), [[309\(2005\)](#)], [arXiv:astro-ph/0511595 \[astro-ph\]](#) .
- [50] J. Lesgourgues and S. Pastor, “Massive neutrinos and cosmology,” *Phys. Rept.* **429**, 307–379 (2006), [arXiv:astro-ph/0603494 \[astro-ph\]](#) .
- [51] A. D. Dolgov, “Cosmology and Neutrino Properties,” *Physics of Fundamental Interactions Moscow, Russia, November 25-30, 2007*, *Phys. Atom. Nucl.* **71**, 2152–2164 (2008), [arXiv:0803.3887 \[hep-ph\]](#) .
- [52] S. Hannestad, “Neutrino physics from precision cosmology,” *Prog. Part. Nucl. Phys.* **65**, 185–208 (2010), [arXiv:1007.0658 \[hep-ph\]](#) .
- [53] Y. Y. Y. Wong, “Neutrino mass in cosmology: status and prospects,” *Ann. Rev. Nucl. Part. Sci.* **61**, 69–98 (2011), [arXiv:1111.1436 \[astro-ph.CO\]](#) .
- [54] A. B. Balantekin and G. M. Fuller, “Neutrinos in Cosmology and Astrophysics,” *Prog. Part. Nucl. Phys.* **71**, 162–166 (2013), [arXiv:1303.3874 \[nucl-th\]](#) .

References

- [55] J. Lesgourgues and S. Pastor, “Neutrino cosmology and Planck,” *New J. Phys.* **16**, 065002 (2014), [arXiv:1404.1740 \[hep-ph\]](#) .
- [56] L. Verde, “Neutrino properties from cosmology,” *Proceedings, Topical Research Meeting on Prospects in Neutrino Physics (NuPhys2013): London, UK, December 19–20, 2013*, *J. Phys. Conf. Ser.* **598**, 012010 (2015).
- [57] K. N. Abazajian and M. Kaplinghat, “Neutrino Physics from the Cosmic Microwave Background and Large-Scale Structure,” *Ann. Rev. Nucl. Part. Sci.* **66**, 401–420 (2016).
- [58] M. Archidiacono, T. Brinckmann, J. Lesgourgues, and V. Poulin, “Neutrino properties from cosmology,” in *Proceedings, Prospects in Neutrino Physics (NuPhys2016): London, UK, December 12–14, 2016* (2017) [arXiv:1705.00496 \[astro-ph.CO\]](#) .
- [59] M. Gerbino, “Neutrino properties from cosmology,” in *Proceedings, Prospects in Neutrino Physics (NuPhys2017): London, UK, December 20–22, 2017* (2018) pp. 52–52, [arXiv:1803.11545 \[astro-ph.CO\]](#) .
- [60] W. Hu and S. Dodelson, “Cosmic Microwave Background Anisotropies,” *Ann. Rev. Astron. Astrophys.* **40**, 171–216 (2002), [arXiv:astro-ph/0110414 \[astro-ph\]](#) .
- [61] Z. Hou *et al.*, “Constraints on Cosmology from the Cosmic Microwave Background Power Spectrum of the 2500 deg² SPT-SZ Survey,” *Astrophys. J.* **782**, 74 (2014), [arXiv:1212.6267 \[astro-ph.CO\]](#) .

References

- [62] W. Hu, D. J. Eisenstein, and M. Tegmark, “Weighing neutrinos with galaxy surveys,” *Phys. Rev. Lett.* **80**, 5255–5258 (1998), [arXiv:astro-ph/9712057 \[astro-ph\]](#) .
- [63] J. Brandbyge, S. Hannestad, T. Haugbølle, and B. Thomsen, “The Effect of Thermal Neutrino Motion on the Non-linear Cosmological Matter Power Spectrum,” *JCAP* **0808**, 020 (2008), [arXiv:0802.3700 \[astro-ph\]](#) .
- [64] S. Saito, M. Takada, and A. Taruya, “Nonlinear power spectrum in the presence of massive neutrinos: perturbation theory approach, galaxy bias and parameter forecasts,” *Phys. Rev.* **D80**, 083528 (2009), [arXiv:0907.2922 \[astro-ph.CO\]](#) .
- [65] S. Hannestad, T. Haugbolle, and C. Schultz, “Neutrinos in Non-linear Structure Formation - a Simple SPH Approach,” *JCAP* **1202**, 045 (2012), [arXiv:1110.1257 \[astro-ph.CO\]](#) .
- [66] A. Mead, C. Heymans, L. Lombriser, J. Peacock, O. Steele, and H. Winther, “Accurate halo-model matter power spectra with dark energy, massive neutrinos and modified gravitational forces,” *Mon. Not. Roy. Astron. Soc.* **459**, 1468–1488 (2016), [arXiv:1602.02154 \[astro-ph.CO\]](#) .
- [67] F. De Bernardis, T. D. Kitching, A. Heavens, and A. Melchiorri, “Determining the Neutrino Mass Hierarchy with Cosmology,” *Phys. Rev.* **D80**, 123509 (2009), [arXiv:0907.1917 \[astro-ph.CO\]](#) .

- [68] R. Jimenez, T. Kitching, C. Pena-Garay, and L. Verde, “Can we measure the neutrino mass hierarchy in the sky?” *JCAP* **1005**, 035 (2010), [arXiv:1003.5918 \[astro-ph.CO\]](#) .
- [69] R. Jimenez, C. P. Garay, and L. Verde, “Neutrino footprint in Large Scale Structure,” *Phys. Dark Univ.* **15**, 31–34 (2017), [arXiv:1602.08430 \[astro-ph.CO\]](#) .
- [70] L. Verde, “A practical guide to Basic Statistical Techniques for Data Analysis in Cosmology,” (2007), [arXiv:0712.3028 \[astro-ph\]](#) .
- [71] R. Trotta, “Bayes in the sky: Bayesian inference and model selection in cosmology,” *Contemp. Phys.* **49**, 71–104 (2008), [arXiv:0803.4089 \[astro-ph\]](#) .
- [72] A. Heavens, “Statistical techniques in cosmology,” (2009), [arXiv:0906.0664 \[astro-ph.CO\]](#) .
- [73] L. Verde, “Statistical methods in cosmology,” *Lect. Notes Phys.* **800**, 147–177 (2010), [arXiv:0911.3105 \[astro-ph.CO\]](#) .
- [74] R. Trotta, “Bayesian Methods in Cosmology,” (2017) [arXiv:1701.01467 \[astro-ph.CO\]](#) .
- [75] R. Bayes, “An essay toward solving a problem in the doctrine of chances,” *Phil. Trans. Roy. Soc. Lond.* **53**, 370–418 (1764).
- [76] S. Hannestad and T. Schwetz, “Cosmology and the neutrino mass ordering,” *JCAP* **1611**, 035 (2016), [arXiv:1606.04691 \[astro-ph.CO\]](#) .

- [77] M. Gerbino, M. Lattanzi, O. Mena, and K. Freese, “A novel approach to quantifying the sensitivity of current and future cosmological datasets to the neutrino mass ordering through Bayesian hierarchical modeling,” *Phys. Lett. B* **775**, 239–250 (2017), [arXiv:1611.07847 \[astro-ph.CO\]](#) .
- [78] S. Vagnozzi, E. Giusarma, O. Mena, K. Freese, M. Gerbino, S. Ho, and M. Lattanzi, “Unveiling ν secrets with cosmological data: neutrino masses and mass hierarchy,” *Phys. Rev. D* **96**, 123503 (2017), [arXiv:1701.08172 \[astro-ph.CO\]](#) .
- [79] W. Handley and M. Millea, “Maximum-Entropy Priors with Derived Parameters in a Specified Distribution,” *Entropy* **21**, 272 (2019), [arXiv:1804.08143 \[math.ST\]](#) .
- [80] F. Simpson, R. Jimenez, C. Pena-Garay, and L. Verde, “Strong Bayesian Evidence for the Normal Neutrino Hierarchy,” *JCAP* **1706**, 029 (2017), [arXiv:1703.03425 \[astro-ph.CO\]](#) .
- [81] T. Schwetz, K. Freese, M. Gerbino, E. Giusarma, S. Hannestad, M. Lattanzi, O. Mena, and S. Vagnozzi, “Comment on ”Strong Evidence for the Normal Neutrino Hierarchy”,” (2017), [arXiv:1703.04585 \[astro-ph.CO\]](#) .
- [82] B. Audren, J. Lesgourgues, S. Bird, M. G. Haehnelt, and M. Viel, “Neutrino masses and cosmological parameters from a Euclid-like survey: Markov Chain Monte Carlo forecasts including theoretical errors,” *JCAP* **1301**, 026 (2013), [arXiv:1210.2194 \[astro-ph.CO\]](#) .

References

- [83] G. J. X.-L. M. Steve Brooks, Andrew Gelman, *Handbook of Markov Chain Monte Carlo* (CRC Press, 2011).
- [84] A. Lewis and S. Bridle, “Cosmological parameters from CMB and other data: A Monte Carlo approach,” *Phys. Rev.* **D66**, 103511 (2002), [arXiv:astro-ph/0205436 \[astro-ph\]](#) .
- [85] S. Roy Choudhury and S. Choubey, “Updated Bounds on Sum of Neutrino Masses in Various Cosmological Scenarios,” *JCAP* **1809**, 017 (2018), [arXiv:1806.10832 \[astro-ph.CO\]](#) .
- [86] E. Di Valentino, E. Giusarma, O. Mena, A. Melchiorri, and J. Silk, “Cosmological limits on neutrino unknowns versus low redshift priors,” *Phys. Rev.* **D93**, 083527 (2016), [arXiv:1511.00975 \[astro-ph.CO\]](#) .
- [87] P. A. R. Ade *et al.* (Planck), “Planck 2015 results. XIII. Cosmological parameters,” *Astron. Astrophys.* **594**, A13 (2016), [arXiv:1502.01589 \[astro-ph.CO\]](#) .
- [88] N. Palanque-Delabrouille *et al.*, “Neutrino masses and cosmology with Lyman-alpha forest power spectrum,” *JCAP* **1511**, 011 (2015), [arXiv:1506.05976 \[astro-ph.CO\]](#) .
- [89] A. J. Cuesta, V. Niro, and L. Verde, “Neutrino mass limits: robust information from the power spectrum of galaxy surveys,” *Phys. Dark Univ.* **13**, 77–86 (2016), [arXiv:1511.05983 \[astro-ph.CO\]](#) .

- [90] Q.-G. Huang, K. Wang, and S. Wang, “Constraints on the neutrino mass and mass hierarchy from cosmological observations,” *Eur. Phys. J.* **C76**, 489 (2016), [arXiv:1512.05899 \[astro-ph.CO\]](#) .
- [91] S. Wang, Y.-F. Wang, and D.-M. Xia, “Constraints on the sum of neutrino masses using cosmological data including the latest extended Baryon Oscillation Spectroscopic Survey DR14 quasar sample,” *Chin. Phys.* **C42**, 065103 (2018), [arXiv:1707.00588 \[astro-ph.CO\]](#) .
- [92] R. C. Nunes and A. Bonilla, “Probing the properties of relic neutrinos using the cosmic microwave background, the Hubble Space Telescope and galaxy clusters,” *Mon. Not. Roy. Astron. Soc.* **473**, 4404–4409 (2018), [arXiv:1710.10264 \[astro-ph.CO\]](#) .
- [93] F. Capozzi, E. Di Valentino, E. Lisi, A. Marrone, A. Melchiorri, and A. Palazzo, “Global constraints on absolute neutrino masses and their ordering,” *Phys. Rev.* **D95**, 096014 (2017), [arXiv:1703.04471 \[hep-ph\]](#) .
- [94] E. Di Valentino, E. Giusarma, M. Lattanzi, O. Mena, A. Melchiorri, and J. Silk, “Cosmological Axion and neutrino mass constraints from Planck 2015 temperature and polarization data,” *Phys. Lett.* **B752**, 182–185 (2016), [arXiv:1507.08665 \[astro-ph.CO\]](#) .
- [95] P. A. R. Ade *et al.* (BICEP2, Keck Array), “Improved Constraints on Cosmology and Foregrounds from BICEP2 and Keck Array Cosmic Microwave

References

- Background Data with Inclusion of 95 GHz Band,” *Phys. Rev. Lett.* **116**, 031302 (2016), [arXiv:1510.09217 \[astro-ph.CO\]](#) .
- [96] A. Padilla, “Lectures on the Cosmological Constant Problem,” (2015), [arXiv:1502.05296 \[hep-th\]](#) .
- [97] M. Chevallier and D. Polarski, “Accelerating universes with scaling dark matter,” *Int. J. Mod. Phys.* **D10**, 213–224 (2001), [arXiv:gr-qc/0009008 \[gr-qc\]](#) .
- [98] E. V. Linder, “Exploring the expansion history of the universe,” *Phys. Rev. Lett.* **90**, 091301 (2003), [arXiv:astro-ph/0208512 \[astro-ph\]](#) .
- [99] J.-Z. Ma and X. Zhang, “Probing the dynamics of dark energy with novel parametrizations,” *Phys. Lett.* **B699**, 233–238 (2011), [arXiv:1102.2671 \[astro-ph.CO\]](#) .
- [100] S. Vagnozzi, S. Dhawan, M. Gerbino, K. Freese, A. Goobar, and O. Mena, “Constraints on the sum of the neutrino masses in dynamical dark energy models with $w(z) \geq -1$ are tighter than those obtained in Λ CDM,” *Phys. Rev.* **D98**, 083501 (2018), [arXiv:1801.08553 \[astro-ph.CO\]](#) .
- [101] R. R. Caldwell, M. Kamionkowski, and N. N. Weinberg, “Phantom energy and cosmic doomsday,” *Phys. Rev. Lett.* **91**, 071301 (2003), [arXiv:astro-ph/0302506 \[astro-ph\]](#) .
- [102] S. P. Brooks and A. Gelman, “General methods for monitoring convergence

References

- of iterative simulations,” *Journal of Computational and Graphical Statistics* **7**, 434–455 (1998).
- [103] R. Takahashi, M. Sato, T. Nishimichi, A. Taruya, and M. Oguri, “Revising the Halofit Model for the Nonlinear Matter Power Spectrum,” *Astrophys. J.* **761**, 152 (2012), [arXiv:1208.2701 \[astro-ph.CO\]](#) .
- [104] S. Bird, M. Viel, and M. G. Haehnelt, “Massive Neutrinos and the Non-linear Matter Power Spectrum,” *Mon. Not. Roy. Astron. Soc.* **420**, 2551–2561 (2012), [arXiv:1109.4416 \[astro-ph.CO\]](#) .
- [105] R. Adam *et al.* (Planck), “Planck 2015 results. I. Overview of products and scientific results,” *Astron. Astrophys.* **594**, A1 (2016), [arXiv:1502.01582 \[astro-ph.CO\]](#) .
- [106] P. A. R. Ade *et al.* (Planck), “Planck 2015 results. XV. Gravitational lensing,” *Astron. Astrophys.* **594**, A15 (2016), [arXiv:1502.01591 \[astro-ph.CO\]](#) .
- [107] S. Alam *et al.* (BOSS), “The clustering of galaxies in the completed SDSS-III Baryon Oscillation Spectroscopic Survey: cosmological analysis of the DR12 galaxy sample,” *Mon. Not. Roy. Astron. Soc.* **470**, 2617–2652 (2017), [arXiv:1607.03155 \[astro-ph.CO\]](#) .
- [108] A. J. Ross, L. Samushia, C. Howlett, W. J. Percival, A. Burden, and M. Manera, “The clustering of the SDSS DR7 main Galaxy sample – I. A 4 per cent distance measure at $z = 0.15$,” *Mon. Not. Roy. Astron. Soc.* **449**, 835–847 (2015), [arXiv:1409.3242 \[astro-ph.CO\]](#) .

References

- [109] F. Beutler, C. Blake, M. Colless, D. H. Jones, L. Staveley-Smith, L. Campbell, Q. Parker, W. Saunders, and F. Watson, “The 6dF Galaxy Survey: Baryon Acoustic Oscillations and the Local Hubble Constant,” *Mon. Not. Roy. Astron. Soc.* **416**, 3017–3032 (2011), [arXiv:1106.3366 \[astro-ph.CO\]](#) .
- [110] D. M. Scolnic *et al.*, “The Complete Light-curve Sample of Spectroscopically Confirmed SNe Ia from Pan-STARRS1 and Cosmological Constraints from the Combined Pantheon Sample,” *Astrophys. J.* **859**, 101 (2018), [arXiv:1710.00845 \[astro-ph.CO\]](#) .
- [111] M. Betoule *et al.* (SDSS), “Improved cosmological constraints from a joint analysis of the SDSS-II and SNLS supernova samples,” *Astron. Astrophys.* **568**, A22 (2014), [arXiv:1401.4064 \[astro-ph.CO\]](#) .
- [112] J. E. Carlstrom *et al.*, “The 10 Meter South Pole Telescope,” *Publ. Astron. Soc. Pac.* **123**, 568–581 (2011), [arXiv:0907.4445 \[astro-ph.IM\]](#) .
- [113] M. Birkinshaw, “The Sunyaev-Zel’dovich effect,” *Phys. Rept.* **310**, 97–195 (1999), [arXiv:astro-ph/9808050 \[astro-ph\]](#) .
- [114] N. Aghanim *et al.* (Planck), “Planck intermediate results. XLVI. Reduction of large-scale systematic effects in HFI polarization maps and estimation of the reionization optical depth,” *Astron. Astrophys.* **596**, A107 (2016), [arXiv:1605.02985 \[astro-ph.CO\]](#) .
- [115] A. G. Riess *et al.*, “A 2.4% Determination of the Local Value of the Hubble Constant,” *Astrophys. J.* **826**, 56 (2016), [arXiv:1604.01424 \[astro-ph.CO\]](#) .

References

- [116] V. Bonvin *et al.*, “H0LiCOW – V. New COSMOGRAIL time delays of HE 0435–1223: H_0 to 3.8 per cent precision from strong lensing in a flat Λ CDM model,” *Mon. Not. Roy. Astron. Soc.* **465**, 4914–4930 (2017), [arXiv:1607.01790 \[astro-ph.CO\]](#) .
- [117] Y. Chen, S. Kumar, and B. Ratra, “Determining the Hubble constant from Hubble parameter measurements,” *Astrophys. J.* **835**, 86 (2017), [arXiv:1606.07316 \[astro-ph.CO\]](#) .
- [118] A. G. Riess, S. Casertano, W. Yuan, L. M. Macri, and D. Scolnic, “Large Magellanic Cloud Cepheid Standards Provide a 1% Foundation for the Determination of the Hubble Constant and Stronger Evidence for Physics beyond Λ CDM,” *Astrophys. J.* **876**, 85 (2019), [arXiv:1903.07603 \[astro-ph.CO\]](#) .
- [119] R. Allison, P. Caucal, E. Calabrese, J. Dunkley, and T. Louis, “Towards a cosmological neutrino mass detection,” *Phys. Rev.* **D92**, 123535 (2015), [arXiv:1509.07471 \[astro-ph.CO\]](#) .
- [120] A. Lewis and A. Challinor, “Weak gravitational lensing of the CMB,” *Phys. Rept.* **429**, 1–65 (2006), [arXiv:astro-ph/0601594 \[astro-ph\]](#) .
- [121] C. L. Reichardt, “Understanding the epoch of cosmic reionization: Challenges and progress,” (Springer International Publishing, Cham, Switzerland, 2016) pp. 227–245.
- [122] P. Astier, “Can luminosity distance measurements probe the equation of

- state of dark energy,” *Phys. Lett.* **B500**, 8–15 (2001), [arXiv:astro-ph/0008306 \[astro-ph\]](#) .
- [123] M.-M. Zhao, Y.-H. Li, J.-F. Zhang, and X. Zhang, “Constraining neutrino mass and extra relativistic degrees of freedom in dynamical dark energy models using Planck 2015 data in combination with low-redshift cosmological probes: basic extensions to Λ CDM cosmology,” *Mon. Not. Roy. Astron. Soc.* **469**, 1713–1724 (2017), [arXiv:1608.01219 \[astro-ph.CO\]](#) .
- [124] J. Hamann, S. Hannestad, J. Lesgourgues, C. Rampf, and Y. Y. Y. Wong, “Cosmological parameters from large scale structure - geometric versus shape information,” *JCAP* **1007**, 022 (2010), [arXiv:1003.3999 \[astro-ph.CO\]](#) .
- [125] P. A. R. Ade *et al.* (BICEP2), “Detection of B -Mode Polarization at Degree Angular Scales by BICEP2,” *Phys. Rev. Lett.* **112**, 241101 (2014), [arXiv:1403.3985 \[astro-ph.CO\]](#) .
- [126] S. Hannestad, “Neutrino masses and the dark energy equation of state - Relaxing the cosmological neutrino mass bound,” *Phys. Rev. Lett.* **95**, 221301 (2005), [arXiv:astro-ph/0505551 \[astro-ph\]](#) .
- [127] E. Di Valentino, A. Melchiorri, E. V. Linder, and J. Silk, “Constraining Dark Energy Dynamics in Extended Parameter Space,” *Phys. Rev.* **D96**, 023523 (2017), [arXiv:1704.00762 \[astro-ph.CO\]](#) .
- [128] G.-B. Zhao *et al.*, “Dynamical dark energy in light of the latest observations,” *Nat. Astron.* **1**, 627–632 (2017), [arXiv:1701.08165 \[astro-ph.CO\]](#) .

References

- [129] L. Feng, J.-F. Zhang, and X. Zhang, “Searching for sterile neutrinos in dynamical dark energy cosmologies,” *Sci. China Phys. Mech. Astron.* **61**, 050411 (2018), [arXiv:1706.06913 \[astro-ph.CO\]](#) .
- [130] W. Yang, R. C. Nunes, S. Pan, and D. F. Mota, “Effects of neutrino mass hierarchies on dynamical dark energy models,” *Phys. Rev.* **D95**, 103522 (2017), [arXiv:1703.02556 \[astro-ph.CO\]](#) .
- [131] G. Lambiase, S. Mohanty, A. Narang, and P. Parashari, “Testing dark energy models in the light of σ_8 tension,” *Eur. Phys. J.* **C79**, 141 (2019), [arXiv:1804.07154 \[astro-ph.CO\]](#) .
- [132] V. Poulin, K. K. Boddy, S. Bird, and M. Kamionkowski, “Implications of an extended dark energy cosmology with massive neutrinos for cosmological tensions,” *Phys. Rev.* **D97**, 123504 (2018), [arXiv:1803.02474 \[astro-ph.CO\]](#) .
- [133] D. Wang, “Dark Energy Constraints in light of Pantheon SNe Ia, BAO, Cosmic Chronometers and CMB Polarization and Lensing Data,” *Phys. Rev.* **D97**, 123507 (2018), [arXiv:1801.02371 \[astro-ph.CO\]](#) .
- [134] X. Zhang, “Weighing neutrinos in dynamical dark energy models,” *Sci. China Phys. Mech. Astron.* **60**, 060431 (2017), [arXiv:1703.00651 \[astro-ph.CO\]](#) .
- [135] X. Zhang, “Impacts of dark energy on weighing neutrinos after Planck 2015,” *Phys. Rev.* **D93**, 083011 (2016), [arXiv:1511.02651 \[astro-ph.CO\]](#) .
- [136] A. Vikman, “Can dark energy evolve to the phantom?” *Phys. Rev.* **D71**, 023515 (2005), [arXiv:astro-ph/0407107 \[astro-ph\]](#) .

- [137] W. Fang, W. Hu, and A. Lewis, “Crossing the Phantom Divide with Parameterized Post-Friedmann Dark Energy,” *Phys. Rev.* **D78**, 087303 (2008), [arXiv:0808.3125 \[astro-ph\]](#) .
- [138] K. J. Ludwick, “The viability of phantom dark energy: A review,” *Mod. Phys. Lett.* **A32**, 1730025 (2017), [arXiv:1708.06981 \[astro-ph.CO\]](#) .
- [139] E. V. Linder, “The Dynamics of Quintessence, The Quintessence of Dynamics,” *Gen. Rel. Grav.* **40**, 329–356 (2008), [arXiv:0704.2064 \[astro-ph\]](#) .
- [140] R. R. Caldwell and E. V. Linder, “The Limits of quintessence,” *Phys. Rev. Lett.* **95**, 141301 (2005), [arXiv:astro-ph/0505494 \[astro-ph\]](#) .
- [141] S. Roy Choudhury and A. Naskar, “Strong Bounds on Sum of Neutrino Masses in a 12 Parameter Extended Scenario with Non-Phantom Dynamical Dark Energy ($w(z) \geq -1$) with CPL parameterization,” *Eur. Phys. J.* **C79**, 262 (2019), [arXiv:1807.02860 \[astro-ph.CO\]](#) .
- [142] F. Renzi, E. Di Valentino, and A. Melchiorri, “Cornering the Planck A_{lens} anomaly with future CMB data,” *Phys. Rev.* **D97**, 123534 (2018), [arXiv:1712.08758 \[astro-ph.CO\]](#) .
- [143] E. Calabrese, A. Slosar, A. Melchiorri, G. F. Smoot, and O. Zahn, “Cosmic Microwave Weak lensing data as a test for the dark universe,” *Phys. Rev.* **D77**, 123531 (2008), [arXiv:0803.2309 \[astro-ph\]](#) .
- [144] H. Böhringer, G. Chon, and C. A. Collins, “The extended ROSAT-ESO Flux Limited X-ray Galaxy Cluster Survey (REFLEX II) IV. X-ray Luminosity

References

- Function and First Constraints on Cosmological Parameters,” *Astron. Astrophys.* **570**, A31 (2014), [arXiv:1403.2927 \[astro-ph.CO\]](#) .
- [145] C. Heymans *et al.*, “CFHTLenS: The Canada-France-Hawaii Telescope Lensing Survey,” *Mon. Not. Roy. Astron. Soc.* **427**, 146 (2012), [arXiv:1210.0032 \[astro-ph.CO\]](#) .
- [146] H. Hildebrandt *et al.*, “KiDS-450: Cosmological parameter constraints from tomographic weak gravitational lensing,” *Mon. Not. Roy. Astron. Soc.* **465**, 1454 (2017), [arXiv:1606.05338 \[astro-ph.CO\]](#) .
- [147] E. Di Valentino, A. Melchiorri, and J. Silk, “Beyond six parameters: extending Λ CDM,” *Phys. Rev.* **D92**, 121302 (2015), [arXiv:1507.06646 \[astro-ph.CO\]](#) .
- [148] E. Di Valentino, A. Melchiorri, and J. Silk, “Reconciling Planck with the local value of H_0 in extended parameter space,” *Phys. Lett.* **B761**, 242–246 (2016), [arXiv:1606.00634 \[astro-ph.CO\]](#) .
- [149] E. Di Valentino, A. Melchiorri, and J. Silk, “Cosmological constraints in extended parameter space from the Planck 2018 Legacy release,” (2019), [arXiv:1908.01391 \[astro-ph.CO\]](#) .
- [150] R. Adam *et al.* (Planck), “Planck intermediate results. XLVII. Planck constraints on reionization history,” *Astron. Astrophys.* **596**, A108 (2016), [arXiv:1605.03507 \[astro-ph.CO\]](#) .
- [151] G. Efstathiou, “Constraining the equation of state of the universe from distant type Ia supernovae and cosmic microwave background anisotropies,” *Mon.*

References

- Not. Roy. Astron. Soc. **310**, 842–850 (1999), [arXiv:astro-ph/9904356](#) [astro-ph] .
- [152] H. K. Jassal, J. S. Bagla, and T. Padmanabhan, “WMAP constraints on low redshift evolution of dark energy,” *Mon. Not. Roy. Astron. Soc.* **356**, L11–L16 (2005), [arXiv:astro-ph/0404378](#) [astro-ph] .
- [153] S. Roy Choudhury and S. Choubey, “Constraining light sterile neutrino mass with the BICEP2/Keck Array 2014 B-mode polarization data,” *Eur. Phys. J.* **C79**, 557 (2019), [arXiv:1807.10294](#) [astro-ph.CO] .
- [154] A. Aguilar-Arevalo *et al.* (LSND), “Evidence for neutrino oscillations from the observation of anti-neutrino(electron) appearance in a anti-neutrino(muon) beam,” *Phys. Rev.* **D64**, 112007 (2001), [arXiv:hep-ex/0104049](#) [hep-ex] .
- [155] A. A. Aguilar-Arevalo *et al.* (MiniBooNE), “Improved Search for $\bar{\nu}_\mu \rightarrow \bar{\nu}_e$ Oscillations in the MiniBooNE Experiment,” *Phys. Rev. Lett.* **110**, 161801 (2013), [arXiv:1303.2588](#) [hep-ex] .
- [156] T. A. Mueller *et al.*, “Improved Predictions of Reactor Antineutrino Spectra,” *Phys. Rev.* **C83**, 054615 (2011), [arXiv:1101.2663](#) [hep-ex] .
- [157] J. Kopp, M. Maltoni, and T. Schwetz, “Are there sterile neutrinos at the eV scale?” *Phys. Rev. Lett.* **107**, 091801 (2011), [arXiv:1103.4570](#) [hep-ph] .
- [158] J. R. Kristiansen, ø. Elgarøy, C. Giunti, and M. Laveder, “Cosmology with sterile neutrino masses from oscillation experiments,” (2013), [arXiv:1303.4654](#) [astro-ph.CO] .

References

- [159] C. Giunti, M. Laveder, Y. F. Li, and H. W. Long, “Pragmatic View of Short-Baseline Neutrino Oscillations,” *Phys. Rev.* **D88**, 073008 (2013), [arXiv:1308.5288 \[hep-ph\]](#) .
- [160] F. Capozzi, C. Giunti, M. Laveder, and A. Palazzo, “Joint short- and long-baseline constraints on light sterile neutrinos,” *Phys. Rev.* **D95**, 033006 (2017), [arXiv:1612.07764 \[hep-ph\]](#) .
- [161] M. Dentler, Á. Hernández-Cabezudo, J. Kopp, P. Machado, M. Maltoni, I. Martinez-Soler, and T. Schwetz, “Updated Global Analysis of Neutrino Oscillations in the Presence of eV-Scale Sterile Neutrinos,” (2018), [arXiv:1803.10661 \[hep-ph\]](#) .
- [162] A. A. Aguilar-Arevalo *et al.* (MiniBooNE), “Observation of a Significant Excess of Electron-Like Events in the MiniBooNE Short-Baseline Neutrino Experiment,” (2018), [arXiv:1805.12028 \[hep-ex\]](#) .
- [163] K. N. Abazajian, “Sterile neutrinos in cosmology,” *Phys. Rept.* **711-712**, 1–28 (2017), [arXiv:1705.01837 \[hep-ph\]](#) .
- [164] X. Chu, B. Dasgupta, and J. Kopp, “Sterile neutrinos with secret interactions—lasting friendship with cosmology,” *JCAP* **1510**, 011 (2015), [arXiv:1505.02795 \[hep-ph\]](#) .
- [165] S. Hannestad, I. Tamborra, and T. Tram, “Thermalisation of light sterile neutrinos in the early universe,” *JCAP* **1207**, 025 (2012), [arXiv:1204.5861 \[astro-ph.CO\]](#) .

- [166] A. Melchiorri, O. Mena, S. Palomares-Ruiz, S. Pascoli, A. Slosar, and M. Sorel, “Sterile Neutrinos in Light of Recent Cosmological and Oscillation Data: A Multi-Flavor Scheme Approach,” *JCAP* **0901**, 036 (2009), [arXiv:0810.5133 \[hep-ph\]](#) .
- [167] M. Archidiacono, E. Giusarma, S. Hannestad, and O. Mena, “Cosmic dark radiation and neutrinos,” *Adv. High Energy Phys.* **2013**, 191047 (2013), [arXiv:1307.0637 \[astro-ph.CO\]](#) .
- [168] S. Bashinsky and U. Seljak, “Neutrino perturbations in CMB anisotropy and matter clustering,” *Phys. Rev.* **D69**, 083002 (2004), [arXiv:astro-ph/0310198 \[astro-ph\]](#) .
- [169] S. Hannestad, “Structure formation with strongly interacting neutrinos - Implications for the cosmological neutrino mass bound,” *JCAP* **0502**, 011 (2005), [arXiv:astro-ph/0411475 \[astro-ph\]](#) .
- [170] J. Hamann, S. Hannestad, G. G. Raffelt, and Y. Y. Y. Wong, “Sterile neutrinos with eV masses in cosmology: How disfavoured exactly?” *JCAP* **1109**, 034 (2011), [arXiv:1108.4136 \[astro-ph.CO\]](#) .
- [171] M. Archidiacono, S. Hannestad, R. S. Hansen, and T. Tram, “Cosmology with self-interacting sterile neutrinos and dark matter - A pseudoscalar model,” *Phys. Rev.* **D91**, 065021 (2015), [arXiv:1404.5915 \[astro-ph.CO\]](#) .
- [172] J.-F. Zhang, J.-J. Geng, and X. Zhang, “Neutrinos and dark energy after

References

- Planck and BICEP2: data consistency tests and cosmological parameter constraints,” *JCAP* **1410**, 044 (2014), [arXiv:1408.0481 \[astro-ph.CO\]](#) .
- [173] M. Archidiacono, N. Fornengo, C. Giunti, and A. Melchiorri, “Testing 3+1 and 3+2 neutrino mass models with cosmology and short baseline experiments,” *Phys. Rev.* **D86**, 065028 (2012), [arXiv:1207.6515 \[astro-ph.CO\]](#) .
- [174] M. Archidiacono, N. Fornengo, C. Giunti, S. Hannestad, and A. Melchiorri, “Sterile neutrinos: Cosmology versus short-baseline experiments,” *Phys. Rev.* **D87**, 125034 (2013), [arXiv:1302.6720 \[astro-ph.CO\]](#) .
- [175] S. Gariazzo, C. Giunti, and M. Laveder, “Light Sterile Neutrinos in Cosmology and Short-Baseline Oscillation Experiments,” *JHEP* **11**, 211 (2013), [arXiv:1309.3192 \[hep-ph\]](#) .
- [176] C. Dvorkin, M. Wyman, D. H. Rudd, and W. Hu, “Neutrinos help reconcile Planck measurements with both the early and local Universe,” *Phys. Rev.* **D90**, 083503 (2014), [arXiv:1403.8049 \[astro-ph.CO\]](#) .
- [177] L. Feng, J.-F. Zhang, and X. Zhang, “Search for sterile neutrinos in a universe of vacuum energy interacting with cold dark matter,” (2017), [arXiv:1712.03148 \[astro-ph.CO\]](#) .
- [178] N. Song, M. C. Gonzalez-Garcia, and J. Salvado, “Cosmological constraints with self-interacting sterile neutrinos,” (2018), [arXiv:1805.08218 \[astro-ph.CO\]](#) .

References

- [179] F. Forastieri, M. Lattanzi, G. Mangano, A. Mirizzi, P. Natoli, and N. Saviano, “Cosmic microwave background constraints on secret interactions among sterile neutrinos,” *JCAP* **1707**, 038 (2017), [arXiv:1704.00626 \[astro-ph.CO\]](#) .
- [180] M.-M. Zhao, D.-Z. He, J.-F. Zhang, and X. Zhang, “Search for sterile neutrinos in holographic dark energy cosmology: Reconciling Planck observation with the local measurement of the Hubble constant,” *Phys. Rev.* **D96**, 043520 (2017), [arXiv:1703.08456 \[astro-ph.CO\]](#) .
- [181] S. Kumar and R. C. Nunes, “Echo of interactions in the dark sector,” *Phys. Rev.* **D96**, 103511 (2017), [arXiv:1702.02143 \[astro-ph.CO\]](#) .
- [182] M. A. Acero and J. Lesgourgues, “Cosmological constraints on a light non-thermal sterile neutrino,” *Phys. Rev.* **D79**, 045026 (2009), [arXiv:0812.2249 \[astro-ph\]](#) .
- [183] P. A. R. Ade *et al.* (Planck), “Planck 2013 results. XVI. Cosmological parameters,” *Astron. Astrophys.* **571**, A16 (2014), [arXiv:1303.5076 \[astro-ph.CO\]](#) .
- [184] S. Dodelson and L. M. Widrow, “Sterile-neutrinos as dark matter,” *Phys. Rev. Lett.* **72**, 17–20 (1994), [arXiv:hep-ph/9303287 \[hep-ph\]](#) .
- [185] A. Peimbert, M. Peimbert, and V. Luridiana, “The primordial helium abundance and the number of neutrino families,” *Rev. Mex. Astron. Astrofis.* **52**, 419 (2016), [arXiv:1608.02062 \[astro-ph.CO\]](#) .

References

- [186] H. Akaike, “A new look at the statistical model identification,” *IEEE Transactions on Automatic Control* **19**, 716–723 (1974).
- [187] Y. Akrami *et al.* (Planck), “Planck 2018 results. X. Constraints on inflation,” (2018), [arXiv:1807.06211 \[astro-ph.CO\]](#) .
- [188] P. A. R. Ade *et al.* (BICEP2, Keck Array), “BICEP2 / Keck Array x: Constraints on Primordial Gravitational Waves using Planck, WMAP, and New BICEP2/Keck Observations through the 2015 Season,” *Phys. Rev. Lett.* **121**, 221301 (2018), [arXiv:1810.05216 \[astro-ph.CO\]](#) .
- [189] A. Aghamousa *et al.* (DESI), “The DESI Experiment Part I: Science, Targeting, and Survey Design,” (2016), [arXiv:1611.00036 \[astro-ph.IM\]](#) .
- [190] L. Amendola *et al.*, “Cosmology and fundamental physics with the Euclid satellite,” *Living Rev. Rel.* **21**, 2 (2018), [arXiv:1606.00180 \[astro-ph.CO\]](#) .
- [191] P. A. Abell *et al.* (LSST Science, LSST Project), “LSST Science Book, Version 2.0,” (2009), [arXiv:0912.0201 \[astro-ph.IM\]](#) .
- [192] K. N. Abazajian *et al.* (CMB-S4), “CMB-S4 Science Book, First Edition,” (2016), [arXiv:1610.02743 \[astro-ph.CO\]](#) .
- [193] P. Ade *et al.* (Simons Observatory), “The Simons Observatory: Science goals and forecasts,” *JCAP* **1902**, 056 (2019), [arXiv:1808.07445 \[astro-ph.CO\]](#) .

References

- [194] T. Matsumura *et al.*, “Mission design of LiteBIRD,” (2013), [10.1007/s10909-013-0996-1](https://doi.org/10.1007/s10909-013-0996-1), [J. Low. Temp. Phys.176,733(2014)], [arXiv:1311.2847](https://arxiv.org/abs/1311.2847) [astro-ph.IM] .
- [195] A. Kogut *et al.*, “The Primordial Inflation Explorer (PIXIE): A Nulling Polarimeter for Cosmic Microwave Background Observations,” *JCAP* **1107**, 025 (2011), [arXiv:1105.2044](https://arxiv.org/abs/1105.2044) [astro-ph.CO] .
- [196] T. Essinger-Hileman *et al.*, “CLASS: The Cosmology Large Angular Scale Surveyor,” *Proceedings, SPIE Astronomical Telescopes + Instrumentation 2014: Millimeter, Submillimeter, and Far-Infrared Detectors and Instrumentation for Astronomy VII: Montreal, Quebec, Canada, June 24-27, 2014*, *Proc. SPIE Int. Soc. Opt. Eng.* **9153**, 91531I (2014), [arXiv:1408.4788](https://arxiv.org/abs/1408.4788) [astro-ph.IM] .
- [197] C. Dvorkin *et al.*, “Neutrino Mass from Cosmology: Probing Physics Beyond the Standard Model,” (2019), [arXiv:1903.03689](https://arxiv.org/abs/1903.03689) [astro-ph.CO] .
- [198] K. N. Abazajian *et al.* (Topical Conveners: K.N. Abazajian, J.E. Carlstrom, A.T. Lee), “Neutrino Physics from the Cosmic Microwave Background and Large Scale Structure,” *Astropart. Phys.* **63**, 66–80 (2015), [arXiv:1309.5383](https://arxiv.org/abs/1309.5383) [astro-ph.CO] .
- [199] A. C. Hall and A. Challinor, “Probing the neutrino mass hierarchy with CMB weak lensing,” *Mon. Not. Roy. Astron. Soc.* **425**, 1170–1184 (2012), [arXiv:1205.6172](https://arxiv.org/abs/1205.6172) [astro-ph.CO] .

References

- [200] W. L. K. Wu, J. Errard, C. Dvorkin, C. L. Kuo, A. T. Lee, P. McDonald, A. Slosar, and O. Zahn, “A Guide to Designing Future Ground-based Cosmic Microwave Background Experiments,” *Astrophys. J.* **788**, 138 (2014), [arXiv:1402.4108 \[astro-ph.CO\]](#) .
- [201] Z. Pan and L. Knox, “Constraints on neutrino mass from Cosmic Microwave Background and Large Scale Structure,” *Mon. Not. Roy. Astron. Soc.* **454**, 3200–3206 (2015), [arXiv:1506.07493 \[astro-ph.CO\]](#) .
- [202] J. Hamann, S. Hannestad, and Y. Y. Y. Wong, “Measuring neutrino masses with a future galaxy survey,” *JCAP* **1211**, 052 (2012), [arXiv:1209.1043 \[astro-ph.CO\]](#) .
- [203] T. Brinckmann, D. C. Hooper, M. Archidiacono, J. Lesgourgues, and T. Sprenger, “The promising future of a robust cosmological neutrino mass measurement,” *JCAP* **1901**, 059 (2019), [arXiv:1808.05955 \[astro-ph.CO\]](#) .
- [204] S. Gariazzo, M. Archidiacono, P. F. de Salas, O. Mena, C. A. Ternes, and M. Tórtola, “Neutrino masses and their ordering: Global Data, Priors and Models,” *JCAP* **1803**, 011 (2018), [arXiv:1801.04946 \[hep-ph\]](#) .
- [205] F. Capozzi, E. Lisi, A. Marrone, and A. Palazzo, “Current unknowns in the three neutrino framework,” *Prog. Part. Nucl. Phys.* **102**, 48–72 (2018), [arXiv:1804.09678 \[hep-ph\]](#) .
- [206] P. F. De Salas, S. Gariazzo, O. Mena, C. A. Ternes, and M. Tórtola, “Neutrino Mass Ordering from Oscillations and Beyond: 2018 Status and Future

References

- Prospects,” *Front. Astron. Space Sci.* **5**, 36 (2018), [arXiv:1806.11051 \[hep-ph\]](#) .
- [207] C. D. Kreisch, F.-Y. Cyr-Racine, and O. Doré, “The Neutrino Puzzle: Anomalies, Interactions, and Cosmological Tensions,” (2019), [arXiv:1902.00534 \[astro-ph.CO\]](#) .
- [208] M. Park, C. D. Kreisch, J. Dunkley, B. Hadzhiyska, and F.-Y. Cyr-Racine, “ Λ CDM or self-interacting neutrinos: How CMB data can tell the two models apart,” *Phys. Rev.* **D100**, 063524 (2019), [arXiv:1904.02625 \[astro-ph.CO\]](#) .
- [209] G. Barenboim, P. B. Denton, and I. M. Oldengott, “Constraints on inflation with an extended neutrino sector,” *Phys. Rev.* **D99**, 083515 (2019), [arXiv:1903.02036 \[astro-ph.CO\]](#) .
- [210] I. M. Oldengott, T. Tram, C. Rampf, and Y. Y. Y. Wong, “Interacting neutrinos in cosmology: exact description and constraints,” *JCAP* **1711**, 027 (2017), [arXiv:1706.02123 \[astro-ph.CO\]](#) .
- [211] M. Archidiacono and S. Hannestad, “Updated constraints on non-standard neutrino interactions from Planck,” *JCAP* **1407**, 046 (2014), [arXiv:1311.3873 \[astro-ph.CO\]](#) .
- [212] B. Dasgupta and J. Kopp, “Cosmologically Safe eV-Scale Sterile Neutrinos and Improved Dark Matter Structure,” *Phys. Rev. Lett.* **112**, 031803 (2014), [arXiv:1310.6337 \[hep-ph\]](#) .

References

- [213] S. Hannestad, R. S. Hansen, and T. Tram, “How Self-Interactions can Reconcile Sterile Neutrinos with Cosmology,” *Phys. Rev. Lett.* **112**, 031802 (2014), [arXiv:1310.5926 \[astro-ph.CO\]](#) .
- [214] M. Archidiacono, S. Gariazzo, C. Giunti, S. Hannestad, R. Hansen, M. Laveder, and T. Tram, “Pseudoscalar–sterile neutrino interactions: reconciling the cosmos with neutrino oscillations,” *JCAP* **1608**, 067 (2016), [arXiv:1606.07673 \[astro-ph.CO\]](#) .
- [215] Y. S. Jeong, S. Palomares-Ruiz, M. H. Reno, and I. Sarcevic, “Probing secret interactions of eV-scale sterile neutrinos with the diffuse supernova neutrino background,” *JCAP* **1806**, 019 (2018), [arXiv:1803.04541 \[hep-ph\]](#) .
- [216] T. Rehagen and G. B. Gelmini, “Effects of kination and scalar-tensor cosmologies on sterile neutrinos,” *JCAP* **1406**, 044 (2014), [arXiv:1402.0607 \[hep-ph\]](#) .
- [217] Y.-Z. Chu and M. Cirelli, “Sterile neutrinos, lepton asymmetries, primordial elements: How much of each?” *Phys. Rev.* **D74**, 085015 (2006), [arXiv:astro-ph/0608206 \[astro-ph\]](#) .
- [218] G. Gelmini, S. Palomares-Ruiz, and S. Pascoli, “Low reheating temperature and the visible sterile neutrino,” *Phys. Rev. Lett.* **93**, 081302 (2004), [arXiv:astro-ph/0403323 \[astro-ph\]](#) .
- [219] J. Dakin, J. Brandbyge, S. Hannestad, T. Haugbølle, and T. Tram,

References

- “ ν CONCEPT: Cosmological neutrino simulations from the non-linear Boltzmann hierarchy,” *JCAP* **1902**, 052 (2019), [arXiv:1712.03944 \[astro-ph.CO\]](#) .
- [220] T. Tram, J. Brandbyge, J. Dakin, and S. Hannestad, “Fully relativistic treatment of light neutrinos in N -body simulations,” *JCAP* **1903**, 022 (2019), [arXiv:1811.00904 \[astro-ph.CO\]](#) .
- [221] J. Brandbyge, S. Hannestad, and T. Tram, “Momentum space sampling of neutrinos in N -body simulations,” *JCAP* **1903**, 047 (2019), [arXiv:1806.05874 \[astro-ph.CO\]](#) .
- [222] A. Banerjee, D. Powell, T. Abel, and F. Villaescusa-Navarro, “Reducing Noise in Cosmological N -body Simulations with Neutrinos,” *JCAP* **1809**, 028 (2018), [arXiv:1801.03906 \[astro-ph.CO\]](#) .
- [223] J. Liu, S. Bird, J. M. Z. Matilla, J. C. Hill, Z. Haiman, M. S. Madhavacheril, A. Petri, and D. N. Spergel, “MassiveNuS: Cosmological Massive Neutrino Simulations,” *JCAP* **1803**, 049 (2018), [arXiv:1711.10524 \[astro-ph.CO\]](#) .
- [224] A. Banerjee and N. Dalal, “Simulating nonlinear cosmological structure formation with massive neutrinos,” *JCAP* **1611**, 015 (2016), [arXiv:1606.06167 \[astro-ph.CO\]](#) .
- [225] S. Vagnozzi, T. Brinckmann, M. Archidiacono, K. Freese, M. Gerbino, J. Lesgourgues, and T. Sprenger, “Bias due to neutrinos must not uncorrect’d go,” *JCAP* **1809**, 001 (2018), [arXiv:1807.04672 \[astro-ph.CO\]](#) .

- [226] C.-T. Chiang, M. LoVerde, and F. Villaescusa-Navarro, “First detection of scale-dependent linear halo bias in N -body simulations with massive neutrinos,” *Phys. Rev. Lett.* **122**, 041302 (2019), [arXiv:1811.12412 \[astro-ph.CO\]](#) .
- [227] S. Vagnozzi, “Cosmological searches for the neutrino mass scale and mass ordering,” (2019), [arXiv:1907.08010 \[astro-ph.CO\]](#) .
- [228] A. I. Lonappan, S. Kumar, Ruchika, B. R. Dinda, and A. A. Sen, “Bayesian evidences for dark energy models in light of current observational data,” *Phys. Rev.* **D97**, 043524 (2018), [arXiv:1707.00603 \[astro-ph.CO\]](#) .
- [229] A. Diaz Rivero, V. Miranda, and C. Dvorkin, “Observable Predictions for Massive-Neutrino Cosmologies with Model-Independent Dark Energy,” *Phys. Rev.* **D100**, 063504 (2019), [arXiv:1903.03125 \[astro-ph.CO\]](#) .
- [230] F. Gerardi, M. Martinelli, and A. Silvestri, “Reconstruction of the Dark Energy equation of state from latest data: the impact of theoretical priors,” *JCAP* **1907**, 042 (2019), [arXiv:1902.09423 \[astro-ph.CO\]](#) .
- [231] S. Kumar, R. C. Nunes, and S. K. Yadav, “Dark sector interaction: a remedy of the tensions between CMB and LSS data,” *Eur. Phys. J.* **C79**, 576 (2019), [arXiv:1903.04865 \[astro-ph.CO\]](#) .
- [232] E. Di Valentino, A. Melchiorri, O. Mena, and S. Vagnozzi, “Interacting dark energy after the latest Planck, DES, and H_0 measurements: an excellent solu-

- tion to the H_0 and cosmic shear tensions,” (2019), [arXiv:1908.04281 \[astro-ph.CO\]](#) .
- [233] S. Pan, W. Yang, E. Di Valentino, E. N. Saridakis, and S. Chakraborty, “Interacting scenarios with dynamical dark energy: observational constraints and alleviation of the H_0 tension,” *Phys. Rev.* **D100**, 103520 (2019), [arXiv:1907.07540 \[astro-ph.CO\]](#) .
- [234] W. Yang, S. Vagnozzi, E. Di Valentino, R. C. Nunes, S. Pan, and D. F. Mota, “Listening to the sound of dark sector interactions with gravitational wave standard sirens,” *JCAP* **1907**, 037 (2019), [arXiv:1905.08286 \[astro-ph.CO\]](#) .
- [235] W. Yang, S. Pan, A. Paliathanasis, S. Ghosh, and Y. Wu, “Observational constraints of a new unified dark fluid and the H_0 tension,” *Mon. Not. Roy. Astron. Soc.* **490**, 2071–2085 (2019), [arXiv:1904.10436 \[gr-qc\]](#) .
- [236] W. Yang, N. Banerjee, A. Paliathanasis, and S. Pan, “Reconstructing the dark matter and dark energy interaction scenarios from observations,” *Phys. Dark Univ.* **26**, 100383 (2019), [arXiv:1812.06854 \[astro-ph.CO\]](#) .
- [237] G. Cheng, Y. Ma, F. Wu, J. Zhang, and X. Chen, “Testing interacting dark matter and dark energy model with cosmological data,” (2019), [arXiv:1911.04520 \[astro-ph.CO\]](#) .
- [238] L. Feng, D.-Z. He, H.-L. Li, J.-F. Zhang, and X. Zhang, “Constraints on active and sterile neutrinos in an interacting dark energy cosmology,” (2019), [arXiv:1910.03872 \[astro-ph.CO\]](#) .

References

- [239] B. D. Wandelt, R. Dave, G. R. Farrar, P. C. McGuire, D. N. Spergel, and P. J. Steinhardt, “Selfinteracting dark matter,” in *Sources and detection of dark matter and dark energy in the universe. Proceedings, 4th International Symposium, DM 2000, Marina del Rey, USA, February 23-25, 2000* (2000) pp. 263–274, [arXiv:astro-ph/0006344 \[astro-ph\]](#) .
- [240] S. Tulin and H.-B. Yu, “Dark Matter Self-interactions and Small Scale Structure,” *Phys. Rept.* **730**, 1–57 (2018), [arXiv:1705.02358 \[hep-ph\]](#) .
- [241] E. Di Valentino, C. Bøehm, E. Hivon, and F. R. Bouchet, “Reducing the H_0 and σ_8 tensions with Dark Matter-neutrino interactions,” *Phys. Rev.* **D97**, 043513 (2018), [arXiv:1710.02559 \[astro-ph.CO\]](#) .